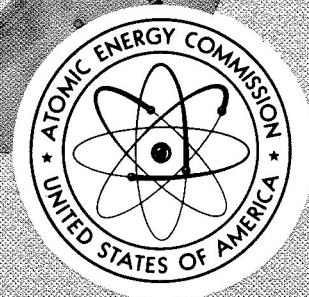


STL-517-0049 vol 6

FACILITY FORM 602

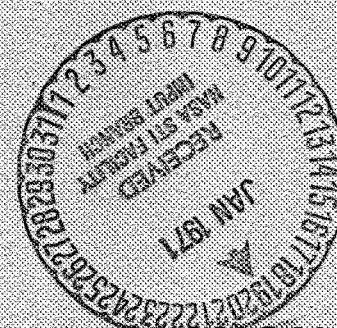
(ACCESSION NUMBER)
N71-70419
(PAGES)
115
CR-115843
(NASA CR OR TMX OR AD NUMBER)

(THRU)
(CODE)
(CATEGORY)

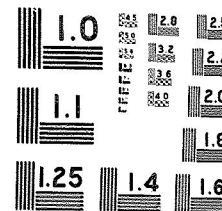


A Facsimile Report

Reproduced by
**UNITED STATES
ATOMIC ENERGY COMMISSION**
Division of Technical Information
P.O. Box 62 Oak Ridge, Tennessee 37830



1 OF 2
STL 517
0049
VOL. 6



MICROCOPY RESOLUTION TEST CHART
NATIONAL BUREAU OF STANDARDS-1963

CEMEX PRICES

H.C. \$ 3.00 MN 65

RADIOISOTOPE PROPULSION TECHNOLOGY PROGRAM (POODLE)

FINAL REPORT

(1 October 1965—31 March 1967)

VOLUME VI—POODLE SYSTEMS ANALYSES

STL-517-0049

April 1967

Contract No. AT(04-3)-517
Modification No. 7

Approved G. E. Austin

Authors:

M. King
R. Simms
J. C. Stansel

G. E. Austin
POODLE Project Manager

Approved D. Jortner

D. Jortner, Manager
Nuclear Technology Department

TRW
SYSTEMS GROUP

LEGAL NOTICE

This report was prepared as an account of Government sponsored work. Neither the United States, nor the Commission, nor any person acting on behalf of the Commission:

A. Makes any warranty or representation, expressed or implied, with respect to the accuracy, completeness, or usefulness of the information contained in this report, or that the use of any information, apparatus, method, or process disclosed in this report may not infringe privately owned rights; or

B. Assumes any liabilities with respect to the use of, or for damages resulting from the use of any information, apparatus, method, or process disclosed in this report.

As used in the above, "person acting on behalf of the Commission" includes any employee or contractor of the Commission, or employee of such contractor, in the extent that such employee or contractor of the Commission, or employee of such contractor prepares, disseminates, or provides access to, any information pursuant to his employment or contract with the Commission, or his employment with such contractor.

FOREWORD

The work reported herein covers Task 6 and portions of Task 2 of the statement of work contained in Modification No. 7, 28 June 1966, to contract AT(04-3)-517, Radioisotope Propulsion Technology (POODLE) for the AEC Division of Isotopes Development and the Joint AEC/NASA Space Nuclear Propulsion Office. Sections on thruster design, re-entry configurations, and performance of advanced upper stages were prepared by M. King, J. C. Stansel, and R. Simms, respectively. The complete final report on Modification 7 consists of this volume and others as listed below:

<u>Volume</u>	<u>Title</u>
I	Capsule Creep Strain Measurements and Analyses
IIA	Analytical Program for Creep in Axisymmetric Shells (CRASH)
IIB	Analytical Program for Creep in Axisymmetric Bodies (CRAB)
III	Oxidation and Diffusion in Noble Metal Alloy Claddings
IV	Performance of Low Thrust Nozzles
V	Simulation of High-Temperature Radioisotope Heat Source
VI	POODLE System Analyses

CONTENTS

	Page
1. INTRODUCTION	1-1
2. THRUSTER DESIGN	2-1
2.1 PURPOSE AND SCOPE	2-1
2.2 CAPSULE DESIGN ANALYSIS	2-2
2.2.1 Temperature Profiles	2-2
2.2.2 Cladding Technology	2-9
2.2.2.1 Interdiffusion of W-25Re	2-13
and Rh-30Ir Cladding	
2.2.2.2 Oxidation of Rh-Ir Claddings	2-14
2.2.2.3 Conclusions	2-21
2.2.3 Creep Analysis	2-22
2.2.4 Final Capsule Isotope Loadings	2-25
2.3 THRUSTER DESIGN ANALYSIS	2-30
2.3.1 Insulation and Thermal Performance	2-30
2.3.1.1 Insulation Design Considerations ..	2-30
2.3.1.2 Thermal Performance	2-34
2.3.2 Mechanical Design Considerations	2-38
2.3.2.1 Flow Module	2-38
2.3.2.2 Outer Thruster Module	2-38
2.3.3 Re-entry Considerations	2-40
2.3.3.1 Oxidation Resistant Coatings	2-40
2.3.3.2 Re-entry Aids	2-41
2.3.4 Nozzle Performance	2-44
2.4 THRUSTER DESIGN	2-46
2.5 CONCLUSIONS AND RECOMMENDATIONS	2-50
3. RE-ENTRY CONFIGURATIONS	3-1
3.2 HYPERSONIC WIND TUNNEL TESTS	3-2
3.3 SUBSONIC WIND TUNNEL TESTS	3-7
3.4 FIN SIZING ANALYSIS	3-14
3.5 CONCLUSIONS AND RECOMMENDATIONS	3-22

CONTENTS

	Page
4. PERFORMANCE COMPARISON OF	4-1
ADVANCED UPPER STAGES FOR	
POTENTIAL NASA MISSIONS	
4.1 INTRODUCTION	4-1
4.2 VEHICLE DESCRIPTION	4-1
4.2.1 POODLE Stage	4-1
4.2.2 Hydrogen-Fluorine Upper Stage	4-4
4.3 LAUNCH VEHICLE/UPPER STAGE	4-4
PAYLOAD CAPABILITY	
4.4 MISSIONS	4-7
4.4.1 Solar Probes	4-7
4.4.2 Out-of-Ecliptic Probes	4-11
4.4.3 Missions to the Outer Planets	4-12
4.4.4 Orbital Transfers	4-23
4.5 CONCLUSIONS	4-23

APPENDIX

A	VELOCITY PENALTY ASSOCIATED	A-1
	WITH POODLE FOR ESCAPE MISSIONS	

ILLUSTRATIONS

	Page
2-1 End of Mission Temperature Profile for Three Capsule Off-Loaded Thruster Configuration ($Q_{Launch} = 5.0$ Kw)	2-3
2-2 Capsule Temperature Profiles in Three Capsule Thruster-Emissivity = 0.7 ($Q_{Launch} = 5.0$ Kw)	2-5
2-3 Capsule Temperature Profiles in Three Capsule Thruster - Emissivity = 0.45 ($Q_{Launch} = 5.0$ Kw)	2-6
2-4 Capsule Temperature Profile in Three Capsule Thruster - Emissivity = 0.2 ($Q_{Launch} = 5.0$ Kw)	2-7
2-5 POODLE Capsule Configuration	2-8
2-6 Peak Capsule Temperature While Within Thruster Radiating to Space (Initial Capsule Power = 3.72 Kw)	2-10
2-7 Temperature Vs Time For Capsule Lying on the Ground (Initial Capsule Power = 3.72 Kw)	2-11
2-8 Correlation of Measured Interdiffusion Zone Thickness from Reference 2-3	2-15
2-9 Correlation of Oxidation Penetration Rate Based on Experimental Data in Reference 2-3	2-17
2-10 Parameter "A" in Correlation of Uniaxial Creep Data for W-25Re	2-22
2-11 Pressure in Maximum Loaded Capsule While Within 5.0 Kw at Launch Thruster	2-23
2-12 Temperature Profile During Propellant Flow for Three Capsule Off-Loaded Thruster Configuration ($Q_{Launch} = 5.6$ Kw)	2-25
2-13 Capsule Temperature Profile in Three Capsule Thruster - Emissivity = 0.70 ($Q_{Launch} = 5.6$ Kw)	2-26
2-14 Capsule Temperature Profiles in Three Capsule Thruster - Emissivity = 0.45 ($Q_{Launch} = 5.6$ Kw)	2-27

ILLUSTRATIONS

	Page
2-15 Peak Capsule Temperature While Within 5.6 Kw Thruster Radiating to Space ($Q_o = 3.72$ Kw)	2-29
2-16 Theoretical Thermal Conductance for 46 Tantalum and Tungsten Shields	2-32
2-17 Capsule Wall Temperature Profile (Off-Loaded Three Capsule Thruster Configuration) for Various Thermal Efficiencies	2-34
2-18 Capsule Wall Temperature Profile (Tapered Capsule Thruster Configuration) for Various Thermal Efficiencies	2-35
2-19 Relative Insulation Effectiveness Required to Achieve Given Thermal Efficiency	2-37
2-20 Thruster Orientation for Re-entry Analysis	2-42
2-21 Thruster Weight Vs Sea Level Impact Velocity for Various Fin Configurations	2-43
2-22 Experimentally Measured Nozzle Efficiency Vs Throat Reynolds Number	2-45
2-23 POODLE Thruster Assembly	2-47
3-1 POODLE Model Test Conditions Compared to Full Scale Flight Regime	3-5
3-2 Thruster Configuration Referenced in Fin-Sizing Analysis	3-15
3-3 Fin Thickness Variation Versus Fin Span	3-17
3-4 Sea Level Impact Velocity Versus Total POODLE Weight	3-19
3-5 Re-entry Aid Weight Versus Fin Span	3-20
4-1 Variation of Structure Factor with POODLE Stage Ignition Weight	4-4
4-2 Payload as a Function of Equivalent Burnout Velocity	4-6

ILLUSTRATIONS

	Page
4-3 Solar Probe	4-8
4-4 Propulsion Requirements for Solar Probes	4-9
4-5 Payloads for Solar Probes	4-10
4-6 Schematic Diagram of a Probe in Degrees Out of the Plane of the Ecliptic	4-12
4-7 Propulsion Requirements for Out-of-Ecliptic Probes	4-13
4-8 Payload for the Out-of-Ecliptic Mission	4-14
4-9 Heliocentric Transfer to Target Planet	4-16
4-10 Transit Time to the Outer Planets as a Function of Injection Energy	4-18
4-11 Variation of Payload With Transit Time to Encounter With the Planet Jupiter (1971 Type 1 Trajectory)	4-19
4-12 Variation of Payload with Transit Time to Encounter With the Planet Saturn (Direct Trajectory)	4-20
4-13 Variation of Payload with Transit Time to Encounter With the Planet Uranus (Direct Trajectory)	4-21
4-14 Variation of Payload with Transit Time to Encounter With the Planet Neptune (Direct Trajectory)	4-22
4-15 Low Thrust Orbit Transfer Trajectory	4-24
4-16 Orbital Transfer Velocity Requirements	4-25
A-1 Low-Thrust Penalty for Low-Thrust Escape from Elliptical Orbits	A-3
A-2 Low-Thrust Penalty for High-Thrust Escape from Parking Orbit	A-3

TABLES

	Page
2-1 Calculated Thickness of Interdiffusion Zone After 30 Days at Constant Temperature	2-13
2-2 Calculated Rh-30Ir/W-25Re Interdiffusion Zone Thickness after 320 Days for Capsule with Maximum Fuel Load	2-14
2-3 Calculated Lifetimes of 100-Mil RhIr Claddings in Air ...	2-18
2-4 Minimum Rh-30Ir Cladding Thickness to Resist Oxidation for 320 Days - Maximum Loaded Capsule Lying on the Ground	2-19
2-5 Minimum Rh-30Ir Cladding Thickness to Resist Oxidation and Interdiffusion for 320 Days - Maximum Loaded Capsule Lying on the Ground	2-19
2-6 Capsule O.D. Strain During 30-Day Mission After 30-Day Hold Period	2-21
2-7 I.D. Strain of 3.72 Kw Capsule After 30 Day Hold and 320 Days Within Thruster in Orbit	2-21
2-8 Capsule Creep Deformation for Thruster Containing 6.5 Kw at Time of Encapsulation	2-28
2-9 Number of Ideal Tantalum Shields to Obtain Various Thermal Efficiencies	2-36
2-10 Required Thickness of Outer Thruster Module	2-39
2-11 POODLE Thruster Power and Performance	2-48
2-12 POODLE Thruster Materials and Weights	2-49
3-1 Thruster Model Configuration for Hypersonic Spin Tests	3-3
3-2 Subsonic Model Test Summary	3-9 3-10 3-11
4-1 Detailed Breakdown of POODLE Stage Designs	4-3
4-2 Description of 7000 Pound Hydrogen-Fluorine High Energy Kick Stage	4-5

TABLES

	Page
4-3 Distance of Closest Approach to Sun for 500- and 1000-Pound Payloads	4-11
4-4 Orbital Parameters for the Outer Planets	4-15
4-5 Comparative Orbital Payload Capabilities	4-26
4-6 Mission Payloads (pounds) for Boost Vehicle Combinations	4-28

1. INTRODUCTION

Other volumes of this final report have treated special technologies underlying the thruster development program, viz., creep of refractory alloy capsule structures, behavior of oxidation-resistant noble-metal-alloy capsule claddings, efficiency of low-thrust nozzles, and simulation of radioisotope heat sources. In this volume, work relating more generally to the thruster system is reported. Findings on creep, claddings, and nozzles are applied in updating the thruster design; the study of thruster bodies with re-entry fins is summarized; and the performance of upper stages with POODLE thrusters is evaluated for several classes of missions.

In Section 2, the thruster design is refined by obtaining capsule temperature profiles as a function of time in the operating mode and in two particular abort modes, and relating these temperature histories to the creep strain and cladding degradation experienced. The total fuel inventory is distributed unequally among the three capsules to take advantage of propellant cooling effects in the operating mode. Calculated creep strain and required cladding thickness are then used in an iterative procedure to arrive at a final fuel distribution which maximizes thruster performance while maintaining capsule integrity for the environments considered.

In the previous program phase, the effectiveness of longitudinal fins in aiding the re-entry of POODLE thrusters was analyzed, experimental confirmation of the subsonic behavior of finned thrusters was obtained, and wind tunnel tests of the hypersonic behavior of subscale models was initiated. The hypersonic tests were finished during the program period covered by this report and results are given in Section 3, together with a fin-sizing analysis.

In Section 4, the utility of a POODLE upper stage is indicated for missions of potential interest to NASA. It will be noted, that the POODLE performance is based on design objectives, which should ultimately be realized, rather than on state-of-the-art characteristics as presented in the thruster design of Section 2. Thus, attention is confined to the specific impulse range from 750 to 800 seconds.

2. THRUSTER DESIGN

2.1 PURPOSE AND SCOPE

In this and previous phases of the POODLE program, considerable information has been generated on high-temperature materials and on other technologies critical to the design of a POODLE thruster, including data in the following specific areas:

- Creep of pressurized refractory-alloy capsules
- Oxidation of noble-metal alloy claddings
- Interdiffusion between substrate and cladding materials
- Efficiency of low-thrust nozzles
- Thermal performance of thruster systems
- Minimum-weight re-entry configurations

It was the purpose of the design analysis task presented herein to evaluate the information which has been accumulated, to apply it in updating the POODLE thruster configuration, and to indicate where additional information of a fundamental nature is needed.

The basis for selecting a thruster configuration, in original POODLE designs, was limited to meeting performance specifications in normal operation and to satisfying safety requirements in launch aborts and early re-entry from orbit. A systematic evaluation of safety in the variety of other possible situations was necessarily deferred because of level of effort limitations. In the program phase just completed, safety analyses were extended to cover two additional cases.

The first case was concerned with the effect of sustained periods in orbit prior to re-entry--periods in which degradation of coatings, claddings, and structural substrates must be minimized to insure their effectiveness in subsequent environments.

The second case was concerned with the post-impact mode in which capsules, with cladding intact, are separated from the thruster and lay exposed on the ground. In both cases, the temperature-time profile is of key importance, since it determines the rate at which

creep, interdiffusion, oxidation and corrosion proceed.

It is clear that a number of other cases also need to be analyzed, particularly the case of earth burial, with configurational variations to include capsules which are housed and not housed by the thruster body. In general, however, such analyses require empirical data not presently available and must be preceded by experimental testing.

Design approaches to exploit the axial temperature gradient due to propellant flow were investigated. Consideration was given to redistributing the fuel in unequal amounts among the three end-to-end cylindrical capsules so that the fuel inventory per capsule increased from hot to cold ends of the thruster. Without changing the external envelope occupied by the three capsules, consideration was also given to substituting a single capsule with an internally tapered wall, thickest at the hot end.

While a significant reduction in creep strain could be shown for an idealized tapered capsule (Reference 2-1), this approach was not pursued further because it required a fuel form which would not migrate in the presence of a temperature gradient, because the fabricability and impact survival of a single capsule were open to question, and because the advantages sought appeared to be achievable by using three unequally loaded capsules.

2.2 CAPSULE DESIGN ANALYSIS

2.2.1 Temperature Profiles

In order to determine the effects of creep, oxidation, and interdiffusion on capsule integrity, capsule temperatures for operational and abort situations were computed. Detailed temperature profiles were obtained using the TRW thermal analyzer digital computer program as described in Reference 2-1.

The computations were based on a total fuel loading of 5.81 kilowatts at time of encapsulation, with 3.72, 1.28, and 0.81 kilowatts in forward, middle, and aft capsules respectively. Temperature profiles were obtained for the operating condition 60 days after encapsulation (Figure 2-1). They were also obtained for aborts in

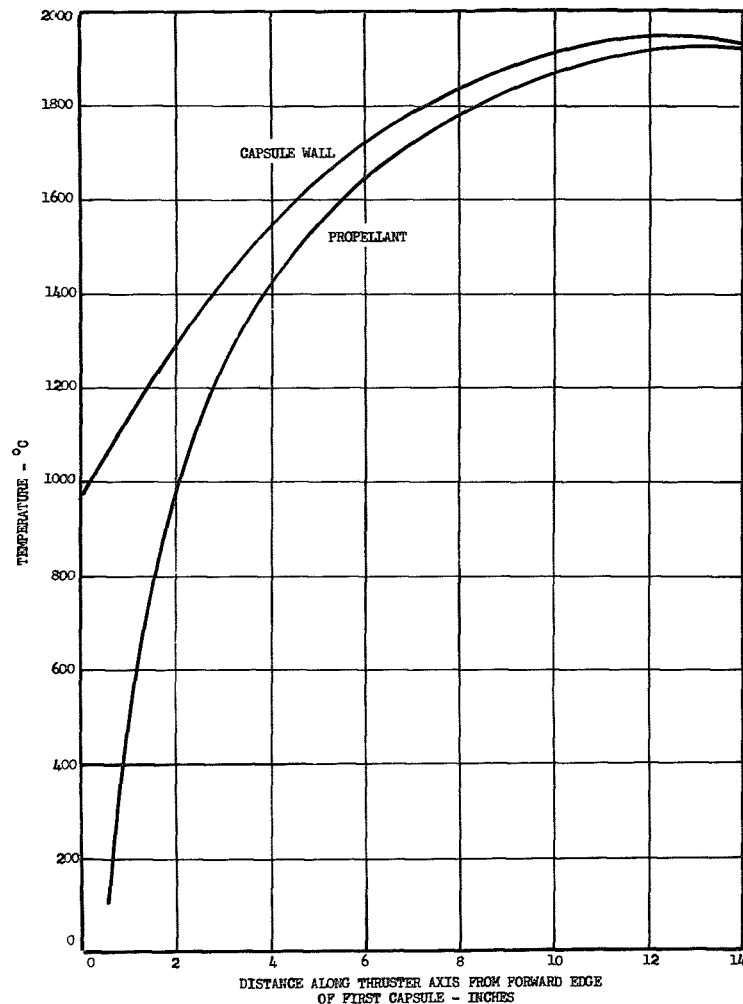


Figure 2-1. End of Mission Temperature Profile for Three Capsule Off-Loaded Thruster Configuration ($Q_{\text{Launch}} = 5.0 \text{ Kw}$)

space with insulation ejected at 30, 60, 180, and 320 days after encapsulation and with thruster surface emissivities of 0.7, 0.45, and 0.2 (Figures 2-2 through 2-4).

In all of the analyses, substrate-to-cladding and capsule-to-capsule heat transfer was assumed to occur by conduction. In order to minimize temperature drops if conductive bonds cannot be achieved, a high conductivity gas such as helium may be used between cladding and substrate. A preliminary estimate of the thermal expansion coefficient for the noble metal alloy used in the cladding indicates that it is about twice that of the W-25Re substrate. If a 1-mil gap is left between the cladding and capsule at low temperatures, the gap will grow to 5 mils at operating temperatures. Gaseous conduction across the 5-mil gap results in a 65°C temperature drop for the case of a capsule containing 3.72 Kw at time of encapsulation.

The configuration of the capsule without external cladding and internal liner is shown in Figure 2-5. This was selected as the baseline configuration for the design analysis. With three such capsules, equally loaded, creep strain during operation is most severe in the aft (hottest) capsule. The other two capsules experience less strain because they are cooler. If the fuel is redistributed in the manner suggested above, the strains can be more nearly equalized and a higher total inventory can be accommodated. The extent to which this "off-loading" may be carried is limited by abort rather than operating conditions, the abort temperature of the most heavily loaded capsule becoming critical.

As previously established for a nominal POODLE thruster (Reference 2-2), the total fuel inventory per thruster was taken to be 5.81 Kw at time of encapsulation (decaying to 5.0 Kw after a 30-day hold period) and the propellant exit gas temperature was assumed to be in the range $1925\text{--}1950^{\circ}\text{C}$. The assumed thermal efficiency was reduced from 95 to 90 percent, a value more consistent with the number of thermal insulation shields considered practicable.

Under the foregoing conditions, and with an initial distribution of isotope selected on the basis of preliminary creep analyses,

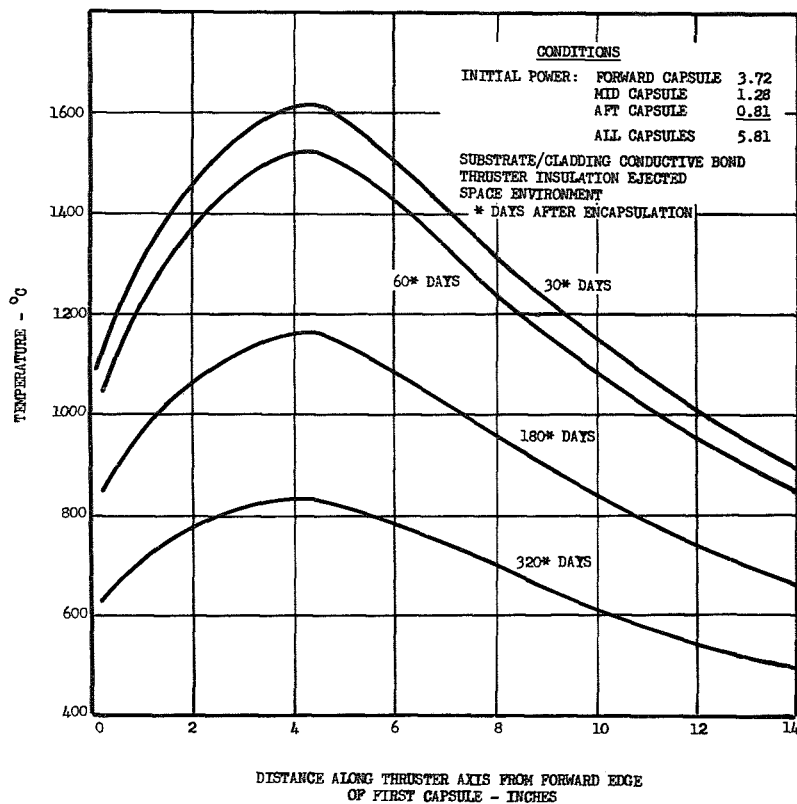


Figure 2-2. Capsule Temperature Profiles in Three Capsule Thruster-Emissivity = 0.7 ($Q_{\text{Launch}} = 5.0 \text{ Kw}$)

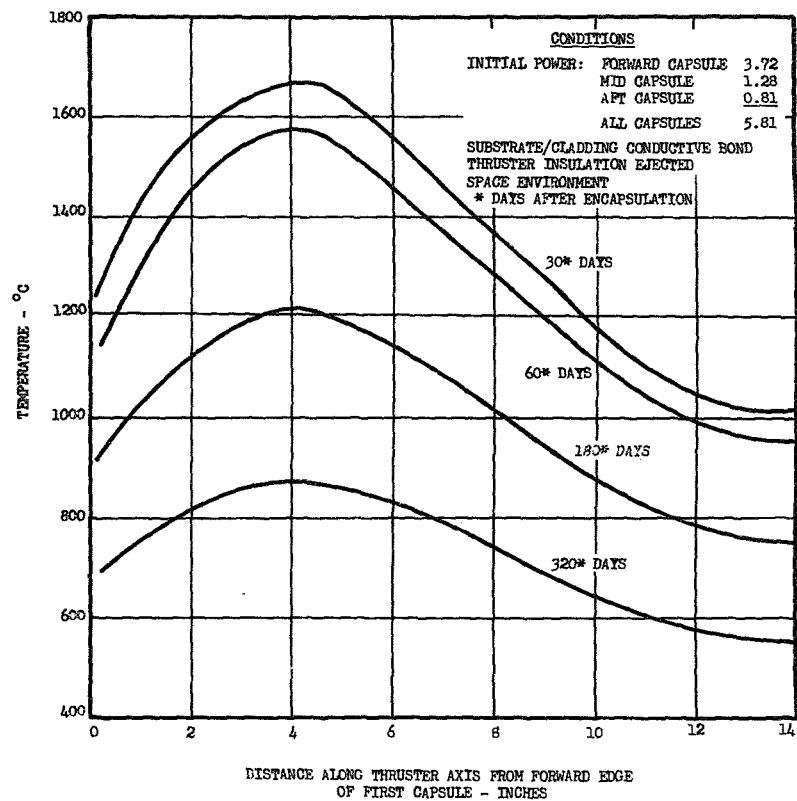


Figure 2-3. Capsule Temperature Profiles in Three Capsule Thruster - Emissivity = 0.45 ($Q_{\text{Launch}} = 5.0 \text{ Kw}$)

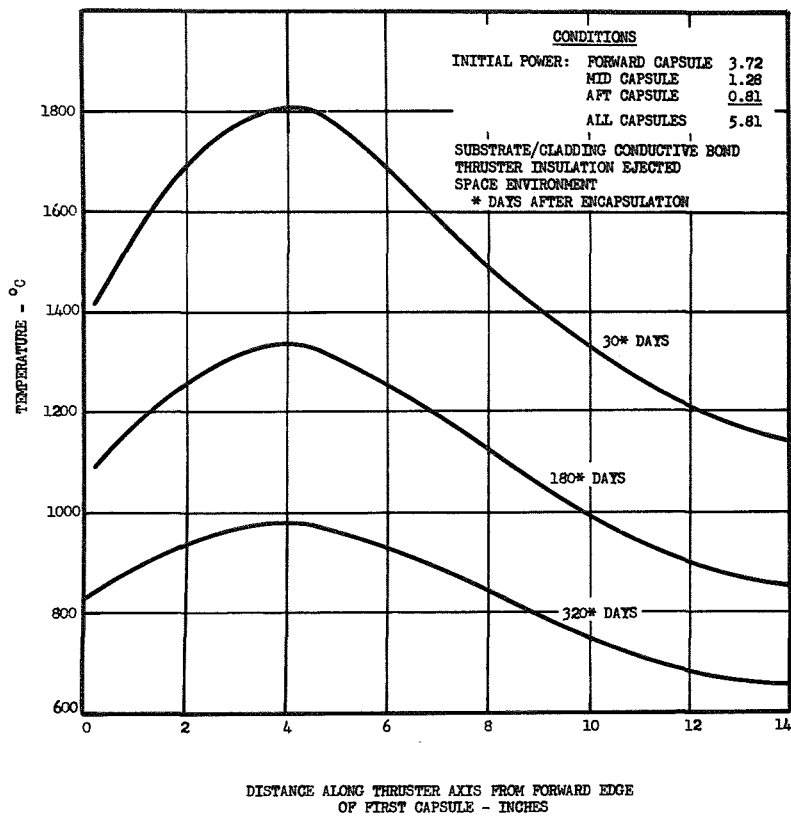


Figure 2-4. Capsule Temperature Profile in Three Capsule Thruster - Emissivity = 0.2 ($Q_{Launch} = 5.0 \text{ Kw}$)

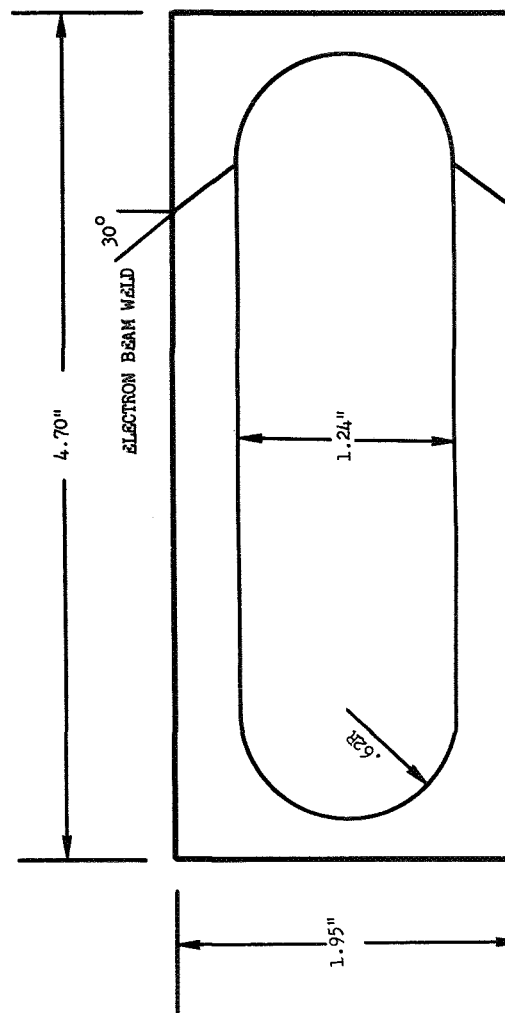


Figure 2-5. POODLE Capsule Configuration

temperature profiles were computed for operating and abort conditions. The computed temperature profiles were used to determine the required capsule cladding thickness and to compute the circumferential midplane capsule creep deformation. A new isotope distribution was then assumed and the calculations repeated. It was found that a total of 6.50 kilowatts could be loaded without exceeding 5 percent O.D. circumferential strain during normal operation and, in the abort situations considered, without exceeding temperatures which would lead to cladding or substrate failure in less than five years after encapsulation.

The peak temperature of the forward capsule, which bears the maximum fuel load, is approximately 1600°C during operation, as seen in Figure 2-1. The temperature of the same capsule as a function of time and thruster emissivity is shown in Figure 2-6 for an abort in space with insulation ejected. It is also shown in Figure 2-7 for the second abort situation considered--a single capsule lying on the ground with cladding intact. In this instance, heat transfer is by natural convection and radiation. Since no emissivity data were available for the Rh-Ir claddings, the temperature histories were computed parametrically for cladding emissivities ranging from the equivalent of platinum to an emissivity of 0.7.

2.2.2 Cladding Technology

The noble metal cladding acts as an oxidation barrier to protect the W-25Re capsule. However, the cladding itself is subject to degradation by oxidation and by interdiffusion of the cladding with the substrate. The rates of both processes are temperature dependent. Extrapolation of available data (Reference 2-3) indicates that below 1000°C cladding degradation due to these processes should be negligible for the time periods (5 years) and cladding thicknesses (100 mils) concerned. Therefore, for the abort situations considered in this analysis, only the degradation occurring prior to 320 days after encapsulation was considered. After that time the capsule temperature remains below 1000°C .

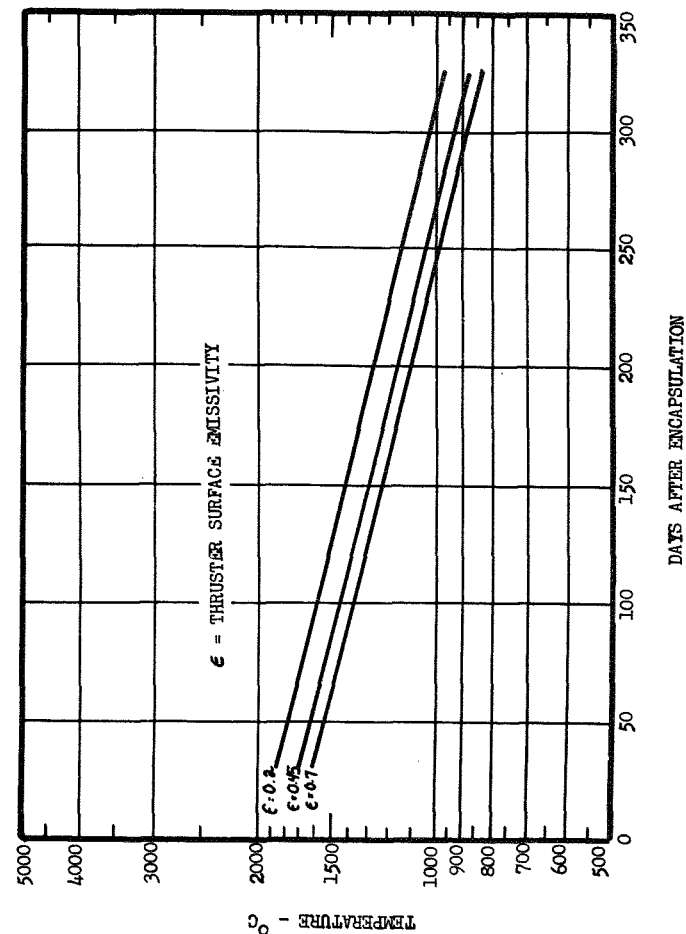


Figure 2-6. Peak Capsule Temperature While Within Thruster Radiating to Space (Initial Capsule Power = 3.72 Kw)

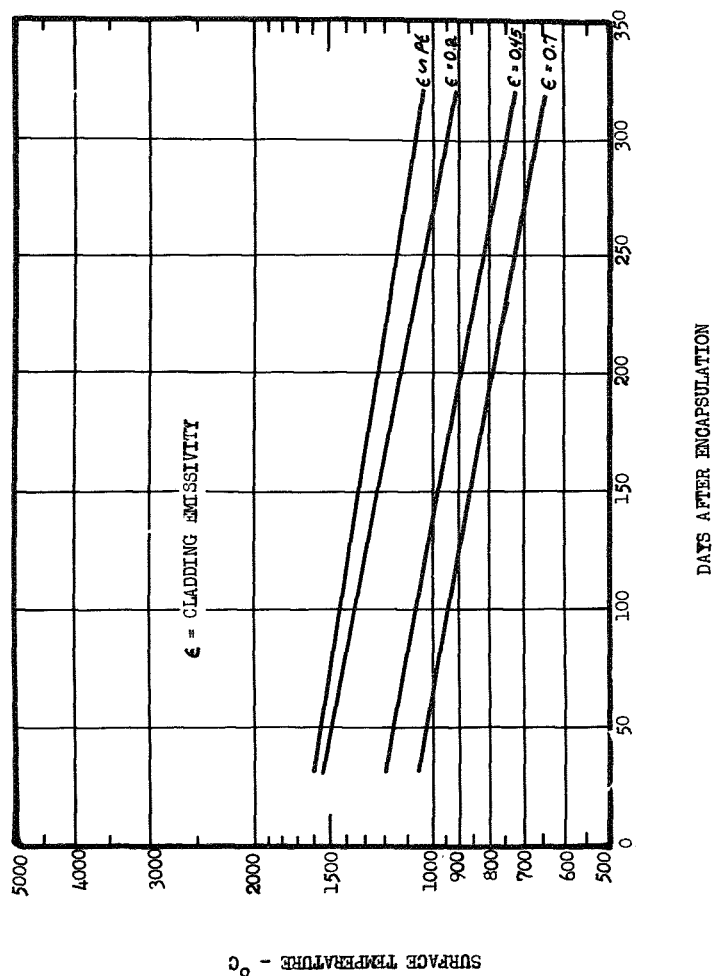


Figure 2-7. Temperature vs Time for Capsule Lying on the Ground
(Initial Capsule Power = 3.72 Kw)

In assessing the consequences of interdiffusion, it was assumed that no oxidation protection is afforded in the zone occupied by diffusion-modified material. The cladding thicknesses required were then estimated by summing the requirements for interdiffusion and oxidation. Experiments should be conducted to determine whether or not interdiffusion and oxidation, proceeding concurrently, will result in more rapid degradation of the cladding than accounted for in this manner.

The alloy selected for the cladding must have a solidus temperature well above the capsule operating temperature and must resist oxidation and diffusion well enough to protect the capsule without requiring excessive cladding thicknesses. In rhodium-iridium alloys, increasing the percentage of rhodium improves oxidation resistance but increases the extent of interdiffusion and lowers the solidus temperature. The composition finally selected (Rh-30a/o Ir) has a solidus temperature of 2140°C, 140°C above the maximum contemplated capsule operating temperature. The relatively high percentage of rhodium reflects the fact that resistance to oxidation is the most critical need.

2.2.2.1 Interdiffusion of W-25Re and Rh-30Ir Cladding

As reported in Reference 2-3, data on interdiffusion between noble metal claddings and the capsule substrate were obtained at temperatures of 1600°, 1800°, and 2000°C. Constant temperature data from short duration tests on thin samples indicated the growth rate of the interdiffusion zone to be parabolic. However, preliminary experiments with thicker samples indicate long duration tests are needed to resolve this question. The interdiffusion zone thicknesses shown in Table 2-1 for a 30 day operational mission were obtained by extrapolating 64-hour exposure data.

Table 2.1. Calculated Thickness of Interdiffusion Zone After 30 Days at Constant Temperature

Cladding	Substrate	Zone Thickness (Mils)		
		1600°C	1800°C	2000°C
Rhodium	W-25Re	7.9	15.0	*
Rh-10 Ir	W-25Re	6.5	15.0	*
Rh-30 Ir	W-25Re	3.9	12.2	29.5
Rh-50 Ir	W-25Re	3.4	5.3	16.0
Iridium	W-25Re	2.9	2.5	2.4

* Above solidus temperature for indicated cladding

In order to calculate the interdiffusion zone thickness for the case of a time-varying temperature, the constant temperature interdiffusion parabolic rate equation was modified. If the thickness of the diffusion zone at constant temperature is

$$X_c = X_o \sqrt{\frac{t}{t_o}} \quad (2-1)$$

then the rate of growth is

$$\dot{X}_c = \frac{1}{2} \sqrt{\frac{X_o}{t_o}} \sqrt{\frac{1}{t}} \quad (2-2)$$

Assuming the form of the growth rate equation to be unchanged, the diffusion zone thickness for a time-dependent temperature is

$$X_T = \frac{1}{2} \int_0^t \sqrt{\frac{X_o(t)}{t_o}} \sqrt{\frac{1}{t}} dt \quad (2-3)$$

where:

X_o = thickness of diffusion-modified material measured at time t_o (constant temperature)

$X_o(t)$ = the value of X_o corresponding to the temperature of the cladding at time t .

Experimental values of X_o at four hours for 1600°, 1800°, and 2000°C fell on a straight line when plotted on semi-log paper as a function of $1/t$ and were extrapolated to lower temperatures (Figure 2.8). Using the temperature histories shown in Figures 2-6 and 2-7, diffusion zone thicknesses for the capsule with maximum fuel were calculated after 320 days in each of the two abort situations. Results are shown in Table 2-2. Approximately 60 percent of the interdiffusion zone thickness is formed within the first 15 days. Use of the parabolic rate and four-hour values of X_o is conservative.

Table 2.2. Calculated Rh-30Ir/W-25Re Interdiffusion Zone Thickness after 320 Days for Capsule With Maximum Fuel Load

Thruster Surface Emissivity	Diffusion Zone Thickness (Inches)	
	Abort in Space	Capsule on Ground
0.7	0.017	0.001
0.45	0.028	0.002
0.2	0.050	0.009
Platinum *	-	0.015

* Temperature dependent

2.2.2.2 Oxidation of Rh-Ir Claddings

In the event of an abort which returns the thruster to earth, the noble-metal-clad capsule will be exposed to an oxidizing environment. The Rh-30Ir cladding is degraded primarily by oxidation of the iridium. The useful lifetime of the cladding was estimated by two different methods as follows:

1. The iridium was assumed to be removed continuously by oxidation at the surface at an average rate determined from experimental measurements of weight loss in a fixed initial period of time. In this case, end-of-life was assumed to occur upon total depletion of iridium.

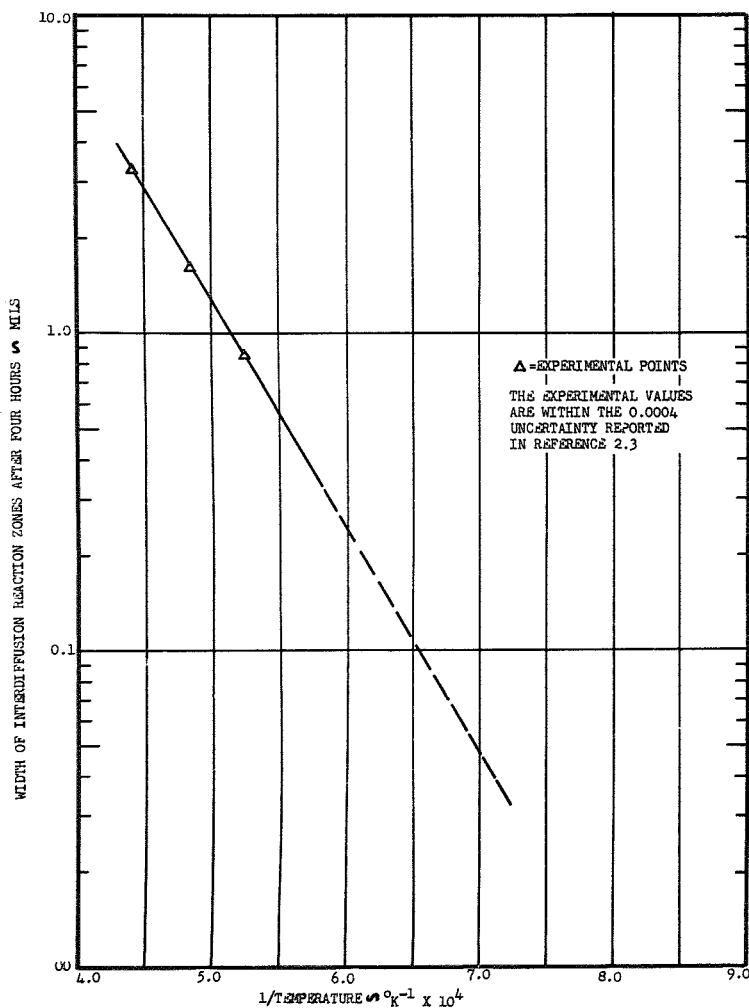


Figure 2-8. Correlation of Measured Interdiffusion Zone Thickness from Reference 2-3

2. An internal concentration gradient of iridium, established by its oxidation and removal at the surface, leads to diffusion of iridium toward the surface along grain boundaries. This results in the formation of an internal porosity layer. The short-time depth of penetration of the porosity zone, observed experimentally, was linearly extrapolated to longer times. When the penetration depth equalled the cladding thickness, useful lifetime was assumed to be terminated. There was some indication that the porosity layer penetration actually proceeds at a lower rate than derived by this linear extrapolation.

Lifetimes calculated as above for a 100-mil cladding are tabulated in Table 2-3 for several temperatures. Actual lifetimes are believed to lie between the extremes shown. However, long-duration data on thick samples must be obtained before firm conclusions can be drawn.

The arithmetic average of the lifetimes obtained by the two methods was used to estimate cladding thicknesses required for oxidation protection of POODLE capsules. The average lifetimes were converted to rates of penetration which, when plotted on semi-log paper as a function of $1/T$, resulted in a straight line (Figure 2-9). The penetration rates were then extrapolated to higher temperatures. The required cladding thicknesses were calculated by graphical integration of the following equation:

$$X = \int_0^t \dot{X}(t) dt \quad (2-4)$$

where:

- X = minimum cladding thickness required
 $\dot{X}(t)$ = oxidation penetration rate for temperature at time t

The temperature histories shown in Figure 2-7 for the maximum loaded capsule were used with the $1/T$ correlation of the penetration rates to obtain $\dot{X}(t)$. The calculated Rh-30Ir cladding thicknesses for the maximum loaded capsule are shown in Table 2-4. The importance of surface emissivity in determining cladding thickness can be seen. It should be noted that a minimum cladding thickness of approximately 50 mils will probably be necessary to assure cladding integrity under impact conditions.

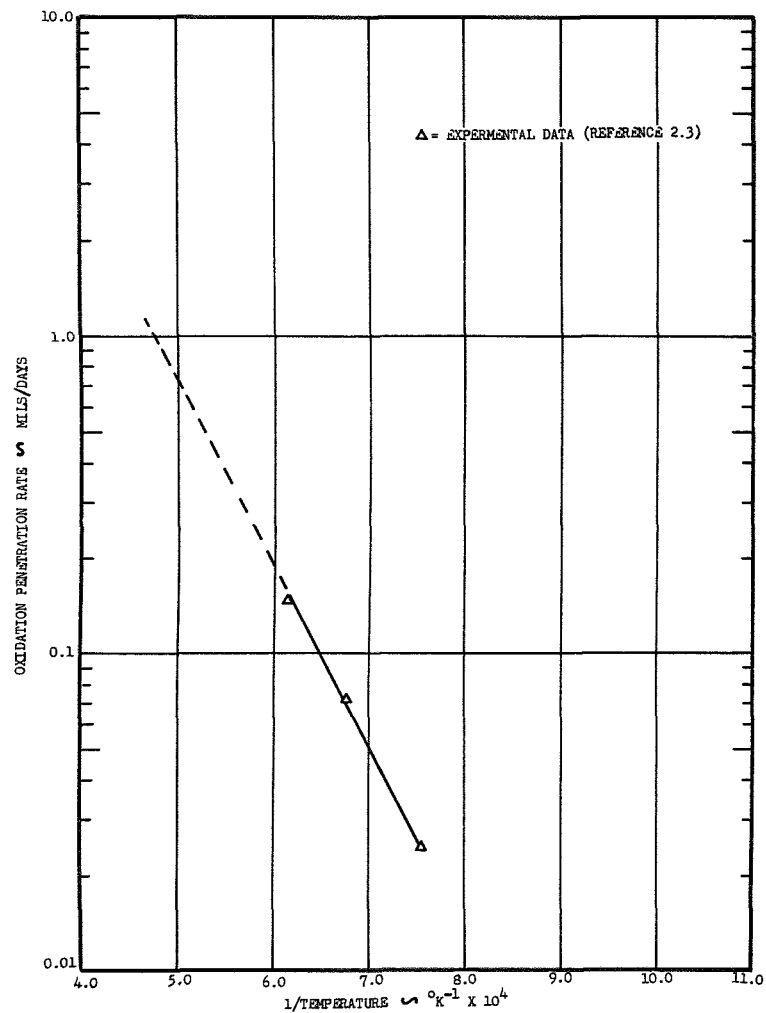


Figure 2-9. Correlation of Oxidation Penetration Rate Based on Experimental Data in Reference 2-3

Table 2-3. Calculated Lifetimes of 100-Mil RhIr Claddings in Air

Assumption *	Cladding Material	Lifetime (days)		
		1050°C	1200°C	1350°C
1.	Rh-10Ir	7,200	2,430	1,215
	Rh-30Ir	7,200	2,420	1,210
	Rh-50Ir	3,600	1,200	600
2.	Rh-10Ir	2,280	750	356
	Rh-30Ir	1,080	365	180
	Rh-50Ir	331	110	56

* See Text

Note: Gravimetric reaction rates vary with air flow and air temperature. The rates used were the highest observed as air flow rate (and therefore air temperature) was varied in the tubular experimental configuration described in Reference 2.3.

Table 2-4. Minimum Rh-30Ir Cladding Thickness to Resist Oxidation for 320 Days - Maximum Loaded Capsule Lying on the Ground

Cladding Emissivity	Cladding Thickness - Inches
Pt	.044
0.2	.035
0.45	.006
0.7	.002

2.2.2.3 Conclusions

Table 2-5 shows the cladding thickness required to resist interdiffusion from the inside as well as oxidation from the outside. This total thickness was obtained by summing the thicknesses required for each effect alone.

Table 2-5. Minimum Rh-30Ir Cladding Thickness to Resist Oxidation and Interdiffusion for 320 Days - Maximum Loaded Capsule Lying on the Ground

Cladding Emissivity	Cladding Thickness Required - Inches		
	Interdiffusion	Oxidation	Total
Pt	.015	.044	.059
0.2	.009	.035	.044
0.45	.002	.006	.008
0.7	.001	.002	.003

Time in orbit prior to re-entry was considered in estimating the required cladding thickness. Because the heat source is decaying, increasing the time in orbit lowers the temperature at which subsequent oxidation occurs. On the other hand, interdiffusion will be more extensive because capsule temperature is higher in orbit than on the ground. As a result, there is an orbital residence time which requires maximum cladding thickness. For a thruster surface emissivity of 0.45 (minimum required for reentry) and for the parabolic rate of interdiffusion assumed, this time is approximately 60 days. The

corresponding maximum increase in cladding thickness is 10 mils. Referring to Table 2-5 and assuming a capsule emissivity equivalent to that of platinum, the required cladding thickness becomes 0.69 inch. A 100-mil cladding is actually specified, giving a safety factor of almost 1.5.

2.2.3 Creep Analysis

The circumferential creep strain at the capsule midplane was calculated using plane strain theory (Reference 2-1). In order to calculate strain when both temperature and stress vary with time, the constant-temperature, constant-stress correlation was modified as follows:

$$\epsilon_c = A\sigma^n t^m \quad (2-5)$$

$$\dot{\epsilon}_c = mA\sigma^n t^{m-1} \quad (2-6)$$

ϵ_c = strain for a constant-temperature constant-stress condition

σ = stress in the capsule wall

t = time

A, m, n = constants derived from uniaxial creep data obtained at fixed temperature and stress

Assuming that a differential equation of the same form as equation 2-6 applies when stress and temperature are variables,

$$\epsilon_T = m \int_0^t A(t)\sigma^n(t)t^{m-1}dt \quad (2-7)$$

where:

ϵ_T = strain for time-varying temperature and stress

$A(t)$ = value of empirical constant corresponding to the temperature of the capsule at time t .

$\sigma(t)$ = stress in the capsule wall corresponding to internal pressure in the capsule at time t

A least squares fit was applied to the available uniaxial creep data for W-25Re with only A assumed to be temperature dependent. The results were $n = 3.61$ and $m = 1.06$. The temperature dependence of A is shown in Figure 2-10. Calculated O.D. strains for the capsules during a 30-day mission beginning 30 days after encapsulation are shown in Table 2-6.

Table 2-6. Capsule O.D. Strain During 30-Day Mission After 30-Day Hold Period

Capsule	Isotope Loading at Encapsulation	Peak Temperature (°C)	O.D. Strain (%)
Forward	3.72	1600	Negligible
Middle	1.28	1860	1.0
Aft	0.81	1960	2.0

The I.D. strain in 320 days for the capsule with maximum load during an abort in space was computed using the temperature history shown in Figure 2-6 and the pressure history shown in Figure 2-11. The results are shown in Table 2-7 for various thruster surface emissivities.

Table 2-7. I.D. Strain of 3.72 Kw Capsule After 30 Day Hold and 320 Days Within Thruster in Orbit

Thruster Surface Emissivity	I.D. Strain (%)
0.2	100
0.45	8
0.7	2

The I.D. strain experienced by the capsule with maximum load when lying on the ground with cladding intact was calculated to be less than 2% for the worst case considered--a cladding emissivity equivalent to that of platinum.

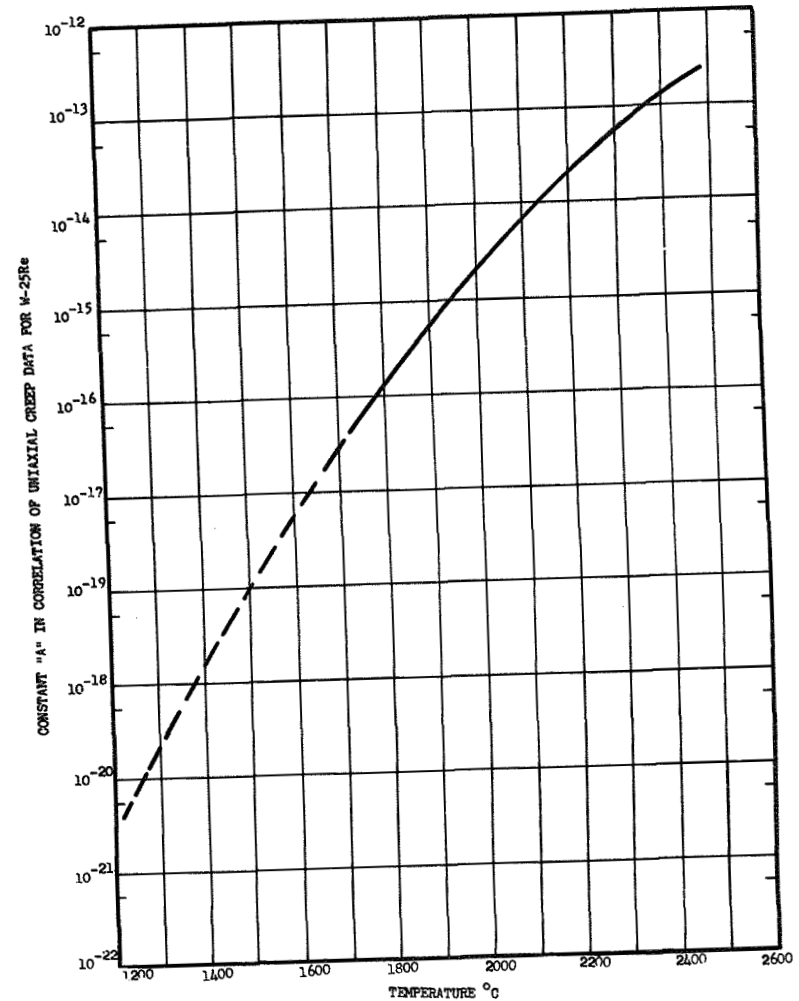


Figure 2-10. Parameter "A" in Correlation of Uniaxial Creep Data for W-25Re

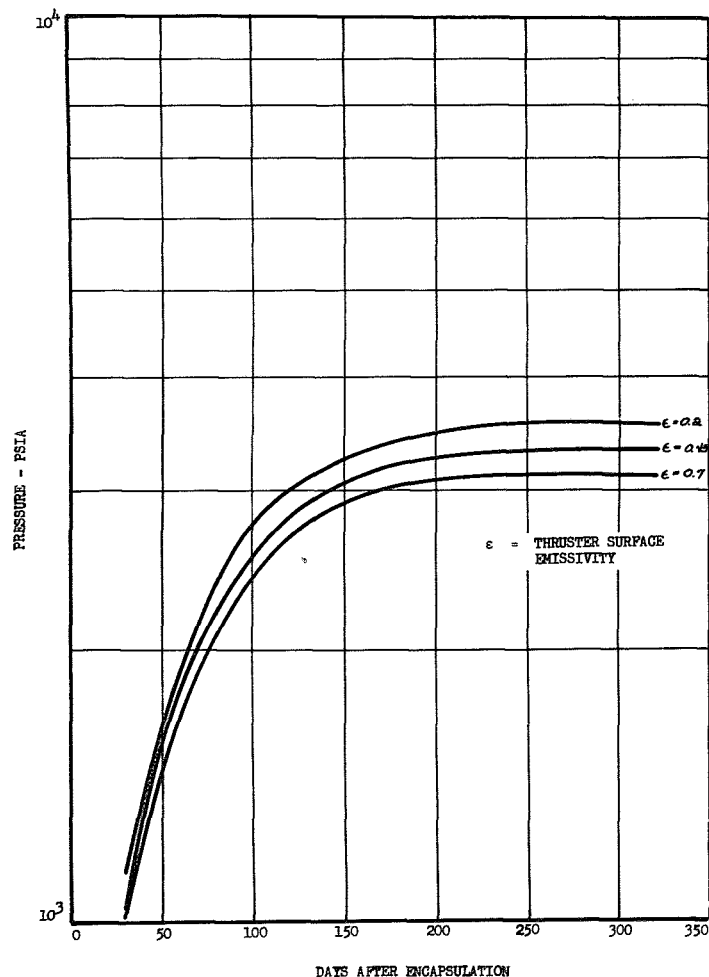


Figure 2-11. Pressure in Maximum Loaded Capsule While Within 5.0 Kw at Launch Thruster

In order to assure intact re-entry of a POODLE thruster in the event of a mission abort, the emissivity of the oxidation-resistant coating on the thruster must be maintained at a high value. Re-entry heating analyses indicate that the temperature of the thruster module will reach approximately 2000°C when the thruster surface emissivity is 0.7 (Reference 2-4). These temperatures increase to 1840°C and 2270°C when the emissivity is reduced to 0.45. Since coating integrity is open to question at 2270°C , a thruster surface emissivity exceeding 0.45 must be maintained for re-entry survival considerations alone. With the allowable emissivity thus bounded, creep deformation in the capsule with maximum load should not exceed 8 percent while in orbit.

The total creep strain at rupture is a function of temperature. W-25Re uniaxial data (Reference 2-5) shows the maximum to exceed 100 percent and to occur at 1850°C . At 1600°C the creep strain at rupture is approximately 80 percent. Although no data are presently available for W-25Re at very low temperatures, it is believed that a circumferential strain of 10-20 percent can be tolerated at abort temperatures encountered without risk of rupture.

2.2.4 Final Capsule Isotope Loadings

Based upon results for a thruster containing a total of 5.81 Kw of isotope at the time of encapsulation distributed among the three capsules as previously indicated, it was concluded that the fuel inventory could be increased in the middle and aft capsules but not in the forward capsule. Accordingly, additional computer analyses were completed for a thruster containing 3.72, 1.78, and 1.0 Kw at time of encapsulation in the forward, middle and aft capsules respectively. This corresponds to a thruster with 5.6 Kw rather than 5.0 Kw at time of launch (30 days after encapsulation). The propellant flow rate was increased to hold the exit gas temperature in the $1925\text{-}1950^{\circ}\text{C}$ range. Addition of a 100-mil cladding to the nominal capsule configuration results in a small increase in thruster O.D. and length. However, it was not necessary to change the basic thermal network described in reference 2-1. The operational temperature profile is shown in Figure 2-12 and the abort-in-orbit temperature profiles are shown in Figures 2-13 and 2-14. Peak temperature of the forward capsule is

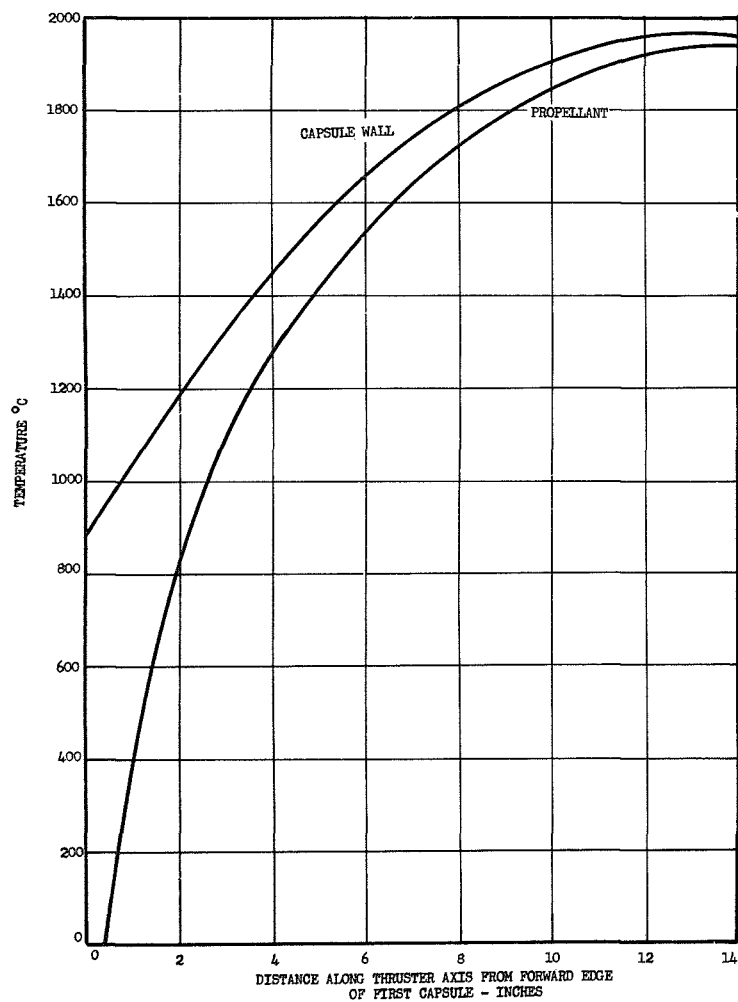


Figure 2-12. Temperature Profile During Propellant Flow for Three Capsule Off-Loaded Thruster Configuration ($Q_{Launch} = 5.6 \text{ Kw}$)

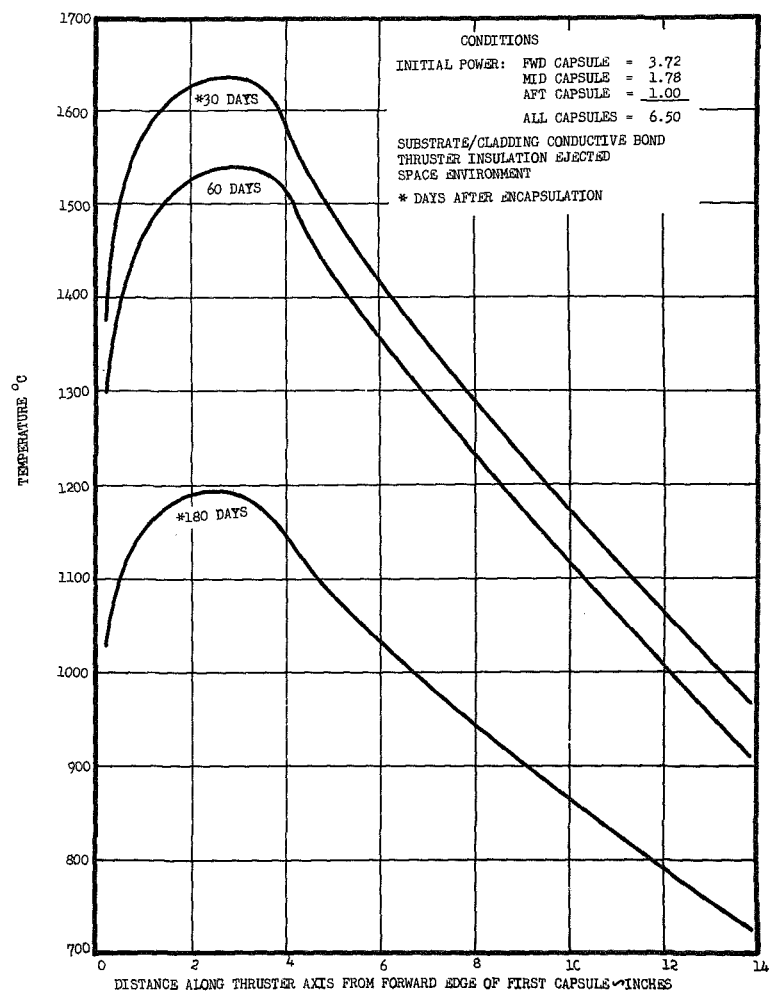


Figure 2-13. Capsule Temperature Profile in Three Capsule Thruster - Emissivity = 0.70 ($Q_{Launch} = 5.6 \text{ Kw}$)

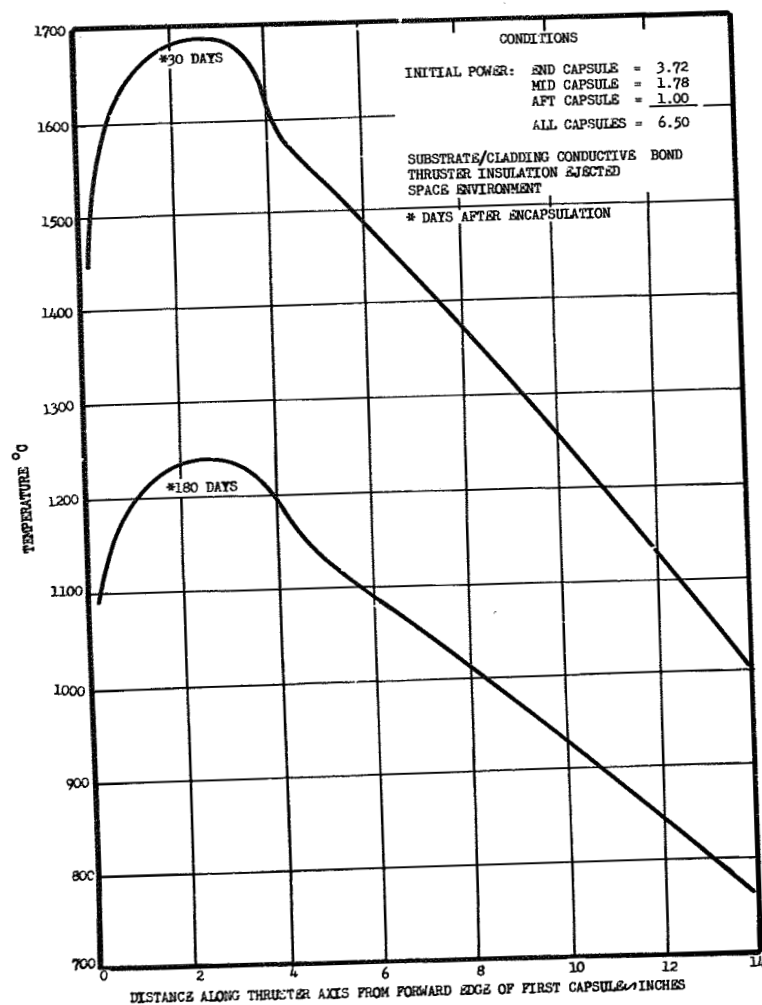


Figure 2-14. Capsule Temperature Profiles in Three Capsule Thruster - Emissivity = 0.45 ($Q_{Launch} = 5.6$ Kw)

plotted in Figure 2-15 as a function of time, with different thruster surface emissivities for the case of an abort in orbit. The calculated creep deformation of the capsules during operation and during an abort in orbit are shown in Table 2-8.

Table 2-8 Capsule Creep Deformation for Thruster Containing 6.5 Kw at Time of Encapsulation

Capsule	Isotope Loading	O.D. Strain During 30 Days Operation	* I.D. Strain After 320 Days in Orbit
Forward	3.72	Negligible	15%
Middle	1.78	4%	Negligible
Aft	1.0	3%	Negligible

* Thruster Surface Emissivity = 0.45

The peak temperature of the forward capsule in a thruster containing 6.5 Kw at time of encapsulation is 40°C higher than in the case of a thruster containing 5.81 Kw at time of encapsulation. The 40°C rise in temperature doubles the creep deformation calculated for an abort in orbit. This extreme sensitivity of creep to temperature must be carefully considered in establishing final design safety margins.

During operation of the thruster (6.5 Kw initial loading) the peak wall temperature on the aft capsule is 150°C below the solidus temperature of the Rh-30Ir cladding (Figure 2-12). Adding fuel to any of the capsules, while increasing propellant flow rate and holding propellant exit temperature constant in order to achieve greater thrust, would drive the cladding temperature higher. Since it is desirable to maintain the 150°C margin between operating and solidus temperatures, the indicated fuel loading represents an upper limit. Thus, at encapsulation, the maximum loading and distribution of isotope for the configuration and abort environments investigated is as follows:

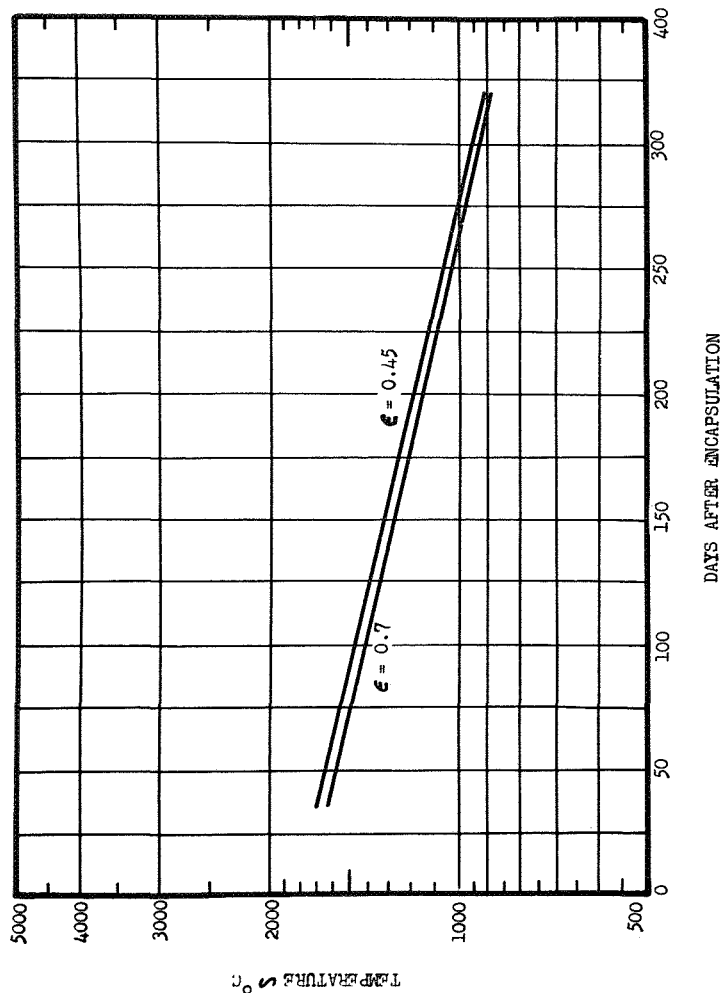


Figure 2-15. Peak Capsule Temperature While Within 5.6 Kw Thruster Radiating to Space ($Q_0 = 3.72 \text{ Kw}$)

Forward Capsule	3.72
Middle Capsule	1.78
Aft Capsule	<u>1.0</u>
All Capsules	6.5 Kw

Loading in the forward capsule is limited by the cladding thickness required to survive the ground abort situation. Loading in the middle and aft capsules is limited by the requirement to hold cladding temperatures 150°C below the solidus temperature.

2.3 THRUSTER DESIGN ANALYSIS

2.3.1 Insulation and Thermal Performance

2.3.1.1 Insulation Design Considerations

The thermal insulation for POODLE must be capable of operation at temperatures up to 2000°C . Radiation shielding fabricated from refractory metal foils is the only type of insulation which can presently be used at these high temperatures. Of the refractory metals, only tungsten and tantalum have sufficiently low vapor pressures to permit operation at 2000°C in vacuum without excessive sublimation during a 30-day mission.

Tantalum is advantageous because its emissivity and density are lower than that of tungsten, but it is very active chemically. The reactions of tantalum with oxygen, nitrogen, and hydrogen were reviewed to determine if degradation or embrittlement of the foils will occur during normal launch and operating conditions. As long as the temperature of the tantalum foils is maintained below 100°C , reactions with O_2 and N_2 should not be important. On the launch pad, sufficient cooling water will have to be supplied to insure that the temperature of the foils does not exceed this limit. For short time periods (30 minutes), the temperature of the foils may increase to approximately 400°C with a one-atmosphere partial pressure of either O_2 or N_2 . Thus, during ascent, with O_2 and N_2 pressures decreasing very rapidly, no degradation of the tantalum should occur.

Tantalum undergoes significant hydriding at temperatures up to 1000°C . Above this temperature the hydrogen solubility in the

metallic lattice is greatly reduced. During thruster operation, the temperature of the forward end of the thruster (H_2 inlet) will be less than 1000°C . Small quantities of H_2 could be present in the insulation due to diffusion or very small leaks in the propellant flow channels. Calculations indicate that a hydrogen partial pressure of 0.01 atmosphere at temperatures below 1000°C is required for significant hydriding to occur (reference 2-6). If the insulation is designed to insure that H_2 gas is exhausted to space, holding its pressure well below 0.01 atmospheres, hydriding of the tantalum foils should not be a problem. Thus, tantalum foils can be considered for use in the POODLE thermal insulation system.

Computer analyses were performed to determine the effective thermal conductance of both tantalum and tungsten foil systems assuming only radiative heat transfer between adjacent cylindrical foils (reference 2-7). The analyses included multiple reflections and temperature dependent emissivities. The calculated thermal conductances as a function of temperature are shown in Figure 2-16. It is seen that the insulation effectiveness of the tantalum system is approximately three times that of tungsten, i.e., a tantalum system will require only one-third the number of shields that a tungsten system requires in order to obtain the same insulation effectiveness.

In practice, however, conductive heat transfer occurs between adjacent foils, since they can never be completely separated. As a result, heat losses are higher than predicted on the basis of pure radiative heat transfer. Conduction can be reduced by minimizing the contact area between adjacent foils or by using a low thermal conductivity spacer between foils. Radiation shielding for operation at 2000°C has been demonstrated during the heater development task (reference 2-8) using 5-mil thick tungsten foils, but much thinner foils will be required for a flight thruster if the weight of the insulation is not to be excessive.

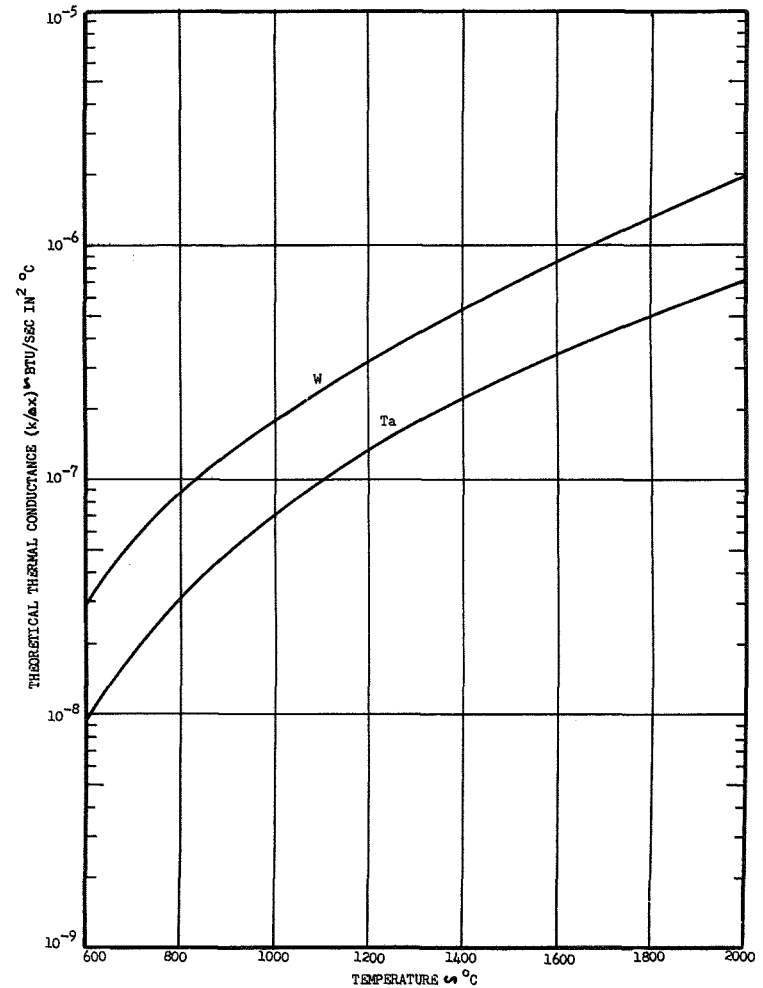


Figure 2-16. Theoretical Thermal Conductance for 46 Tantalum and Tungsten Shields

2.3.1.2 Thermal Performance

Thruster design calculations performed in previous phases of the POODLE Program have been made assuming a thermal efficiency of 95 percent. Since the thermal insulation may represent a major fraction of the total thruster weight, the effect of the amount of insulation on the thruster thermal efficiency was investigated. Thermal analyses were completed for POODLE thrusters employing different effective insulation thicknesses to obtain thermal efficiencies in the 80 to 95 percent range, while maintaining the propellant exit gas temperature between 1925°C and 1950°C. The analyses were conducted for a thruster with 4.3 Kw of isotope, corresponding to conditions at the end of a 30-day mission following a 30-day hold for a thruster originally loaded with 5.81 Kw at the time of encapsulation. The end of mission conditions were used because the thermal efficiency decreases as the isotope power level decays. The three-capsule off-loaded configuration analyzed contained 2.75 Kw, 0.95 Kw and 0.6 Kw in forward, middle and aft capsules respectively. The capsule-to-capsule axial heat transfer was assumed to be by conduction. Similar analyses were also conducted for a thruster at the same power level (4.3 Kw) using a single capsule loaded uniformly in the axial direction and having an inner wall which tapers in that direction. The overall thruster dimensions were the same for both configurations and the tapered single capsule occupied the same volume as the three capsules. The resulting capsule wall temperature profiles are shown in Figures 2-17 and 2-18.

Reducing thruster thermal efficiency results in an increase in capsule wall temperatures. For the case of the three-capsule thruster, the temperature of the middle capsule increases 110°C when the thermal efficiency changes from 93 to 82 percent. This temperature increase would significantly reduce the quantity of isotope which could be contained in the capsule, since creep is very strongly temperature-dependent. The temperature of the capsule wall increases only 30° - 40°C when the thermal

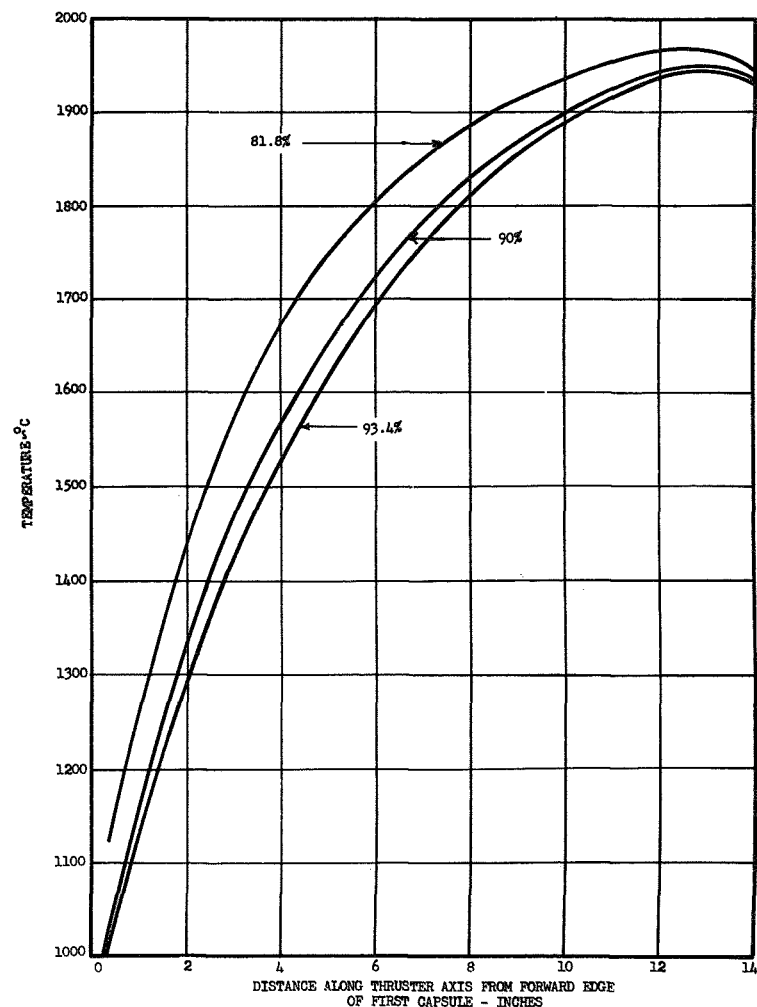


Figure 2-17. Capsule Wall Temperature Profile (Off-Loaded Three Capsule Thruster Configuration) for Various Thermal Efficiencies

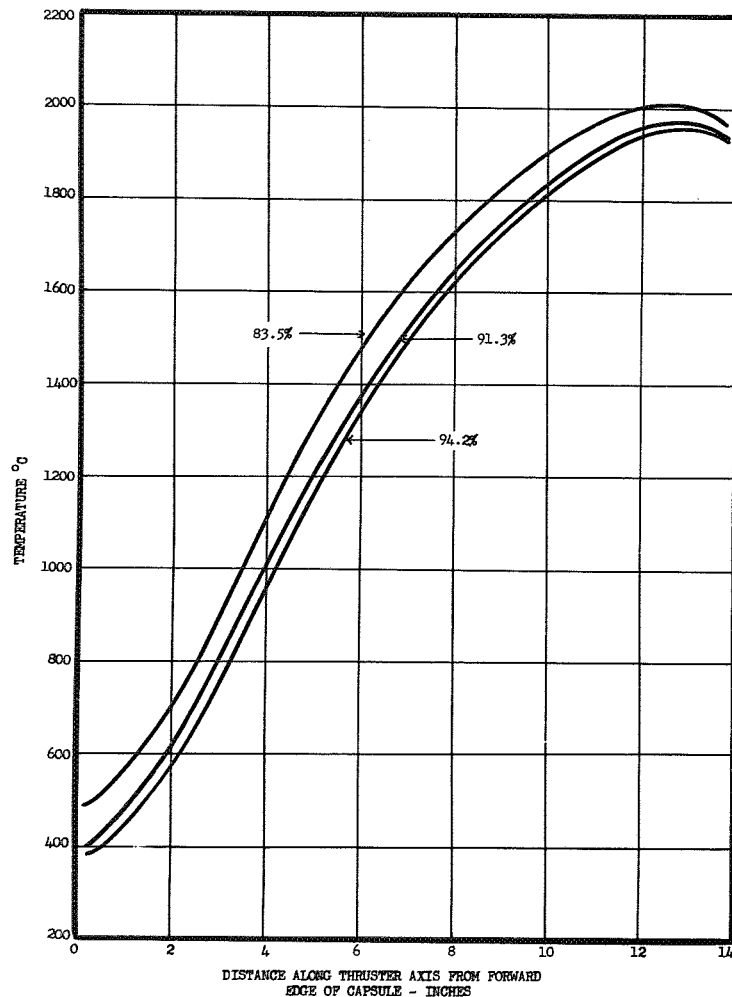


Figure 2-18. Capsule Wall Temperature Profile (Tapered Capsule Thruster Configuration) for Various Thermal Efficiencies

efficiency falls to 90 percent.

The relative insulation effectiveness, defined as the ratio of the number of insulation shields required to achieve a given thermal efficiency divided by the number of insulation shields required to achieve a thermal efficiency of 95 percent, was computed and is shown in Figure 2-19. It is seen that the data for the thruster containing three off-loaded capsules and the thruster containing a single uniformly loaded tapered capsule are correlated by a single curve. The thruster thermal efficiency as a function of thermal insulation requirements in the range cited is apparently independent of the isotope distribution for a fixed total fuel inventory. The number of ideal tantalum shields (assuming only radiative heat transfer between adjacent shields) for the thruster containing three capsules at various efficiencies is shown in Table 2-9.

Table 2-9 Number of Ideal Tantalum Shields to Obtain Various Thermal Efficiencies

Thermal Efficiency %	Number of Shields Required
85	18
90	32
95	78

A thermal efficiency of 90 percent was selected for the design analyses presented herein. This efficiency allows a major reduction in the number of shields required, while producing only a nominal increase in capsule wall temperature. The total number of radiation shields which will be required to achieve it in an actual thruster must be determined experimentally. However, in order to obtain an estimate of the weight of the insulation, the insulation effectiveness was assumed to be one-half the ideal effectiveness computed with only radiative heat transfer between adjacent foils. On the basis of this assumption, the required number of shields was 64.

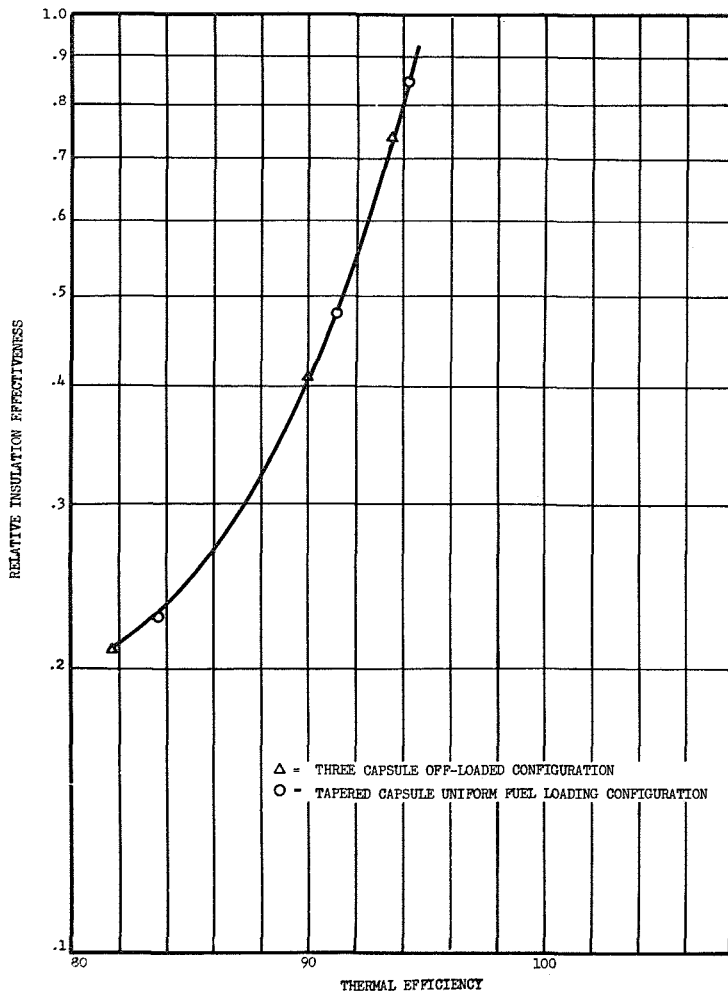


Figure 2-19. Relative Insulation Effectiveness Required To Achieve Given Thermal Efficiency

2.3.2 Mechanical Design Considerations

A preliminary structural analysis was conducted to determine the required thickness of the flow module and the outer thruster module. The flow module is a cylindrical shell concentric with the three cylindrical capsules forming the channel through which the hydrogen propellant passes. The flow module is separated from the capsules by a .050-inch diameter wire which acts as a helical flow guide. The re-entry aids are attached to the outer thruster module.

2.3.2.1 Flow Module

The flow module, fabricated from W-25Re, is subject to internal pressure due to hydrogen flow during operation and external pressure resulting from cooling water flow prior to launch. The hydrogen pressure was assumed to be 15 psi applied at a temperature of 2000°C over a 30-day operating period. For a 0.020-inch module wall thickness, the stress is 850 psi. The creep rupture strength of W-25Re for 30 days at 2000°C is approximately 1200 psi. Hence, the use of a 0.020-inch wall thickness results in a stress on the flow module equal to 70 percent of the rupture stress. This will produce about 5 percent deformation. The external cooling water pressure produces a compressive stress in the flow module. For a 0.020-inch module wall thickness the water pressure can be 200 psi at a temperature of 540°C before buckling will occur. It should be noted that axial and circumferential thermal expansion characteristics require more study in conjunction with the detailed design of the module and other components which interface with it.

2.3.2.2 Outer Thruster Module

Fins attached to the outer thruster module cause it to spin about its longitudinal axis during re-entry. Significant aerodynamic heating accompanied by high surface temperatures occur over the 5- to 10-minute re-entry period. The peak temperature of the outer thruster module was estimated to be 1650°C (Reference 2-4). Hence, the outer thruster module must be able to survive the forces resulting from the spinning motion and the aerodynamic pressure while at peak

temperature. The thickness required for the outer thruster module was computed based on the following assumptions:

1. 2.92-inch thruster diameter
2. 4 psi aerodynamic pressure loading
3. 3000 rpm rotational velocity
4. 1650°C maximum temperature at fin root and outer thruster module
5. 0.5-inch O.D. tube with 0.030-inch wall used for fin bead
6. Fin-tip thickness one-half fin-root thickness

The maximum allowable stress was taken as the creep rupture stress corresponding to a 20 minute loading at 1650°C. The allowable stresses were estimated to be 16,000 psi for Ta-10W (Reference 2-9) and 30,000 psi for W-25Re (Reference 2-1).

A typical section consisting of the outer shell with four fins and the associated beads was analyzed. The forces resulting from the rotational motion and from the aerodynamic pressure were applied to a unit length of this section. The internal forces in the fin were determined by treating it as a cantilevered beam subjected to the external forces mentioned above. The tensile and bending stresses were then evaluated by conventional means. Forces existing at the root of each fin were applied to the shell which was then treated as a ring for evaluating the radial forces, bending moments, and the resulting stresses. Table 2-10 presents the required thickness for the outer thruster module for both Ta-10W and W-25Re.

Table 2-10. Required Thickness of Outer Thruster Module

Fin Span, Inches	W-25Re Module Thickness - Inches	Ta-10W Module Thickness - Inches
1.00	0.040	0.055
2.25	0.065	0.085
3.50	0.105	0.140

Additional calculations were completed to determine the effect of thruster diameter on the required module thickness. In addition, the effect of a two-fin re-entry aid configuration on the thruster module thickness was determined. A 10 percent increase in thruster diameter required only a 5 percent increase in module thickness. For the case of a two-fin re-entry aid, the thruster module thickness is increased approximately 30 percent due to the higher moment coefficient associated with the two-position radial load compared to the four position radial load for the four-fin design (Reference 2-10).

W-25Re was selected for the outer thruster module since the reduction in the required wall thickness when compared to the wall thickness required using Ta-10W more than compensates for the increased density of the W-25Re.

2.3.3 Re-entry Considerations

The POODLE thruster is designed to survive intact in the event of re-entry from earth orbit. Re-entry fins are used to increase the drag of the thruster and to introduce a spinning motion, decreasing aerodynamic heating and impact velocity. In addition, an oxidation-resistant high-emissivity coating must be used to protect the refractory thruster materials. The effects of the coating and the re-entry fins on the thruster design are described below.

2.3.3.1 Oxidation Resistant Coatings

At operating temperatures (1950° - 2000°C), presently available oxidation-resistant coatings deteriorate rapidly (Reference 2-11). In order to assure their integrity if abortive re-entry occurs within 5 years after launch, it is necessary to prevent operation of the thruster whenever such re-entry is possible. In these cases the mission is aborted, the thruster assumes the abort configuration (insulation ejected), and the thruster surface temperature remains low enough to preserve the coating. It remains to be established that the coating/substrate system can endure prolonged exposure in vacuum at abort-

in-orbit temperatures. For an abort during initial orbiting maneuvers (30 days after encapsulation), the maximum thruster surface temperature would be as shown below and would decrease with time due to isotope decay.

<u>Thruster Surface Emissivity</u>	<u>Maximum Thruster Surface Temperature</u>
0.45	1100°C
0.7	900°C

2.3.3.2 Re-entry Aids

As indicated above, fins are used on the thruster body to insure its survival during atmospheric re-entry. The four-fin re-entry aid was selected for the nominal configuration, since considerable analytical and experimental data were available for it. Preliminary subsonic test results indicated that a two-fin re-entry aid configuration may also be acceptable. Use of a two-fin design reduces the area to be insulated, decreasing weight of the insulation 30-40 percent and simplifying its installation. The weight of the nominal thruster configuration (see Section 2.4.1) using both two-fin and four-fin re-entry aids was computed as a function of allowable sea-level impact velocity. The increase in the weight of the outer module as a function of the fin span was also included in the calculations (see Section 2.3.2.2).

The analytical basis for sizing the four-fin re-entry aid configuration is described in Section 3. For the two-fin configuration, the fins were assumed to have a rectangular planform, a trapezoidal cross section and a 0.50" diameter bead with a .030" wall thickness at the fin tip. The rate of spin was assumed to be the same as for the four-fin configuration (3000 RPM). The effective drag coefficient for the spinning two-fin re-entry aid configuration was determined from the broadside drag coefficient, $\alpha = 90^\circ$, by accounting for the reduction in the effective flat-plate drag area due to the spinning motion. The average drag per cycle was compared to the drag for $\alpha = 90^\circ$.

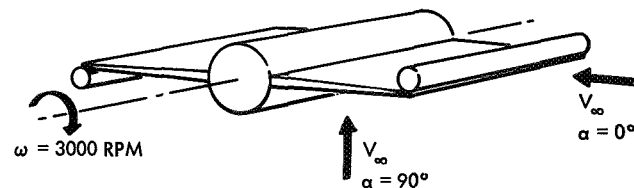


Figure 2-20. Thruster Orientation for Re-entry Analysis

The drag coefficient based on a reference area equal to the planform projection, $L \times D$ is then given by the following equation:

$$C_{D_a = 90^\circ} = \frac{F}{qA} = C_{D_{a = 90^\circ}} \left\{ (.425) + \left(\frac{C_{D_{a = 0^\circ}}}{C_{D_{a = 90^\circ}}} \right) (.575) \right\} \quad (2-8)$$

where:

F = total aerodynamic drag force, lbs. (defined parallel to the re-entry vehicle flight path)

q = free-stream dynamic pressure, psf

A = re-entry vehicle drag reference area, ft^2 (taken to be the planform area of the finned vehicle)

$C_{D_{a = 90^\circ}}$ = flat plate drag coefficient

The total thruster weights for two-fin and four-fin re-entry aid configurations are shown in Figure 2-21. It is seen that the two-fin design cannot achieve a sea level impact velocity of 200 ft/sec. At the present time, the effect of an impact at 240 ft/sec is not well defined. Extensive impact testing of capsules and thrusters will be required to establish the maximum allowable impact velocity. If a 240 ft/sec sea level impact velocity is found to be acceptable, the weight of the re-entry aids can be reduced by decreasing the fin span for the four-fin configuration or by using a two-fin configuration. The direct weight reduction is augmented by the accompanying reduction in insulation weight.

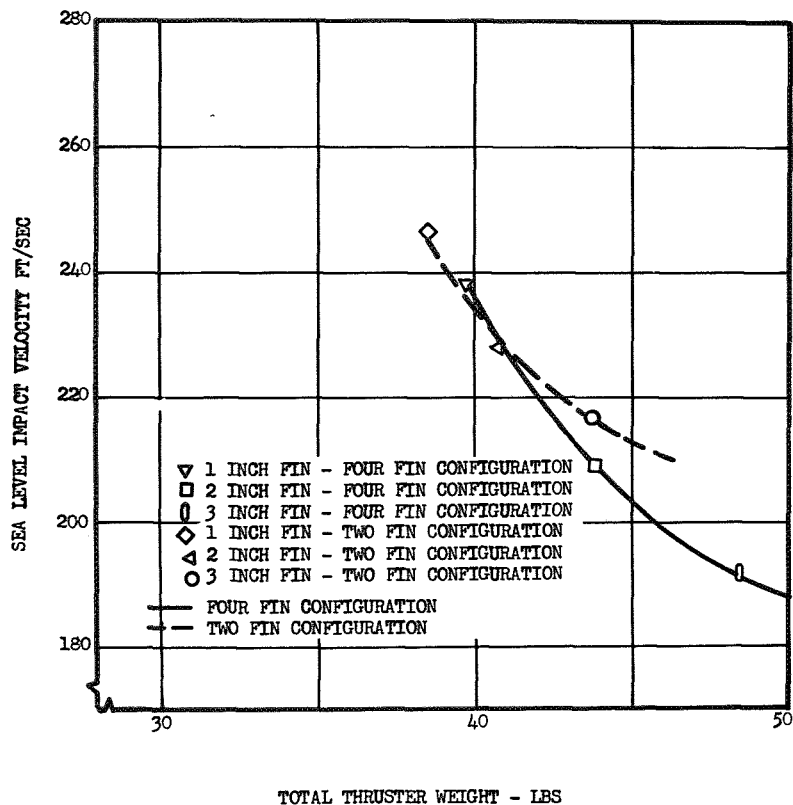


Figure 2-21. Thruster Weight Vs Sea Level Impact Velocity for Various Fin Configurations

A higher impact velocity results from an increase in the ballistic coefficient. Since the stagnation point aerodynamic heating is proportional to the square root of the ballistic coefficient, an increase in the allowable sea level impact velocity to 240 ft/sec will increase the peak aerodynamic heating approximately 20 percent and the peak stagnation temperature approximately 5 percent. However, by increasing the fin tip bead diameter, the increase in the peak stagnation temperature can be offset somewhat since the heating is also inversely proportional to the square root of the body diameter.

2.3.4 Nozzle Performance

As discussed in Reference 2-12, the nozzle efficiency (delivered specific impulse as a percent of the ideal) is a function of the throat Reynolds number. Nozzle efficiencies as high as 94 percent were predicted analytically for typical POODLE flow rates, but measured efficiencies in experimental nozzles were found to be somewhat lower (Figure 2-22). For the thruster design described in Section 2.4.1, the nozzle throat Reynolds number at the beginning of mission is 2150, and the nozzle efficiency is taken to be 87 percent (in accordance with measurements reported in Volume IV).

The POODLE propulsion system design is based on a nominal chamber pressure of 15 psia and a nominal propellant tank pressure of 30 psia (Reference 2-13). Variations in the propellant tank pressure produce changes in thruster chamber conditions which, of course, affect the thruster performance. However, to overcome this problem, orifices are placed in the propellant feed lines to decouple the perturbations in tank pressure from the thruster. The nominal pressure drop in the lines and across the orifice is 15 psi.

The nozzle throat Reynolds number can be increased by increasing the chamber pressure. A detailed analysis of the propulsion subsystem should be conducted to determine if the tank pressure can be increased without incurring a significant weight penalty. In

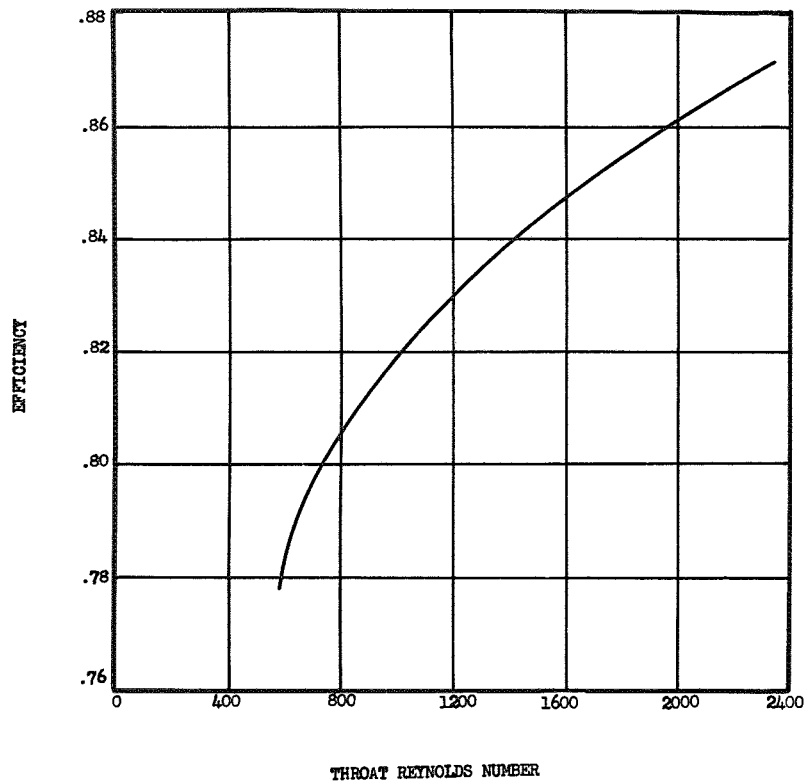


Figure 2-22. Experimentally Measured Nozzle Efficiency Vs Throat Reynolds Number

addition, the pressure ratio across the orifice should be minimized. For example, if the chamber pressure can be increased to 30 psia, the nozzle efficiency will increase 2 percent. This is equivalent to an increase in the I_{sp} of 15 seconds.

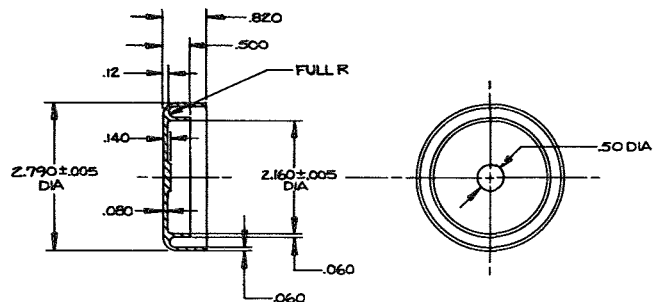
2.4 THRUSTER DESIGN

Results of the foregoing analyses were used in updating the POODLE thruster design, arriving at the revised configuration shown in Figure 2-23 with characteristics as summarized in Tables 2-11 and 2-12. The thruster is designed to endure aerodynamic heating and loads associated with re-entry from orbit and to impact with a sea level velocity of approximately 205 ft/sec.

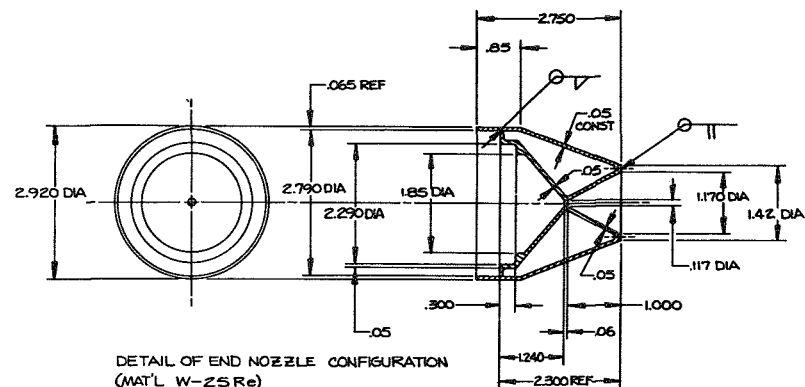
The specific impulse of 706 seconds shown in Table 2-11 corresponds to the measured nozzle efficiency of 87 percent, as reported in Volume IV. If nozzle efficiency can be raised to 94 percent, the specific impulse will increase to 760 seconds. Suggested future work directed toward improved nozzle efficiency is discussed in Volume IV.

Previous thruster designs included a cylindrical module which served as a container for the three capsules and as the inner wall of the propellant flow channel. This module has been deleted in the current design. In addition to the direct weight saving, elimination of the module also reduces cladding weight, since a thinner cladding may be used when not subjected to interdiffusion at its exterior surface. Thus, except at forward and aft ends of the thruster, capsule surfaces are in contact only with the helical flow guide, which is made of the same material as the cladding (Rh-30Ir).

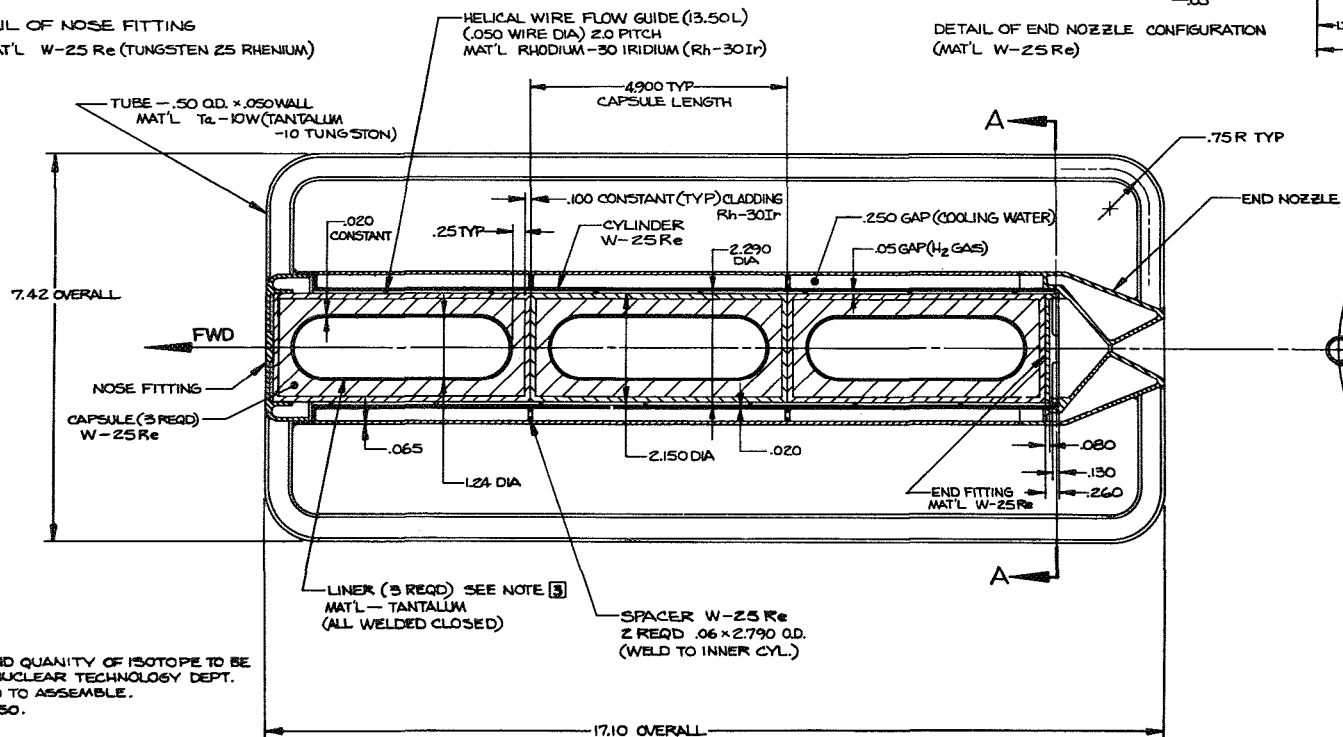
The outer surface of the thruster and the re-entry fins will require an oxidation-resistant, high-emissivity coating to survive reentry. The minimum acceptable emissivity is 0.45. This must be maintained until a point is reached in the trajectory at which an abort leading to reentry is no longer possible, or until the isotope has decayed sufficiently (5 years) so that capsule disintegration upon reentry is permissible. It is reasonable to expect that a high



DETAIL OF NOSE FITTING
MAT'L W-25 Re (TUNGSTEN 25 RHENIUM)



DETAIL OF END NOZZLE CONFIGURATION
(MAT'L W-25 Re)



SECTION A-A

- 5 FUEL FORM AND QUANTITY OF ISOTOPE TO BE SPECIFIED BY NUCLEAR TECHNOLOGY DEPT.
2. WELD AS REQD TO ASSEMBLY.
1. ALL RAD: .050.
NOTES—

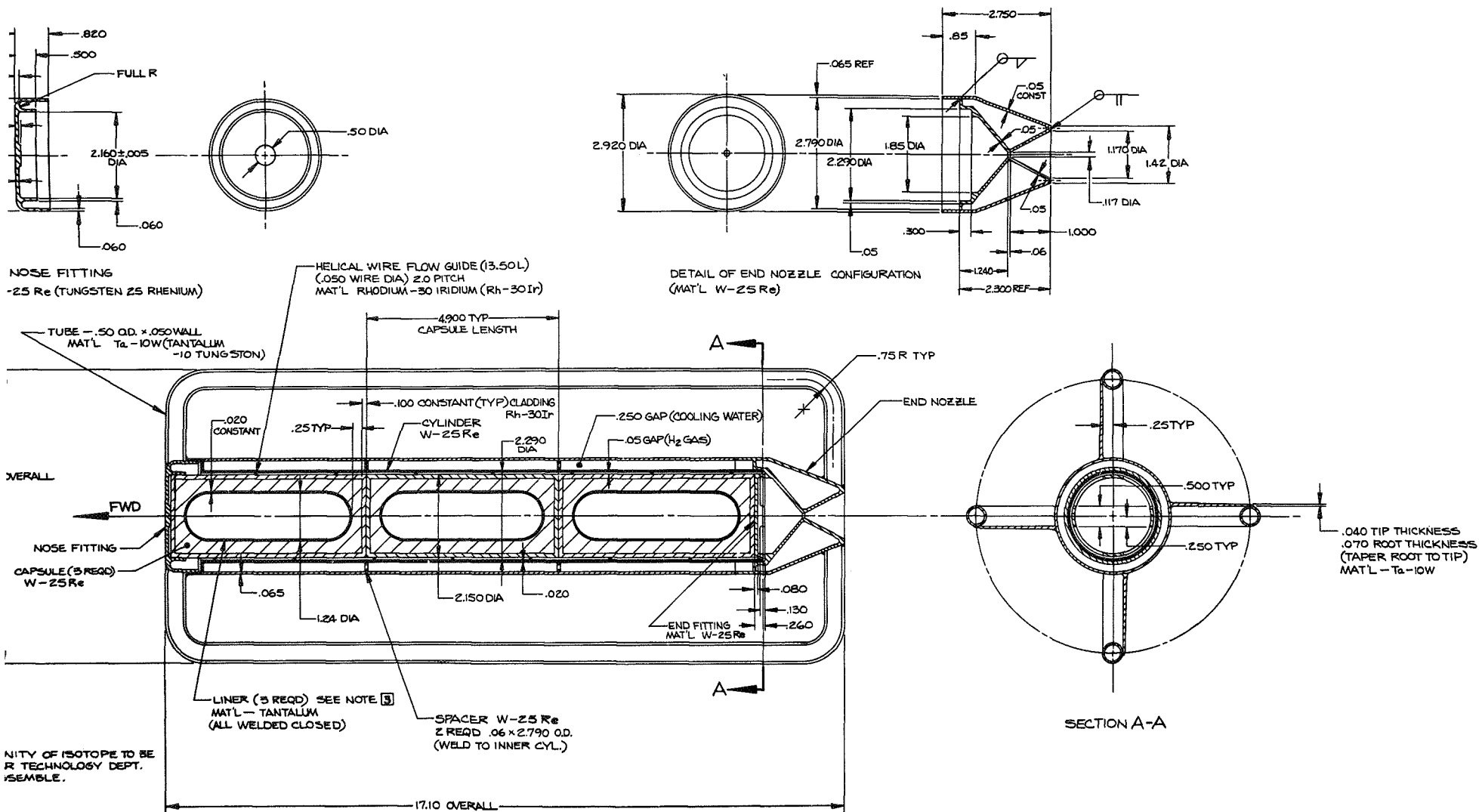


Figure 2-23. POODLE Thruster Assembly

Table 2-11. POODLE Thruster Power and Performance

THERMAL POWER - Kilowatts		At Encapsulation (t = 0)	At Launch (t = 30 Days)	At End of Mission (t = 60 Days)
Forward Capsule		3.70	3.19	2.74
Middle Capsule		1.80	1.55	1.33
Aft Capsule		1.00	0.86	0.74
Total		6.50	5.60	4.81

2-48

PERFORMANCE				
Insulation Efficiency	%	-	90	90
Nozzle Efficiency	%	-	87	86
Chamber Pressure	psia	-	15	15
Propellant Temperature	°C	-	1925	1925
Thrust	lb	-	0.24	0.20
Specific Impulse	sec	-	706	700

a

2-12. POODLE Thruster Materials and Weights

Component	Material	Thickness (mils)	O.D. (inches)	Weight (lb)	Quantity per Thruster	Total Weight (lb)	Note
Capsule Inner Vessel							*
Capsule Substrate	W-25Re	310	1.24	0.8			
Capsule Cladding	Rh-30Ir	100	1.95	6.7			
Composite Capsule			2.15	2.1			
			2.15	9.6	3	28.8	
Helical Flow Guide	Rh-30Ir	50	2.25	1.0	1	1.0	
Flow Channel Wall	W-25Re	20	2.29	1.5	1	1.5	
Outer Cylinder	W-25Re	65	2.92	5.9	1	5.9	**
Re-entry Fin	Ta-10W			1.9	4	7.6	
Coolant Channel Spacers	W-25Re			0.1	2	0.2	
Nose and End Fittings	W-25Re			0.9	1	0.9	
Nozzle	W-25Re			1.4	1	1.4	
Insulation	Ta			4.8	1	4.8	***
Thruster	52.1						

*Weight indicated is for fuel, matrix, and liner and is averaged for non-uniformly loaded capsules.

**Fins are 70 mils at root, 40 mils at tip, 2.25 inches in radial width, and are edged by a 0.5-inch-diameter bead.

***Insulation consists of 64 concentric foils, each 0.25 mils thick.

2-49

emissivity can be maintained because thruster surface temperatures are relatively low in the abort mode.

Although a total thruster weight of 52.1 pounds is shown in Table 2-12, weight reductions up to 13 pounds are possible as follows:

- A 3.2-pound reduction in cladding weight will result if the cladding thickness is changed from 100 mils to 50 mils. The advisability of this change depends upon the capsule surface emissivity attainable. For example, if an emissivity of 0.7 can be assured, a 17-mil cladding thickness is sufficient to resist oxidation and inter-diffusion for the most heavily loaded capsule. Impact considerations would become limiting in this instance, and a 50-mil cladding would be specified.
- A weight reduction of 1.5 to 2.0 pounds will be realized if the outer ends of forward and aft capsules are reshaped (leaving other ends unaltered to retain axial and radial heat transfer characteristics). Excess material at the two extreme ends is removed by changing from right circular cylindrical heads to hemispherical domes, and these are accommodated by redesigning nose and end fittings. Additional small weight savings may be possible if capsule walls are thinned in regions of low stress.
- An 8.0-pound reduction in the weight of fins, outer cylinder, and insulation will be realized if the fin span is reduced from 2.25 inches to 1.0 inch. The advisability of this change must be examined in terms of capsule impact survivability, since sea level impact velocity increases from 205 to 240 ft/sec. Approximately the same weight saving, with the same increase in impact velocity, can be realized by using two 1.25-inch fins. The weight advantage of the two-fin over the four-fin configuration is very slight (because the outer cylinder must be thickened) and there are relatively little data on its aerodynamic behavior. However, the two-fin configuration remains of interest because it simplifies installation of insulation.

2.5 CONCLUSIONS AND RECOMMENDATIONS

Design analyses based on the best available data have led to a 52-pound thruster delivering one-quarter-pound of thrust at a specific impulse of 706 seconds. Possible weight reductions yielding a thruster in the neighborhood of 40 pounds have been described. Areas in which further development work is necessary, either to improve indicated thruster performance or to verify

compatibility with operational and abort environments, are summarized below:

- Development efforts to obtain increased nozzle efficiency should be continued in order to reach specific impulse objectives above 750 seconds. In particular, the performance of spike nozzles designed to reduce the viscous losses associated with thick boundary layers in conventional low-thrust nozzles should be investigated. (See Volume IV)
- The endurance of cladding/substrate systems in air at abort temperatures must be investigated to verify their effectiveness and the analytical methods used in establishing required cladding thicknesses. (See Volume III)
- A more complete definition of post-impact environments is needed together with associated studies of capsule lifetimes in those environments. In particular, capsule temperature history and chemical behavior must be determined for earth burial in representative soils and for representative post-impact configurations.
- The integrity of clad capsules when subjected successively to creep and impact (in either order), and the effectiveness of the thruster body in cushioning capsule impact and shielding capsules from impact abrasion should be investigated.
- Testing of oxidation-resistant, high-emissivity coatings should be carried out to establish that the coating effectiveness during reentry is not impaired by volatility and/or interdiffusion experienced in prior exposure to representative abort environments.
- The development of light-weight, highly-efficient multi-foil thermal insulation for 2000 °C operation should be pursued.

REFERENCES

- 2-1 Radioisotope Propulsion Technology Program (POODLE), Final Report (October 1965 - January 1967), Volume I, "Capsule Creep Strain Measurements and Analyses", STL-517-0049, February 1967, TRW Systems, Redondo Beach
- 2-2 Radioisotope Applications in Space Program, Phase A, Interim Report, STL-517-0022, June 1965, TRW Systems, Redondo Beach
- 2-3 Radioisotope Propulsion Technology Program (POODLE) Final Report (October 1965 - September 1966) Volume III, "Oxidation and Diffusion in Noble Metal Alloy Claddings", STL-517-0049, October 1966, TRW Systems, Redondo Beach, Calif.
- 2-4 Radioisotope Applications in Space Program, Final Report, Volume I, "POODLE Aerospace Safety Analysis," STL-517-0016, February 1965, TRW Systems, Redondo Beach, California (SDI)
- 2-5 High Temperature Materials Program, Progress Report No. 59, Part A, GEMP-59A, May 31, 1966, General Electric Co., Atomic Products Division, Cincinnati, Ohio
- 2-6 F. F. Schmidt, "Tantalum and Tantalum Alloys", DMIC Report 133, July 1960, Defense Metals Information Center, Battelle Memorial Institute, Columbus, Ohio
- 2-7 Interoffice Memo - TRW Systems, N. Bayard De Volo and J. Licari to I. R. Jones, "Theoretical Results of Radiation Shielding Analysis, 9736.4.65-69, July 1965
- 2-8 Radioisotope Propulsion Technology Program (POODLE) Final Report (October 1965 - November 1966) Vol. V, "Simulation of High Temperature Radioisotope Heat Sources", STL-517-0049, December 1966, TRW Systems, Redondo Beach, Calif.
- 2-9 Supplement I to Aerospace Structural Metals Handbook, Volume II, Non-Ferrous Alloys, ASD TDR-63-141, December 1963, Air Force Materials Laboratory, AFSC, Wright Patterson Air Force Base, Ohio
- 2-10 Raymond J. Roark, Formulas for Stress and Strain, Fourth Edition, McGraw Hill, New York, N. Y., 1965
- 2-11 H. J. Nolting and R. A. Jeffreys, "Oxidation Resistant High Temperature Protective Coatings for Tungsten", ASC-TDR
- 2-12 Radioisotope Propulsion Technology Program (POODLE), Final Report (October - 1965 - 1966) Volume IV, "Performance of Low Thrust Nozzles", STL-517-0049, 1966, TRW Systems, Redondo Beach, Calif.
- 2-13 Radioisotope Applications in Space Program, Final Report, Volume IV, "POODLE Propulsion Subsystem Technology, STL-517-0016, February 1965, TRW Systems, Redondo Beach California (OUO)
- 2-14 Radioisotope Propulsion Technology Program (POODLE), Final Report (1 October 1965 - 30 September 1966) Volume IIb, "Analytical Program for Creep in Axisymmetric Bodies (CRAB) STL-517-0049, October 1966, TRW Systems, Redondo Beach, California

3. RE-ENTRY CONFIGURATIONS

Work on POODLE re-entry configurations was concluded in March 1966 and reported in the Quarterly Progress Report for the period 1 January - 31 March 1966, STL-517-0042. That portion of the quarterly report is repeated below for the sake of completeness of this volume.

3.1 INTRODUCTION

Extensive analysis (Reference 3-1) on the re-entry behavior of POODLE thrusters has shown that a significant reduction in both aerodynamic heating and thruster impact velocity can be achieved by the simple addition of relatively lightweight longitudinal fins-provided that the finned vehicle achieves a broadside orientation and spins rapidly about its longitudinal axis. This orientation is essential to (1) achieve the maximum effective drag area, thus reducing both re-entry heating rate and impact velocity, and (2) distribute the aerodynamic heating over the entire thruster surface, thus reducing the peak re-entry temperature to an acceptable value. It was reasoned that the gyroscopic effect of the spin would tend to stabilize the vehicle in the desirable broadside attitude, thus preventing end-over-end tumbling. However, because of the complex nature of the air flow patterns over the re-entry body and the resulting uncertainties associated with both hypersonic and subsonic calculational techniques, it was decided that experimental verification of the finned thruster behavior would be necessary prior to further design improvements.

A series of subsonic drop-tests were performed in previous phases of the POODLE program (Reference 3-2) utilizing full-scale POODLE thruster models dropped from a helicopter hovering at an altitude of approximately 15,000 feet. Ballistic tracking cameras were employed to obtain thruster orientation and trajectory data during descent. Evaluation of the test results indicated that substantial reductions in thruster impact velocities were achieved, as predicted, and that the finned thrusters did spin rapidly (up to 3000 rpm) in an essentially broadside orientation, although the smaller finned models did experience a coning motion as well.

Having verified the subsonic behavior, attention was focused on methods for determining the hypersonic characteristics of the finned configuration. Although free-flight testing appeared most desirable, budgetary and schedule limitations dictated that other means be sought. Accordingly, a series of hypersonic wind tunnel tests were initiated in the previous phase of the POODLE program to determine if the finned thrusters would spin about their longitudinal axes when subjected to hypersonic air flows. A detailed description of the finned models and test procedures was previously reported (Reference 3-2). The testing was finished during this phase of the program and the results are reported in Section 3.2.






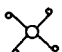

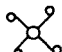
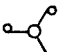

A series of subsonic wind tunnel tests was recently completed in an attempt to resolve some apparent discrepancies between the hypersonic wind tunnel data and the free-flight aerodynamic information obtained from the drop-tests. The results are reported in Section 3.3. Finally, an aerodynamic fin sizing analysis was performed utilizing the previous analytical and experimental results to determine the thruster impact velocity as a function of basic thruster weight and various fin sizes. This data, reported in Section 3.4, will be useful in evaluating the advantages or disadvantages involved in changing the weight and configuration of various thruster components, such as capsules, nozzles and structural shells.

3.2 HYPersonic WIND TUNNEL TESTS

Initially, eight subscale POODLE models, employing several fin configurations, were designed and fabricated. The models were mounted in a specially designed bracket which would allow them to spin. The entire assembly was placed in TRW's hypersonic wind tunnel facility so that the longitudinal axis of the model was normal to the air flow direction. After testing was initiated, two additional models of different configuration were fabricated on the basis of apparent aerodynamic merit. Model configurations, testing procedures and preliminary test data were described in Reference 3-2, but for convenience, the model characteristics are repeated in Table 3-1.

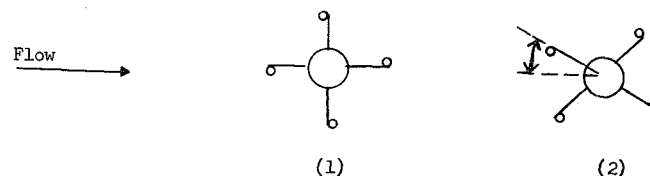
Because of wind tunnel limitations, all the models were initially tested at a Mach number of 5 and a Reynolds number of 722 (based on

Table 3-1. Thruster Model Configuration for Hypersonic Spin Tests

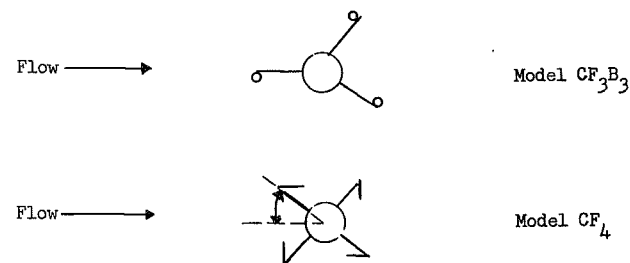
Model Designation	Fin Configuration	Sketch	Model Fin Span (in.)	Bead Diameter (in.)	Moments of Inertia (lb-in ²) $\times 10^{-4}$	Weight (lb)	Fin Material
CF ₁	Four Large Straight Fins		1.79	0	88	0.053	Aluminum
CF ₁ B ₁	Four Large Straight Fins		1.79	0.039	286	0.109	Brass
CF ₁ B ₂	Four Large Straight Fins		1.79	0.066	340	0.116	Brass
CF ₁ B ₃	Four Large Straight Fins		1.79	0.1327	957	0.146	Brass
CF ₂	Four Small Straight Fins		0.76	0	11.6	0.036	Aluminum
CF ₂ B ₁	Four Small Straight Fins		0.76	0.039	52.5	0.059	Brass
CF ₂ B ₂	Four Small Straight Fins		0.76	0.066	106	0.065	Brass
CF ₂ B ₃	Four Small Straight Fins		0.76	0.132	723	0.095	Brass
CF ₃ B ₃	Three Large Straight Fins		1.79	0.132	719	0.11624	Brass
CF ₄	Four Large Straight Fins		1.79		406	0.12946	Copper

* Length of all models = 2.50 inches.

model body diameter of 0.375 inch); all four-finned models sought one of two stable positions shown in the sketch below. The majority of the models showed a preference for position (2).



Models CF₃B₃ and CF₄ sought the following stable positions:



Although some oscillation or quiver was observed once the models had reached their equilibrium position, there was no strong tendency for the models to spin. It was also observed that the aerodynamic forces acting on the finned surfaces, while the models sought stable positions, were rather weak.

To more nearly approach the conditions which would occur during an actual re-entry, it was decided to increase the Reynolds number in the wind tunnel by approximately an order of magnitude. Figure 3-1 shows the POODLE model test conditions compared to a typical re-entry profile. The main difficulty associated with increasing the Reynolds number was the rather large back pressure which occurred in the wind tunnel and caused back-streaming of the diffusion pump oil and eventually flow separation in the wind tunnel flow nozzle.

A second series of tests was conducted at a Reynolds number of 5400. However, the test results were essentially the same as those

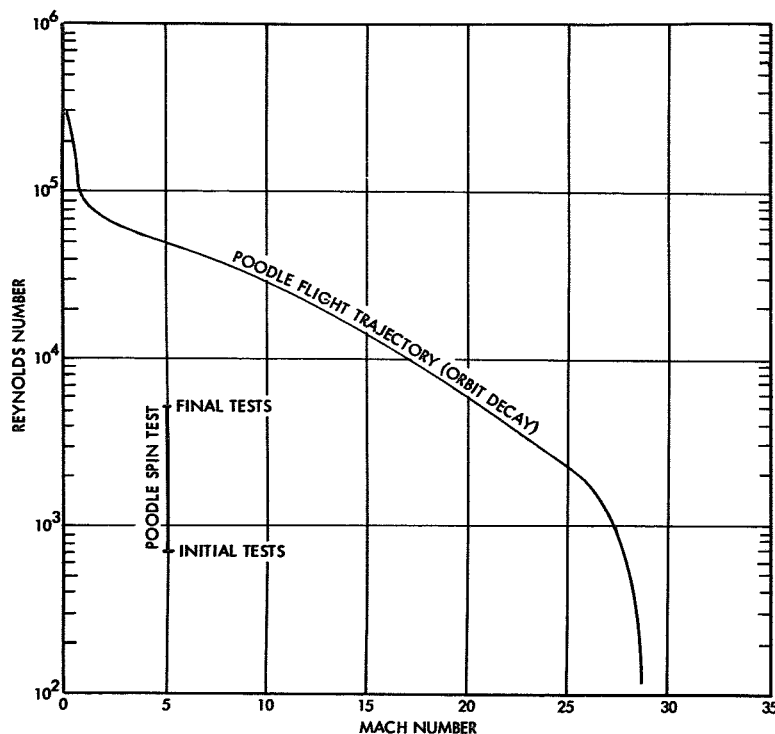


Figure 3-1. POODLE Model Test Conditions Compared to Full Scale Flight Regime

observed in the first test series, i. e. , the models all exhibited a tendency to trim at stable positions rather than spin.

Analysis of the experimental procedures and the test data revealed that the reluctance of the models to achieve a spinning motion could possibly be attributed to any or all of the following factors:

- 1) The one degree of freedom constraint imposed upon the models by the mounting structure
- 2) Weak aerodynamic forces acting on the finned surfaces in hypersonic flow
- 3) Friction in the mounting bearings
- 4) Wind tunnel conditions which did not effectively simulate the actual re-entry conditions
- 5) Relatively large moments of inertia of the models

It was suspected that the first factor was probably the dominant one in explaining why the models would not spin. In free-flight, an initial perturbation induced by some random motion of the vehicle such as tumbling could well be the "triggering" device to facilitate thruster spin up. Hence, it was considered desirable to perturb the model in the wind tunnel to see if spinning could be induced. However, this could not be achieved from the outside, since the wind tunnel was a completely enclosed structure. Hence, the models were repositioned in the wind tunnel where flow discontinuities and assymetrics were known to exist. Under these conditions, spinning was achieved for most model configurations. The large finned models spun up to a relatively steady value, while the smaller finned designs underwent an unsteady spin motion.

The test results were generally regarded as inconclusive with regard to determining the hypersonic behavior of finned re-entry bodies. A number of questions arose as to the validity of the information which could be obtained, even under more refined wind tunnel test conditions. It was finally decided to perform a series of subsonic tests, where free-flight information was available from the drop-tests to correlate wind tunnel results. These tests and the conclusions derived therefrom are given in the following section.

3.3 SUBSONIC WIND TUNNEL TESTS

Since it was desired to have easy access to the models while they were being tested so that a triggering action to induce spin could be imposed if required, a simple unenclosed wind tunnel was constructed. Basically it consisted of a ten-inch ducted fan, a wire-screen grid to alleviate the turbulence, and the model support bracket used in the hypersonic test series. The spin models were mounted horizontally in the support bracket with their longitudinal axes normal to the air flow direction. The flow conditions were somewhat erratic, but, by a trial and error adjustment of model position, a suitable location was found where the same spin and trim characteristics could be duplicated when the models were turned end-for-end in the mounting bracket. Testing of twenty-four models was performed at this location and, on a comparative basis, the results were satisfactory.

The flow conditions at the model location were obtained by using a flat-plate drag techniques: A flat-plate was attached to a light flexible strut and placed at the model location. The drag force was determined by measuring the deflection of the strut and comparing this deflection to a previous calibration of the strut and plate assembly. Since the drag coefficient of the plate was known ($C_D \approx 1.2$), the effective dynamic pressure was determined and the Reynolds number computed (it was found to be approximately 1500). Although this value was quite low compared to the full-scale drop-test values, it was considered adequate for the preliminary screening tests to be performed.

The subscale test models employed the same aluminum cylindrical body used in the hypersonic tests (Dia. = 0.375 inch). Initially, the aluminum and brass fins were also utilized, but later the fins were made from stiff cardboard; and the beads, located on the fin tips, were constructed from balsa wood. The lighter weight fins were used to promote a more lively response of the models to the rather low energy level of the subsonic air stream. A total of twenty-four different spin model configurations were tested, and will be described further in subsequent paragraphs.

During the course of testing, the fan was operated continuously, since model changes were very easily made and required only a few minutes to perform. The test procedure for each model was to place it

in the support bracket, check for free rotation, hold the model steady, then release it and observe its behavior. Most of the models tested would immediately seek a trim point and oscillate slightly or quiver in this stable position (just as the models tested in the hypersonic wind tunnel had done). The model would then be given a gentle push to force it past this stable trim point. Following this triggering action, some of the models would continue to spin, and accelerate up to a steady spin rate. Other models would merely rotate through part of a revolution, stop and trim again. The metal-finned models all behaved in this manner and even very strong initial triggering forces could not produce the desired acceleration to a steady spin rate. Instead the model would eventually return to the stable trimmed position. However, many of the lighter finned models could be made to achieve a stable spin by increasing the force applied in the triggering action.

When the above testing procedure was completed and the results evaluated, the model was turned 180° , end-for-end in its mounting bracket, and the test repeated. This was done to confirm that the observed trimming and spinning characteristics were not a function of any existing tunnel flow asymmetries. Reruns of the models were accomplished many times during the course of testing, especially when attempting to compare the characteristics of one model with another of similar geometry. After a while a good "feel" was developed in evaluating the inherent spinning qualities of each model.

Table 3-2 presents information on the model characteristics and test results for each of the twenty-four different configurations tested. The flow direction arrow associated with the small sketches indicates the the approximate initial trimmed attitude of the model.

Models 1, 2, and 3 were straight-finned POODLE-type configurations with three different fin spans. Model configuration 1a corresponded to the large-finned POODLE drop-test model. The subsonic wind tunnel test results for this configuration showed that the model trimmed initially; but if given a moderate initial spin rate, it would continue to accelerate and reach a steady spin velocity. The tendency to trim initially was in agreement with the hypersonic spin tests, but definitely not in agreement with the full-scale POODLE drop-tests, where it was shown that the

Table 3-2. Subsonic Model Test Summary

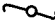
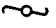




CONFIG NUMBER	CONFIGURATION			TEST RESULTS
	DESCRIPTION	SKETCH	FIN SPAN IN.	HEAD DIA IN.
1a	FOUR-FIN, LARGE-SPAN STRAIGHT PANELS, BEADED. (THIS MODEL CORRESPONDS TO THE LARGE-FINNED POODLE DROP-TEST MODEL)		1.88	0.094
1b	TWO-FIN, LARGE-SPAN STRAIGHT PANELS, BEADED.		1.88	0.094
2a	FOUR-FIN, MEDIUM-SPAN STRAIGHT PANELS, BEADED.		1.28	0.094
2b	TWO-FIN, MEDIUM-SPAN STRAIGHT PANELS, BEADED.		1.28	0.094
3a	FOUR-FIN, SMALL-SPAN STRAIGHT PANELS, BEADED. (THIS MODEL CORRESPONDS TO THE SMALL-FINNED POODLE DROP-TEST MODEL)		0.81	0.094
3b	TWO-FIN, SMALL-SPAN STRAIGHT PANELS, BEADED.		0.81	0.094
4a	FOUR-FIN, VERY LARGE SPAN STRAIGHT PANELS, LARGE BEADS.		3.25	0.26
4b	TWO-FIN, VERY LARGE SPAN STRAIGHT PANELS, LARGE BEADS.		3.25	0.26

Table 3-2. Subsonic Model Test Summary (Continued)

CONFIG NUMBER	CONFIGURATION			TEST RESULTS
	DESCRIPTION	SKETCH	FIN SPAN IN.	HEAD DIA IN.
5	TWO-FIN, LARGE-SPAN STRAIGHT PANELS, NO BEAD.		1.75	0
6	TWO-FIN, MEDIUM-SPAN STRAIGHT PANELS, NO BEAD.		1.19	0
7	TWO-FIN, SMALL-SPAN STRAIGHT PANELS, NO BEAD.		0.81	0
8a	FOUR-FIN, VERY LARGE-SPAN CIRCULAR-ARC SHAPED PANELS, NO BEAD.		3.06	0
8b	TWO-FIN, VERY LARGE-SPAN CIRCULAR-ARC SHAPED PANELS, NO BEAD.		3.06	0
9	TWO-FIN, VERY LARGE-SPAN CURVED PANELS, NO BEAD.		3.24	0
10a	FOUR-FIN, LARGE-SPAN CURVED PANELS, NO BEAD.		1.80	0
10b	TWO-FIN, LARGE-SPAN CURVED PANELS, NO BEAD.		1.80	0
11a	FOUR-FIN, LARGE-SPAN CURVED PANELS, CURLED EDGE.		1.80	0.14*
11b	TWO-FIN, LARGE-SPAN CURVED PANELS, CURLED EDGE.		1.80	0.14*

*ASSUMES AN "EFFECTIVE" HEAD DIAMETER FOR THE CURLED EDGE

Table 3-2. Subsonic Model Test Summary (Continued)

CONFIG NUMBER	CONFIGURATION			TEST RESULTS	
	DESCRIPTION	SKETCH	FIN SPAN IN.	BEAD DIA IN.	
12	TWO-FIN, LARGE-SPAN CURVED PANELS, LARGE CURLED EDGE.		1.80	0.24"	SIMILAR TO CONFIGURATION 11b COMMENTS BUT A LITTLE MORE SLUGGISH IN BUILDING UP THE SPIN.
13	TWO-FIN, MEDIUM-SPAN CURVED PANELS, CURLED EDGE.		1.19	0.124"	TRIMS INITIALLY, BUT IF PUSHED SLIGHTLY WILL ACCELERATE AND MAINTAIN SPIN IN PROPER DIRECTION. WILL NOT MAINTAIN SPIN IN WRONG DIRECTION. PERFORMS WORSE THAN LARGE-SPAN VERSION 11b, AND PERHAPS ABOUT THE SAME AS STRAIGHT-FINNED MODEL 2b.
14a	FOUR-FIN, MEDIUM-SPAN STRAIGHT PANELS, CURLED EDGE.		1.25	0.191"	TRIMS INITIALLY. IF GIVEN A MODERATE SPIN RATE, WILL CONTINUE TO SPIN IN PROPER DIRECTION, BUT THE SPIN RATE IS REDUCED. IF GIVEN ONLY A SMALL SPIN RATE, WILL COAST TO A STOP AND TRIM. SLUGGISH.
14b	TWO-FIN, MEDIUM-SPAN STRAIGHT PANELS, CURLED EDGE.		1.25	0.191"	TRIMS INITIALLY. IF GIVEN A MODERATE SPIN RATE, WILL CONTINUE TO SPIN IN PROPER DIRECTION. PERFORMS BETTER THAN THE FOUR-FIN VERSION 14a, BUT SLIGHTLY WORSE THAN CONFIGURATION 13.
15a	TWO-FIN, MEDIUM-SPAN PANELS, HELICALLY MOUNTED, READLESS.		1.43	0	TRIMS INITIALLY. IF GIVEN A PUSH, WILL MAINTAIN SPIN COUNTER-CLOCKWISE (FROM TEST OBSERVER'S VIEWPOINT); WILL NOT MAINTAIN SPIN IN A CLOCKWISE DIRECTION. RUNS WERE REPEATED FOR MODEL EXCHANGED END-FOR-END WITH SAME RESULTS.
15b	SAME AS 15a, BUT WITH BEADS		1.43	0.094	TRIMS INITIALLY. MUST BE GIVEN A MODERATE SPIN RATE TO INVESTIGATE SPINNING CHARACTERISTICS. WHEN MODEL IS MOUNTED SO THAT BEADS ARE IN POSITION TO INDUCE COUNTER-CLOCKWISE ROTATION, THE MODEL SPINS COUNTER-CLOCKWISE VERY WELL. WHEN MODEL IS EXCHANGED END-FOR-END SO THAT BEADS ARE IN POSITION TO INDUCE CLOCKWISE ROTATION, THE MODEL WILL STILL SPIN BUT AT A LOWER COUNTER-CLOCKWISE RATE. IF GIVEN AN INITIAL CLOCKWISE SPIN RATE, IT WILL COAST TO A STOP AND TRIM.

*ASSUMES AN "EFFECTIVE" BEAD DIAMETER FOR THE CURLED EDGE

large-finned POODLE vehicle exhibited no tendency to trim whatsoever, but spun up very nicely, regardless of the launching orientation.

Model configuration 3a corresponded to the small-finned POODLE drop-test model. The subsonic test results for this configuration showed that the model trimmed initially; and, even if given a large initial spin rate, it would coast to a stop and trim. It is quite likely that if the bearing friction were reduced and the model could maintain a steady spin rate; however, the fact remains that the aerodynamic forces promoting spin for this configuration were very weak. The results from the full-scale POODLE drop-tests on the small-finned POODLE configuration showed there was no tendency to trim, regardless of launch orientation. All five full-scale drop-test models spun up very nicely within 10 to 15 seconds after launching.

Factors contributing to the discrepancy between the thruster behavior in the free-flight drop-tests and in the hypersonic wind tunnel experiments were outlined in the previous section. These same factors apparently also apply to the subsonic wind tunnel experiments as well. The single degree of freedom constraint imposed upon the wind tunnel models by the mounting structure, bearing friction and the initial lack of triggering forces appear to be the major factors in explaining the discrepant behavior. The subsonic test results were instructive in that, when the triggering force was supplied, the large finned model behavior correlated well with the free-flight data.

Continuing with other results of the subsonic spin model tests, it was observed that the two-finned versions of the POODLE-type configurations, Models 1b, 2b, and 3b, performed nearly as well as the four-finned version by maintaining a steady spin rate, whereas the four-finned version could not. A likely explanation of this behavior is that the two-finned version was a lighter model and thus had less bearing friction. However, the test results in general, indicate that additional consideration should be given to determining the free-flight behavior of two-finned thruster configurations since they will probably be lighter than the four-finned designs.

The effect of the beaded edges on the spin characteristics of straight-finned POODLE models was explored with Models 5, 6, and 7 in which the beads were removed. These models had no asymmetries, such as produced by the beads, and yet they exhibited a good tendency to spin. Of course, for an actual re-entry vehicle, the sharp-edged fins would not be realistic because of aerodynamic heating considerations; but these particular results on symmetrical configurations indicate that for free-flight vehicles it may not be difficult to maintain a spin once started, and that the real problem is assuring that a "triggering" action to start the spin is available.

The remainder of the tests were exploratory attempts to find fin configurations that would induce self-spinning of the model. Curved fin arrangements were tried, with various degrees of success. In general, the curved-fin models performed better than the straight-fin models of equal span. Of all the models tested, only two consistently demonstrated a self-spinning behavior: Models 8a and 10a. Model 8a was a four-fin, very large span, circular-arc shaped fin configuration, and does not particularly represent an attractive practical case because the fins are too large. Model 10a was a four-fin, large span, curved fin configuration with a fin span comparable to the large-finned POODLE drop-test vehicle. This configuration is still somewhat impractical for a reentry application. However, it is reasoned that since the subsonic spin model tests apparently produce conservative results compared to the full-scale POODLE drop-tests, this configuration may eventually be made practical by reducing the fin span and/or using a two-fin version.

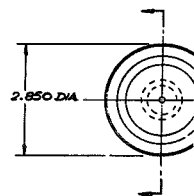
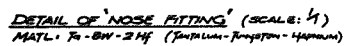
Model 11b, which was a two-fin curved panel configuration, was judged to be the most efficient and perhaps the most promising of the configurations tested, based on a practical application viewpoint. This configuration was almost self-starting in spin, spun-up well when triggered, and had a minimum of fin area for the spin results achieved. Based on the apparent conservative results of the subsonic spin model tests, the ratio of fin span to body diameter of this configuration could probably be reduced significantly and satisfactory spin performance still be obtained on a full-

scale re-entry application. It must be remembered, however, that for the POODLE application, the minimum fin size (i.e., effective drag surface area) will probably be dictated by the allowable impact velocity requirement even after a spinning broadside motion has been guaranteed; in other words, the minimum fin size required for satisfactory impact velocity will probably be larger than the minimum fin size required for satisfactory spin performance. In addition, aerodynamic heating and fabrication problems must also be evaluated prior to selection of a final finned thruster flight configuration.

3.4 FIN SIZING ANALYSIS

A thruster fin sizing analysis was performed utilizing previous analytical and experimental results. The purpose of this endeavor is to provide design information which will be useful in evaluating the advantages or disadvantages involved in changing the basic thruster weight and/or configuration. Such changes may be necessitated as a result of findings from capsule studies now underway.

Although the subsonic windtunnel tests revealed that certain two-finned configurations may have a moderate weight advantage over the four-finned designs, insufficient information currently exists on the free-flight behavior and aerodynamic heating characteristics to justify the selection of two-finned designs as the nominal thruster configuration. Hence, the four-finned thruster design with beads on the fin tips to control the heating rate at this critical location was selected as the nominal design for the purposes of this study. Figure 3-2 is an illustration of this type of thruster configuration. The thruster contains three radioisotope capsules constructed from W-25Re (density = 0.7 lb/in^3). Two structural shells, also made from W-25Re, surround the capsule forming an annular propellant flow passage. The third or outer shell, fins, and hollow beads were assumed to be constructed from Ta-10W, a slightly lighter refractory alloy (density = 0.6 lb/in^3) with an allowable stress of 12,000 psi at a re-entry temperature of approximately 3000°F.



DETAIL C
(MATL: 70-)

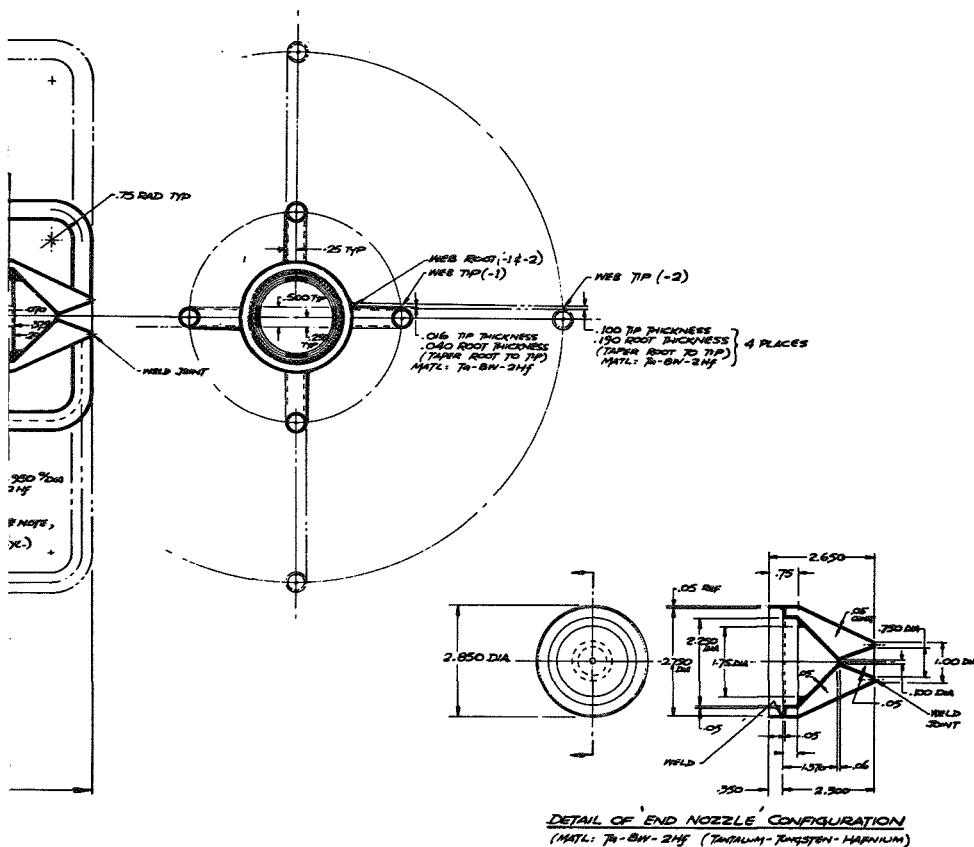


Figure 3-2. Thruster Configuration Referenced in Fin-Sizing Analysis

Four basic cylindrical thruster diameters were assumed: 2.40, 2.85*, 3.15 and 3.90 inches. The corresponding thruster weights were 20.5, 32.2*, 38.0 and 61.0 lbs. These weights were calculated assuming that the ratio of internal-to-external diameters of the capsules remained constant (a requirement imposed by capsule strength and creep considerations). In addition, the thruster and capsule lengths, structural shell thicknesses and the spacing between the three shells were assumed to remain constant and equal to the values shown in Figure 3-2*.

Fins of varying span were designed for each of the four basic POODLE thruster bodies in order to evaluate the vehicle impact velocity as a function of total thruster weight including fins. Results from the several test programs previously discussed were considered in the fin sizing studies.

It was apparent from the drop-tests that a four-finned thruster could be expected to attain a steady spin rate ranging from 2000 rpm to as high as 3000 rpm during the subsonic portion of re-entry. Since no data currently exists on the spin rate during hypersonic flight, it was assumed for the purposes of this study that a spin rate of 3000 rpm prevailed during the entire re-entry period. The drop-tests also revealed that the thruster orientation was essentially broadside and spinning. However, as the thruster fin span was decreased, a coning action was superimposed on the spinning motion which reduced the effective drag area compared to the spinning broadside drag area. Thus, a higher impact velocity was experienced than predicted from the broadside spinning orientation for the smaller finned configuration. However, only one thruster configuration was tested which exhibited this behavior. Extrapolation of the data on this complex motion to other fin sizes cannot presently be accomplished with high reliability; consequently, this effect was not included in this analysis. A broadside spinning orientation was assumed.

The actual fin sizing was accomplished for a fin with a rectangular planform and a span-wise trapezoidal cross section. Tubing, 0.50 inches

* This diameter and weight and the detailed configuration of Figure 3-2 correspond to the nominal 5 KW POODLE at the time the fin-sizing analysis was performed. The design techniques presented here were applied in deriving the more recent thruster configuration described in Section 2.

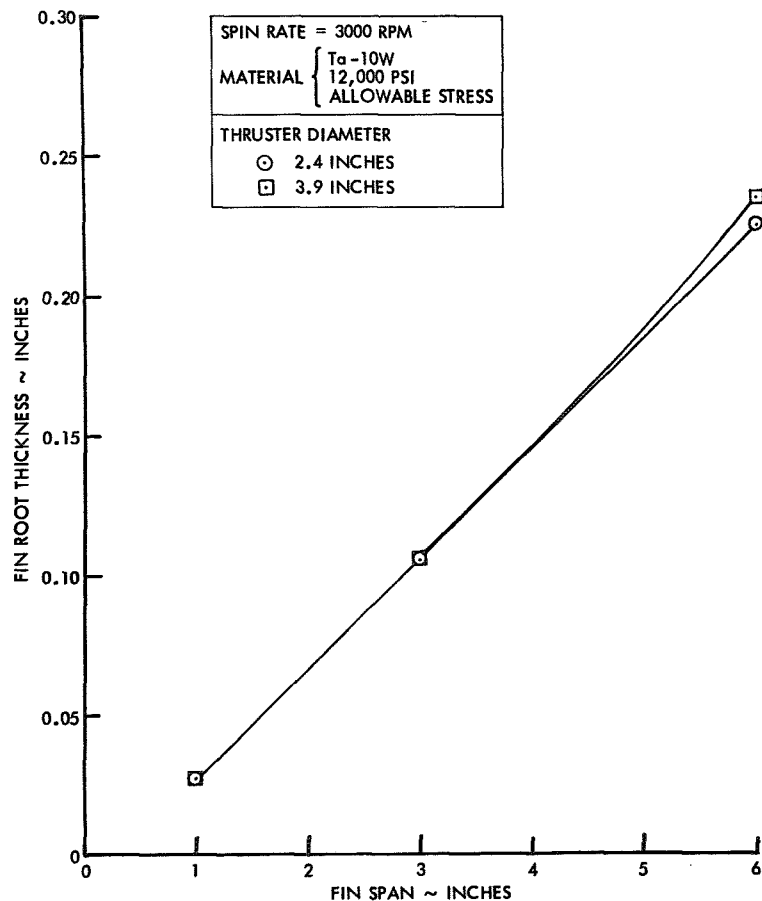


Figure 3-3. Fin Thickness Variation Versus Fin Span

in diameter with a 30 mil wall thickness, was used as the bead structure. Fin root thickness was then determined assuming that the fin was a cantilever beam with (1) a uniform load imposed by aerodynamic pressure forces (a maximum of approximately 4 psi near peak re-entry temperature) and (2) a centrifugal load, at right angles to the pressure forces, arising from the spinning motion of the body. The results are plotted in Figure 3-3. The fin tip thickness was assumed to be one-half of the fin root thickness to allow enough material for adequate welding of the fin and bead. It should be noted that, as the thruster spins about its longitudinal axis, the bending stress acting at the fin root cross section will vary from tension to compression with a period determined by the spinning frequency of the vehicle. Any material fatigue developed as a result of this rapid stress variation was not considered in this analysis.

Assuming various fin span values and using the results shown in Figure 3-3, the weight of the re-entry aids (fin and beads for all four panels) and the total weight of the POODLE vehicle (basic thruster weight plus re-entry aid weight) was computed. The next step was to calculate the thruster impact velocity.

The subsonic drag coefficient for the four-finned POODLE thruster was computed from test information ($C_D = 1.02$). Using this drag coefficient combined with the weights and planform areas for the various POODLE thrusters, the subsonic ballistic coefficients ($\frac{W}{C_D A}$) were calculated. Each vehicle was considered to be in its terminal stage of flight and to satisfy the "free-fall" condition where the weight of the thruster is equal to the aerodynamic drag. The sea level impact velocity was then calculated for each thruster with varying fin spans. The results are shown in Figure 3-4. Note that for all thrusters, a significant reduction in impact velocity occurs with only a moderate increase in total thruster weight (basic cylindrical thruster plus re-entry fins). However, a minimum impact velocity is eventually reached as the fin size is increased, because the total thruster weight increases faster than the drag area produced by the enlarged fins. Thus, the ballistic coefficient at first decreases as the fin spin is increased, but then increases with further increases in fin size. The impact velocity

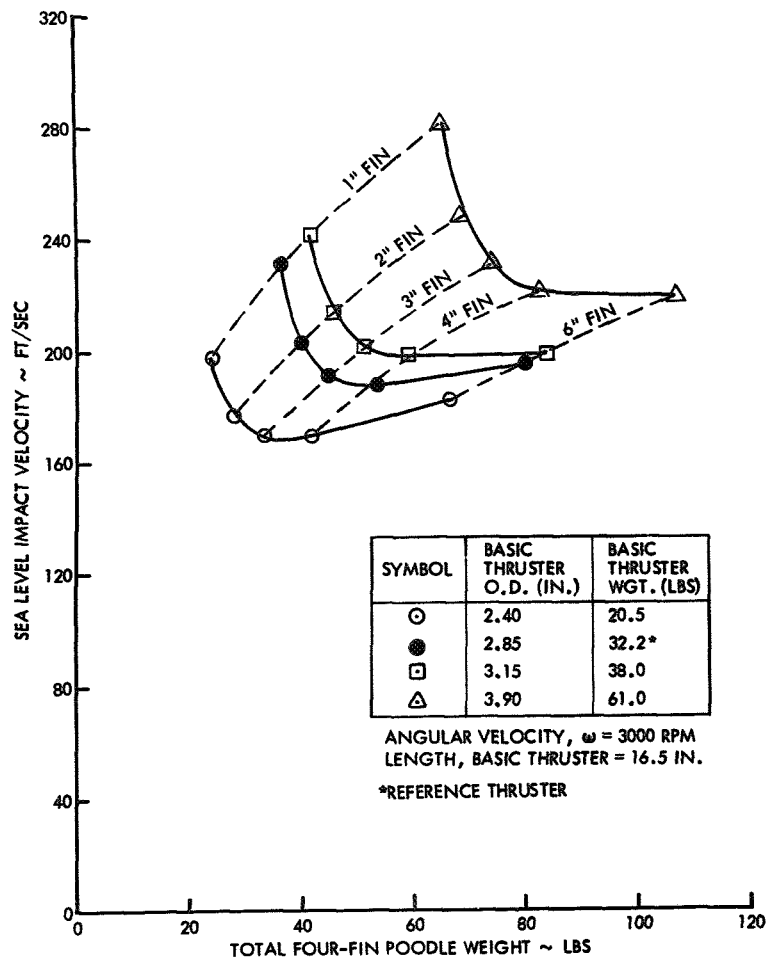


Figure 3-4. Sea Level Impact Velocity Versus Total POODLE Weight

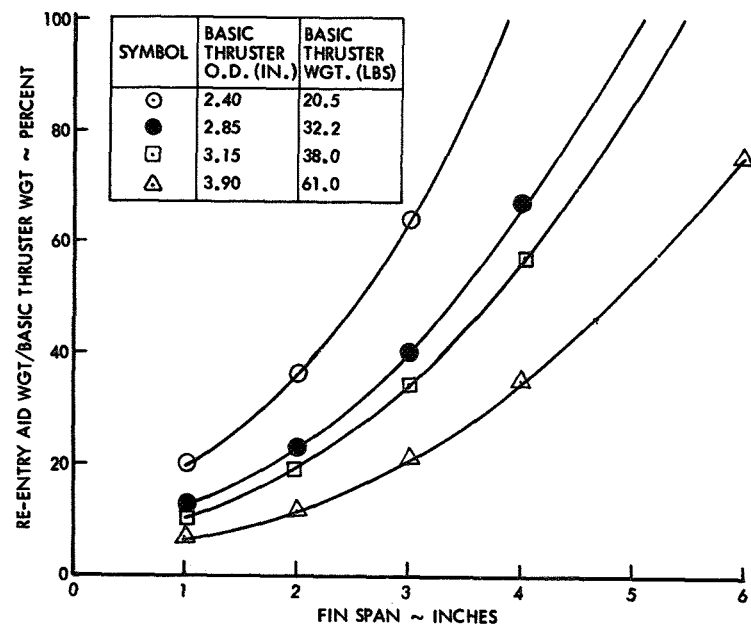


Figure 3-5. Re-entry Aid Weight Versus Fin Span

follows the same trend. It is also seen in Figure 3-4 that the curves become much flatter near the minimum point as the basic thruster weight is increased. A practical minimum impact velocity is reached by adding four fins with spans in the range of 3 to 4 inches. However, it must be remembered that it will not always be necessary to achieve the minimum impact velocity provided capsule integrity can be demonstrated at higher impact velocities.

A plot of re-entry aid weight divided by the basic cylindrical thruster weight versus fin span is shown in Figure 3-5. Using results from this figure and the previous one, it is obvious that impact velocities of less than 230 ft/sec can be obtained for all thrusters by adding longitudinal fins which weigh less than 20% of the basic cylindrical thruster weight.*

Up to this point, it has been assumed that increases in thruster weight arise solely from increases in the diameter, while the thruster length remains constant. However, if the basic engine weight is increased by increasing the thruster length proportionately while holding the diameter constant, the entire curve for the nominal thruster design (shown in Figure 3-4) is translated to the right. For example, if the basic cylindrical thruster weight of 32.2 lbs is increased to 61.0 lbs by increasing the thruster length, the impact velocity for a given fin span may be held constant by simply extending the fins so that their lengths equal the new thruster length. Thus an impact velocity of 200 ft/sec may be achieved for either a 32.2 or a 61.0 lb thruster by adding fins which increase the basic thruster weight by approximately 22%. Reviewing Figure 3-4, it is obvious that adding 22% in fin weight to a thruster initially weighing 61.0 lbs, whose diameter has been increased from the nominal 2.85 inches to 3.90 inches, results in an impact velocity of approximately 230 ft/sec - some 30 ft/sec higher than the previous case. In fact, the minimum impact velocity is 220 ft/sec, no matter how much fin weight is added.

* If a coning motion occurs for some of the smaller finned configurations, a slight increase in fin weight may be required to achieve this impact velocity.

It is apparent that if increases in thruster weight are necessary, an addition to the thruster length is more desirable in limiting impact velocity than an increase in thruster diameter. However, other factors such as minimum capsule L/D ratios, insulation optimization, envelope limitations imposed by the spacecraft, etc. must be considered prior to selection of a final design.

3.5 CONCLUSIONS AND RECOMMENDATIONS

The feasibility of using finned re-entry aids on cylindrical, high temperature heat sources has been established analytically and, to some extent, experimentally. However, it is apparent that additional testing is required to achieve the optimum configuration necessary to assure complete intact re-entry. Reliable data on the hypersonic behavior of finned re-entry bodies are presently of primary interest. It is felt that this information will best be obtained from free-flight tests of simply instrumented models flown by small sounding rockets or piggy-backed aboard larger boost vehicles. Two-finned configurations warrant further consideration in tests of the type just outlined as well as in subsonic drop-tests.

REFERENCES

- 3-1 Radioisotope Applications in Space Program Final Report, Vol. I
POODLE Aerospace Safety Analysis STL-517-0016 dated February
1965
- 3-2 Radioisotope Applications in Space Program (POODLE) Phase A
Final Report Vol. I STL-517-0034 dated October 1965

4. PERFORMANCE COMPARISON OF ADVANCED UPPER STAGES FOR POTENTIAL NASA MISSIONS

4.1 INTRODUCTION

The objective of this study was to compare the performances of a POODLE upper stage and a hydrogen-fluorine High Energy Kick Stage (HEKS) for missions of potential interest to NASA. Missions for which these upper stages have been shown to be useful include:

- a) Solar probes
- b) Out-of-ecliptic probes
- c) Planetary and interplanetary probes
- d) Orbital transfers

In most cases, the performance of existing launch vehicles is substantially improved by addition of the upper stage. In solar probe missions, for example, the Saturn IB/Centaur payload capability drops to zero at a perihelion distance of 0.2 AU. Addition of either POODLE or HEKS extends the perihelion distance which can be reached with useful payloads to the vicinity of 0.1 AU. Once the propulsion capability is available, entire classes of high velocity missions become possible and it is reasonable to expect that planning for these missions will then be definitized.

Cost estimates for developing a high energy upper stage range between 70 and 110 million dollars (Reference 4-1). If the development cost is to be justified, it must be shown that the upper stage is sufficiently versatile for general use in a variety of missions. An appraisal of cost effectiveness also requires a good estimate of the number of missions to be performed. However, advanced missions which may require a high-performance upper stage have not yet been well-defined—a situation at least partially attributable to the fact that such an upper stage does not now exist. Accordingly, a cost effectiveness study was considered to be beyond the scope of this study and objectives were limited to evaluation of performance.

4.2 VEHICLE DESCRIPTION

4.2.1 Poodle Stage

The nominal design for a small POODLE upper stage consists of four POODLE thrusters, hydrogen propellant, insulated hydrogen tanks, and the

hardware necessary for stage operation. The stage and thrusters are designed for operation for approximately 30 days. Provision for hydrogen storage for longer periods of time was not considered here, although it may be feasible. The four POODLE thrusters provide a total of one pound of thrust. The specific impulse range of 750 to 800 seconds has been used in this study, since that range is the performance objective of the current POODLE thruster development program.

The POODLE stage size was selected on the basis of a preliminary systems analysis to determine the best size for the missions considered (Reference 4-2). This study resulted in the selection of a POODLE stage in the 5000-pound class. A detailed breakdown of the stage design is given in Table 4-1. Two alternate configurations were considered, single- and double-shell designs. The single-shell design differs from the double-shell design by a jettisonable aerodynamic fairing (this has the effect of reducing booster payload by about 100 pounds prior to POODLE ignition).

Since POODLE operates for only 30 days, it may be possible to integrate redundant components required for both stage and payload. If the power supply and communications subsystems can be charged to the payload, the effective structure factor (ratio of stage jettison weight to stage ignition weight) is reduced. Table 4-1 gives the structure factors for payload-dependent POODLE stage designs. The payload-independent, single-shell design will have about the same performance as the payload-dependent, double-shell design, since their structure factors are nearly equal.

Figure 4-1 shows the variation of structure factor with stage ignition weight for the three principal POODLE stage designs. The structure factors increase rapidly below 3000 pounds. The payload-independent, single-shell design was chosen as representative of a POODLE stage for this study. The structure factor corresponding to this design is 0.215 and falls within the range of structure factors for the other configurations. Care should be exercised when comparisons are made with electrically propelled spacecraft. Since the latter spacecraft are necessarily fully integrated designs, it should be more consistent to base the comparison on the POODLE payload-dependent, single-shell design.

Table 4-1. Detailed Breakdown of POODLE Stage Designs

Structure	Double-Shell		Item	Double-Shell		Lightweight	Lightweight
	Design 1b	Design 1c		Design 1b	Design 1c	Design 1b	Design 1c
Outer shell	174	291	Orbit Control Equipment	28	28	28	28
Skin	60		Gyro compass (1)	5	5	5	5
Stringers	13		Horizon scanner (1)	12	12	12	12
Miscellaneous fittings and atoms	14		Power supply (1)	6	6	6	6
Payload support trans incl. fittings			Power supply assembly (1)	2	2	2	2
Equipment platform			Programmer (1)				
Engine support structure			Equipment Temperature Control	13	13	13	13
Injection system adaptor			Cold plate	8	8	8	8
Injection system			Lower assembly	5	5	5	5
Miscellaneous fittings and attachments			Power Supply	127	127	127	127
Micrometeoroid shield			MR radioscopes power generators (4)	84	84	84	84
Truss-type interstage adaptor			MR antenna installation	10	10	10	10
(0.998 penetration probability)			Batteries	29	29	29	29
Payload separation mechanism			Cabling, connectors, J-box, converters	4	4	4	4
Propulsion System			Injection System Installation Hardware	110	110	110	110
Propellant tank			Contingency (10 percent)	(1)*	(1)*	(1)*	(1)*
Propellant tank insulation			Stage Dry Weight	1223	992	977	742
Propellant feed system			Residual Propellant	19	19	19	19
Heater and installation			Stage Jettison Weight	1242	1014	996	768
Propellant tank exchange instal.			Usable Propellant	3609	3609	3609	3609
Thrusters (4)			Stage Ignition Weight	4851	4623	4605	4377
Thruster installation			Structure Factor $\frac{W_{jett}}{W_{ign}}$	0.255	0.218	0.215	0.175
Thrusters (4)							
Gimbals (4)							
Actuators and mounts (4)							
Thruster cooling system-dry							
Communications, Telemetry and Guidance							
High-power beacon (1)							
Low-power beacon (1)							
Telemetry transmitter (1)							
Command Receiver (2)							
Telemetry unit (2)							
Data storage unit							
Signal conditioner (1)							
Diplomer-coupler (1)							
Coupler (1)							
Antenna 150/136 Mc (1)							
Antenna 100 Mc (1)							
Antenna cabling (1)							

*Complete Stage
*Payload - dependent stage

*No outer shell is required, but a larger jettisonable fairing will reduce the booster payload by approximately 100 pounds.

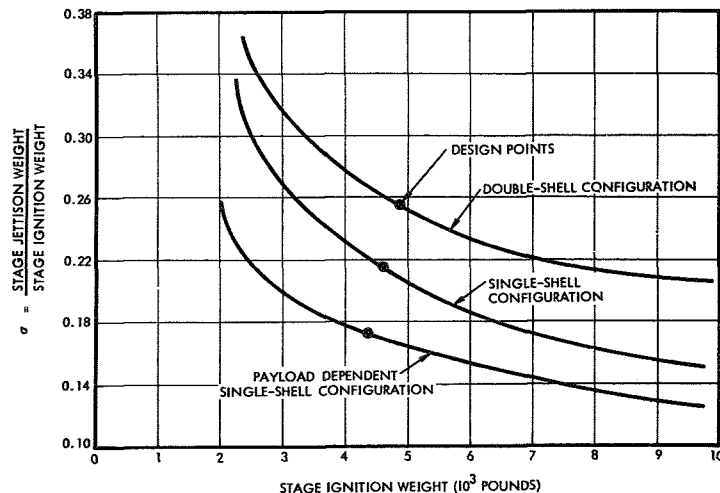


Figure 4-1. Variation of Structure Factor with POODLE Stage Ignition Weight

4.2.2 Hydrogen-Fluorine Upper Stage

The hydrogen-fluorine upper stage (HEKS) is representative of the concepts considered for advanced chemical bipropellant systems. Stage sizing studies (Reference 4-2) indicated that an H_2/F_2 stage in the 7000-pound class could perform a variety of advanced missions and gave near-optimum performance. A breakdown of the H_2/F_2 stage is given in Table 4-2. The delivered specific impulse for this propellant combination is approximately 440 seconds. The two structure factors given in Table 4-2 were used in this study as representative of the design of the H_2/F_2 stage.

4.3 LAUNCH VEHICLE/UPPER STAGE PAYLOAD CAPABILITY

The objective of an upper stage development is to improve performance of existing or potentially available launch vehicles for high velocity missions. In this study, the performance of upper stages was evaluated for the Saturn class of launch vehicles. The launch vehicles considered were:

- Saturn IB/Centaur
- Saturn IB/Nuclear
- Saturn V/Nuclear

Table 4-2. Description of 7000 Pound Hydrogen-Fluorine High Energy Kick Stage

Item	Stage A-1	Stage A-2
	Low Cost Development Weight (lb)	Improved Design Weight (lb)
Structure and Insulation	379	395
Propulsion System	317	317
Guidance	357	150
Attitude and Ullage Control	9	9
Power and Electrical	130	115
Instrumentation	42	42
Contingency	62	103
Stage Weight Empty	1296	1131
Stage Jettison Weight	1370	1209
Stage Gross Weight	7585	7364
Structure Factor	0.18	0.164

The nuclear stage considered, characterized by a structure factor of 0.2 and specific impulse of 800 seconds, is conceivably within the state of the art. Although the Saturn IB/Centaur combination is not, at present, an approved launch vehicle, the work necessary to mate these stages could readily be justified if a mission application were apparent. A POODLE stage in the 20,000-pound class would be required to replace the Centaur if a performance advantage over the Saturn IB is to be realized. However, this study was restricted to the 5000-pound POODLE stage.

Payload, as a function of the equivalent high-thrust burnout velocity, is shown in Figure 4-2. It is important to note that POODLE suffers a ΔV penalty relative to a high-thrust system for which the impulsive approximation is valid. However, once the POODLE stage escapes from Earth's influence, it suffers no significant penalty in the weaker heliocentric gravitational field. A further discussion of low-thrust penalties is given in

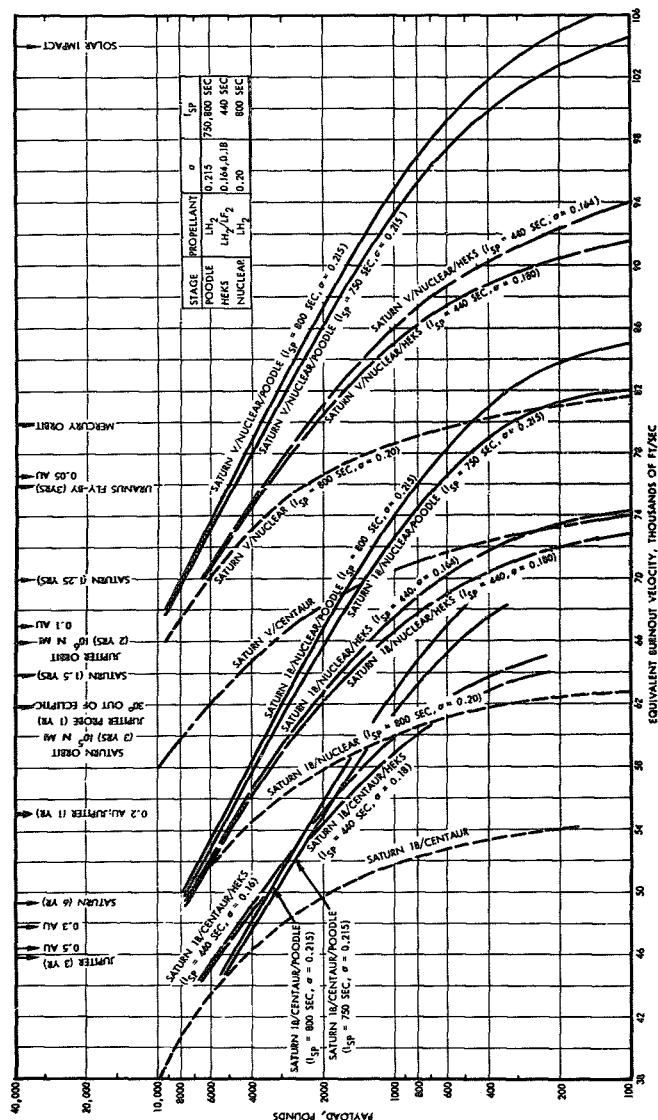


Figure 4-2. Payload as a Function of Equivalent Burnout Velocity

Appendix A. The POODLE results shown in Figure 4-2 can be used only for Earth-escape missions relative to departure from a 100 nautical-mile parking orbit. Figure 4-2 can be used to determine payload once the high-thrust burnout velocity is known for the mission concerned.

It can be seen from Figure 4-2 that the Saturn IB/Nuclear/POODLE combination competes with the Saturn V/Centaur for missions requiring burnout velocities in excess of 68,000 feet/second with payloads less than 1800 pounds. Although missions requiring greater than 68,000 feet/second are rare, the development costs of the Nuclear/POODLE combination could be offset by just a few such missions. It can also be seen that the Saturn V/Nuclear/POODLE combination could inject about 250 pounds of payload into the Sun.

4.4 MISSIONS

4.4.1 Solar Probes

The class of missions generally referred to as solar probes involve the injection of a spacecraft onto a heliocentric trajectory for the purpose of making a close approach to the Sun. Figure 4-3 shows a schematic diagram of a solar probe trajectory. For upper stages on Saturn class vehicles, distances in the vicinity of 0.1 AU are possible. A clarification of scientific objectives in reaching 0.1 AU or less awaits results of precursor probes, such as Pioneer. However, it is reasonable to expect that there will be strong scientific interest in performing deep solar probe missions.

Propulsion requirements for solar probes are given in Figure 4-4. The equivalent burnout velocities required to reach 0.1 and 0.05 AU are 67,000 and 77,000 feet/second, respectively, and that required to reach the Sun is 104,000 feet/second. Because of the magnitude of these velocities, the principal tradeoff for this mission will be payload as a function of perihelion distance. Figure 4-5 shows the variation of delivered spacecraft weight with perihelion distance. It is seen that the Saturn IB/Centaur is not capable of achieving 0.2 AU with any significant payload. In order to reach 0.1 AU, an upper stage is required. POODLE will deliver higher payloads than the HEKS to perihelion distances less than 0.2 AU (on the Saturn IB/Centaur or Saturn IB/Nuclear).

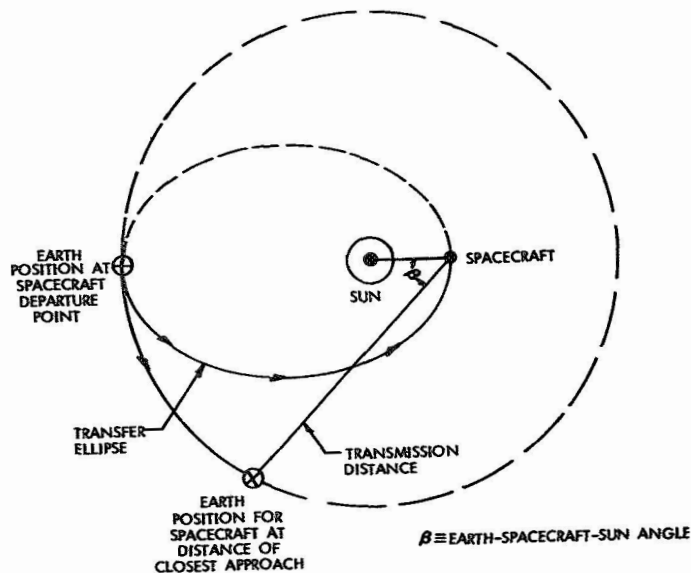


Figure 4-3. Solar Probe

Table 4-3 summarizes capabilities of the launch vehicles and upper stage combinations for 500- and 1000-pound spacecraft. It should be noted that the Saturn IB/Nuclear/POODLE combination can compete with the Saturn V/Centaur in achieving perihelion distances less than 0.09 AU. A Saturn V/Nuclear/POODLE combination could inject 250 pounds into the Sun.

A recent study of solar-electric propulsion (Reference 4-3) indicated that an optimized electrically propelled stage, when placed on the Saturn IB/Centaur, could inject about 1300 pounds to 0.1 AU. The study assumed a power plant specific mass of 75 pounds/kw. However, to achieve 0.1 AU, it would be necessary to operate the electrically propelled stage for over 1 year. POODLE and the high thrust systems complete perihelion passage in less than 80 days and return to perihelion more than once in a year. Any detailed comparison of solar-electric propulsion with POODLE would

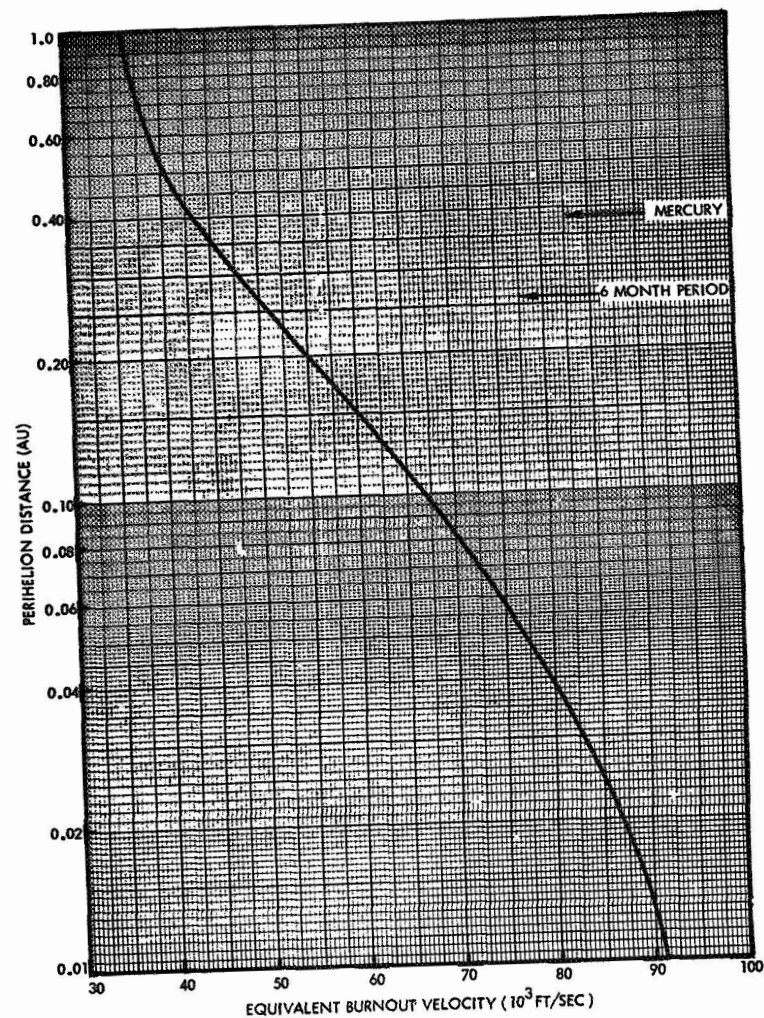


Figure 4-4. Propulsion Requirements for Solar Probes

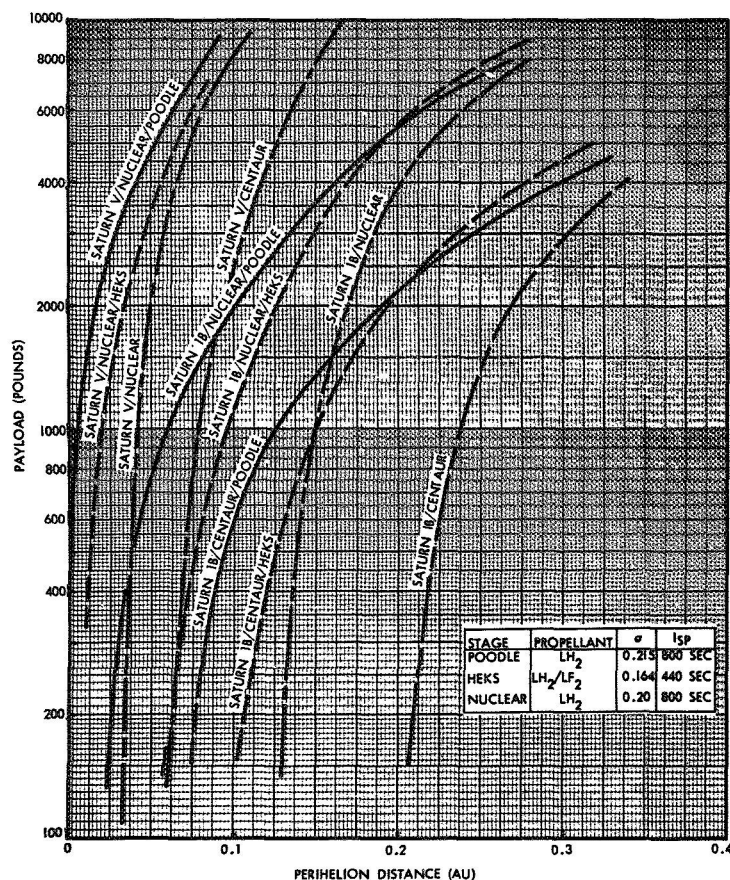


Figure 4-5. Payloads for Solar Probes

involve an extrapolation of POODLE technology to be consistent with the era in which electric propulsion is projected. Such a comparison was considered beyond the scope of this study, but could form the basis of future work.

Table 4-3. Distance of Closest Approach to Sun for 500- and 1000-Pound Payloads

	500-Pound Payload	1000-Pound Payload
Saturn IB/Centaur	0.22	0.24
Saturn IB/Centaur/HEKS	0.135	0.15
Saturn IB/Centaur/POODLE	0.095	0.11
Saturn IB/Nuclear	0.14	0.15
Saturn IB/Nuclear/HEKS	0.075	0.10
Saturn IB/Nuclear/POODLE	0.04	0.06
Saturn V/Centaur	0.07	0.08
Saturn V/Nuclear	0.04	0.04
Saturn V/Nuclear/HEKS	0.012	0.02
Saturn V/Nuclear/POODLE	0.001	0.005

4.4.2 Out-of-Ecliptic Probes

Another test of performance capability generally applied in upper stage studies is the ability to launch a spacecraft to an angle out of the plane of the ecliptic. Figure 4-6 shows a schematic diagram of an out-of-ecliptic probe having a circular orbit of radius 1 AU, assumed here to be desirable.

The investigation of particles and fields out of the ecliptic plane are justified by the increase in knowledge of our solar system which it will provide. No spacecraft has yet been launched to angles greater than 3 degrees out of the ecliptic. Since phenomena may vary only with the cosine of the solar latitude, it is reasonable to expect that angles greater than 30 degrees must be achieved before statistically significant data can be obtained.

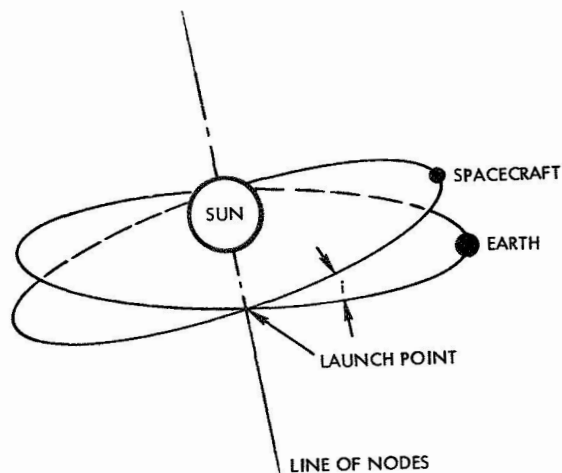


Figure 4-6. Schematic Diagram of a Probe i Degrees Out of the Plane of the Ecliptic

Propulsion requirements for out-of-ecliptic probes at 1 AU are shown in Figure 4-7. Figure 4-7 is combined with Figure 4-2 to obtain the principal tradeoff for the mission—payload as a function of angle out of the ecliptic plane which is shown in Figure 4-8. The POODLE upper stage with Saturn class launch vehicles covers the range of 33 to 55 degrees with a 500-pound spacecraft.

4.4.3 Missions to the Outer Planets

The outer planets (Jupiter, Saturn, Uranus, and Neptune) offer logical targets for scientific investigation during the next 20 years. Orbital characteristics of each planet are listed in Table 4-4. The National Aeronautics and Space Agency has indicated interest in these planetary objectives by funding several spacecraft design studies at Lockheed Missiles and Space Company, TRW Systems, General Dynamics, Hughes Aircraft Company and Electro-Optical Systems. The latter two studies were directed primarily toward the investigation of electric propulsion concepts, whereas, the former studies investigated more conventional spacecraft designs. In addition, NASA has performed in-house studies in this area.

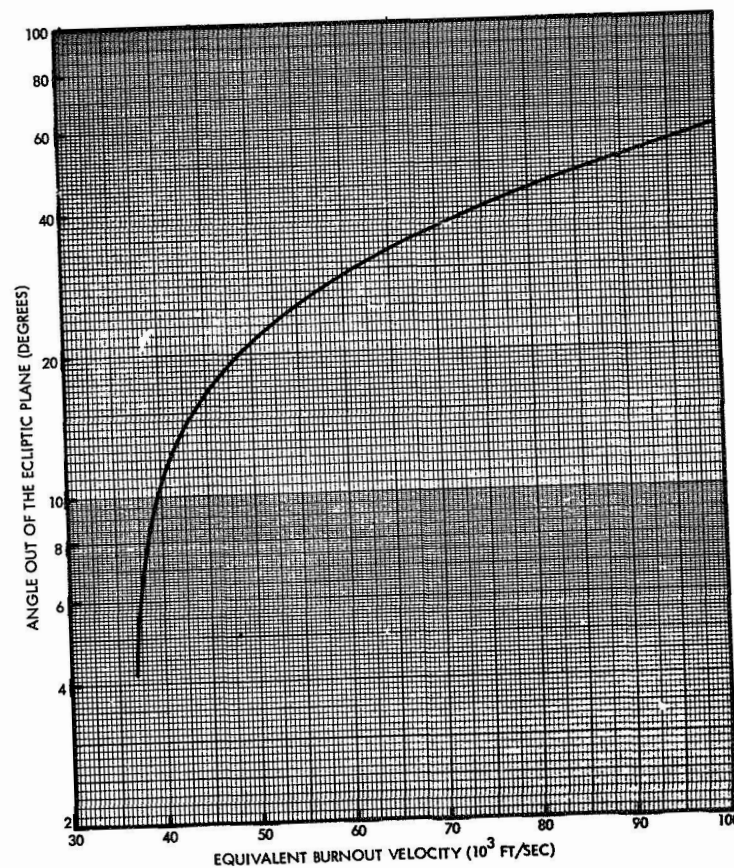


Figure 4-7. Propulsion Requirements for Out-of-Ecliptic Probes

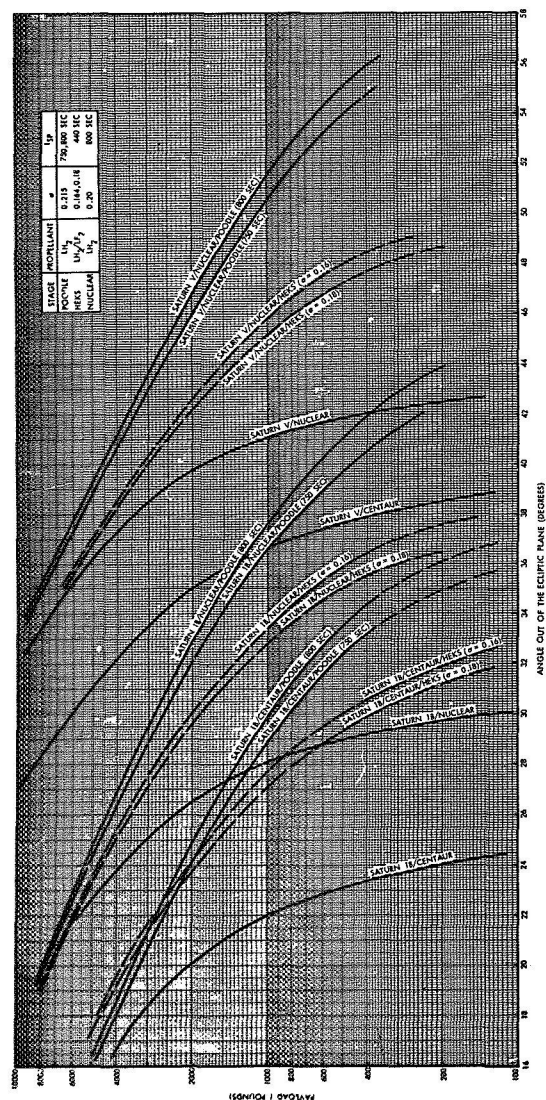


Figure 4-8. Payload for the Out-of-Ecliptic Mission

Table 4-4. Orbital Parameters for the Outer Planets

Quantity	Planet			
	Jupiter	Saturn	Uranus	Neptune
a, semimajor axis, AU	5.2028	9.539	19.18	30.06
Perihelion distance, AU	4.9520	9.008	18.28	29.80
Aphelion distance, AU	5.4536	10.070	20.09	30.32
e, orbital eccentricity	0.0482	0.05162	0.04431	0.00734
i, inclination to ecliptic, deg	1.306	2.487	0.772	1.773
Ω , longitude of ascending node, deg	100.18	113.3	73.7	131.4
ω , longitude of perihelion, deg	13.35	89.6	172.5	25.4

Distances from both Sun and Earth impose severe requirements on spacecraft. The reduction in solar power and increase in communication distance affect designs of the electrical power and communication subsystems. In addition, the long transit times to the outer planets place severe requirements on subsystem reliability. Lockheed, General Dynamics, and TRW Systems have emphasized the use of radioisotope thermoelectric generators in their spacecraft design studies as possible solution to the problem of diminishing solar power.

The class of missions to the outer planets includes planetary flybys and orbiters. At present, planetary landers have not been investigated in detail, probably because of the uncertainty associated with the planetary surfaces and mission difficulty. However, landers may be considered for some of the planetary satellites in the future. Spacecraft weights required for missions to the outer planets, as envisioned today, vary from a few hundred pounds to over 2000 pounds for the more ambitious missions.

The function of the prime propulsion system for unpowered spacecraft is to place the payload onto the proper unpowered interplanetary trajectory. A midcourse maneuver is generally required to correct for injection errors. The heliocentric trajectory may be either an ellipse or a hyperbola. A schematic diagram of the transfer is shown in Figure 4-9. One of the principal objectives of the launch vehicle combination will be to reduce the very long transit times to planetary encounters. Propulsion requirements are generally given in terms of injection energy.

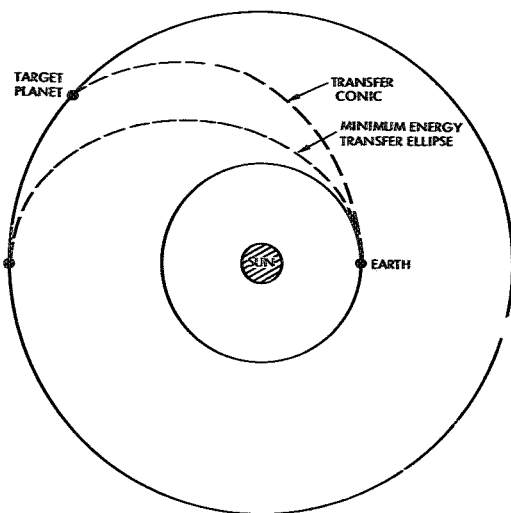


Figure 4-9. Heliocentric Transfer to Target Planet

Figure 4-10 shows the transit time to Jupiter, Saturn, Uranus and Neptune as a function of injection energy. Figures 4-11 through 4-14 show the variation of payload with transit time for the various launch vehicle combinations. Because the injection energy required to reduce transit time becomes enormous, the payload curves decrease sharply and it simply does not pay to reduce transit time below some limit. For planetary orbiters, it should be noted that the reduction in transit time is accompanied by an increase in the relative approach velocity at the target. If propulsive braking is required, the influence of the reduction in transit time will be magnified beyond that indicated. The performance of POODLE and HEKS is about equal for the Jupiter mission. However, beyond Jupiter, POODLE clearly outperforms HEKS in reducing transit times to reasonable periods.

Some consideration has been given to swingby maneuvers, particularly by the Jet Propulsion Laboratory. The maneuver involves a close approach flyby of Jupiter, using its gravitational potential to alter the spacecraft's trajectory. If the proper time and year are chosen, it is possible to reach

radial distances of the other outer planets in time for an encounter, with a savings in injection energy. However, the swingby maneuver is not very effective in reducing mission time and will require more than one mid-course maneuver. This mission mode is presently under further study at various laboratories.

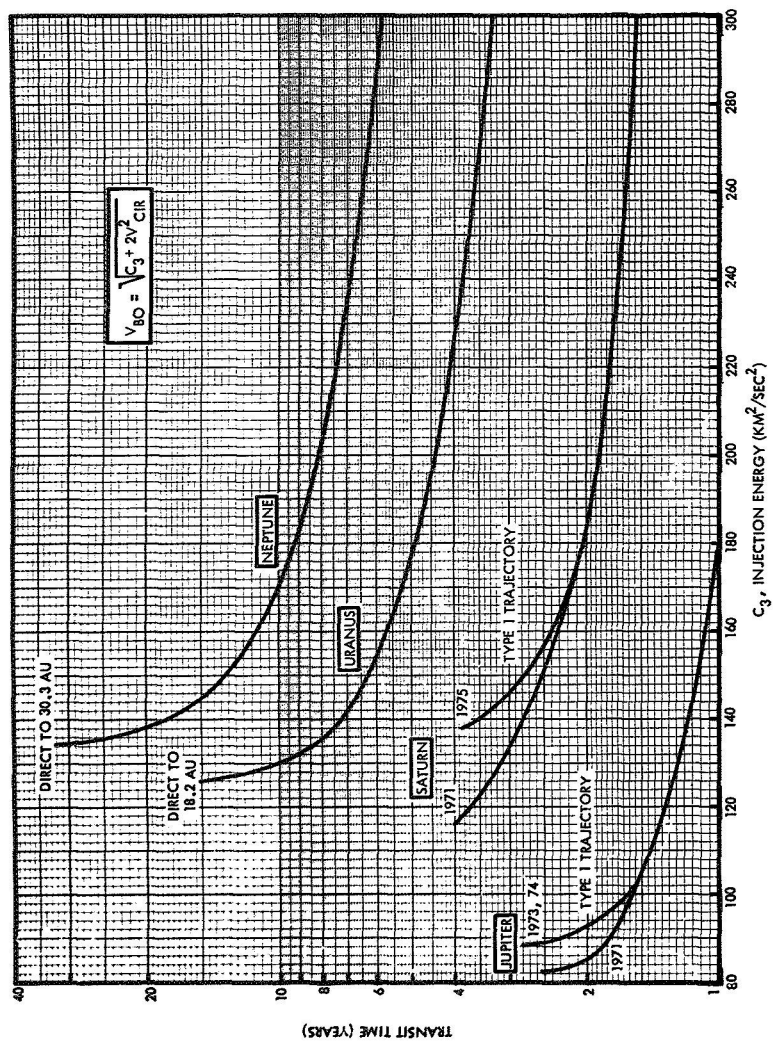


Figure 4-10. Transit Time to the Outer Planets as a Function of Injection Energy

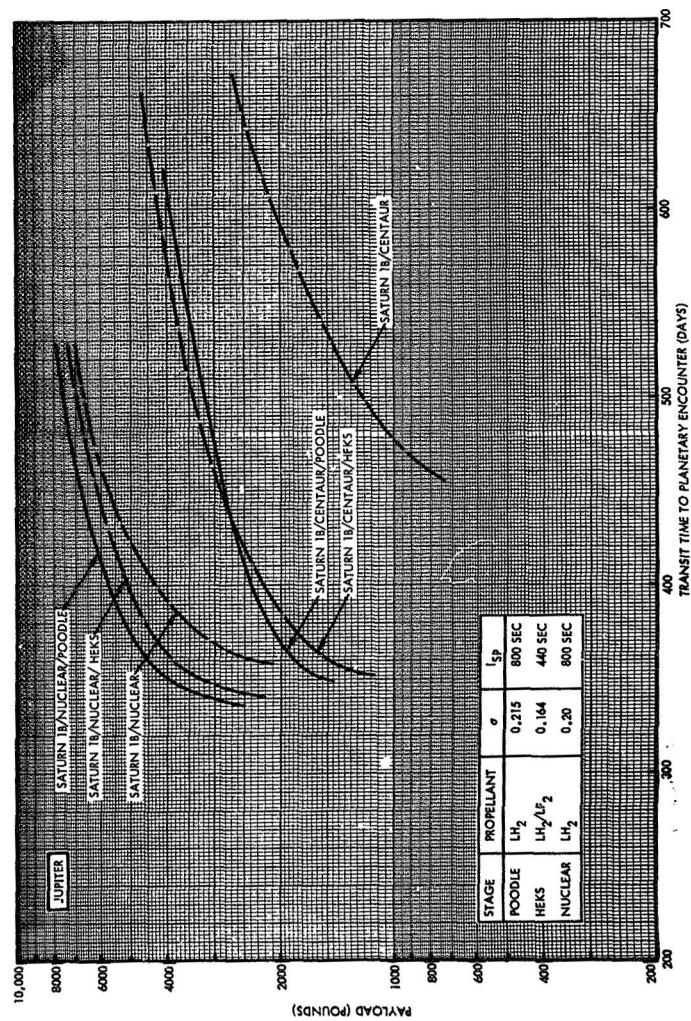


Figure 4-11. Variation of Payload With Transit Time to Encounter With the Planet Jupiter (1971 Type I Trajectory)

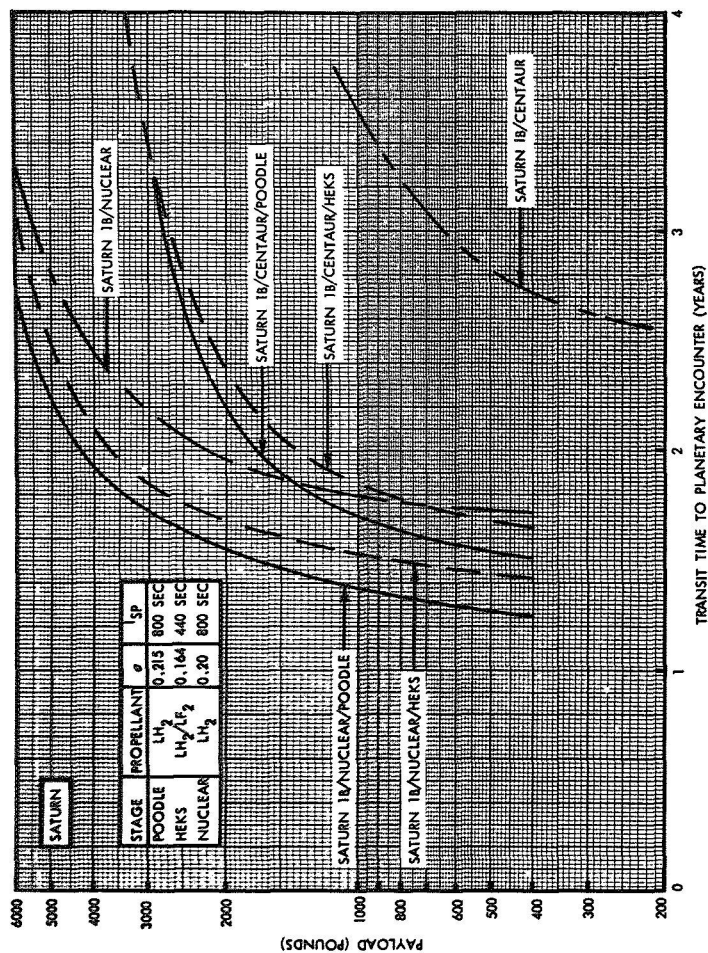


Figure 4-12. Variation of Payload with Transit Time to Encounter With the Planet Saturn (Direct Trajectory)

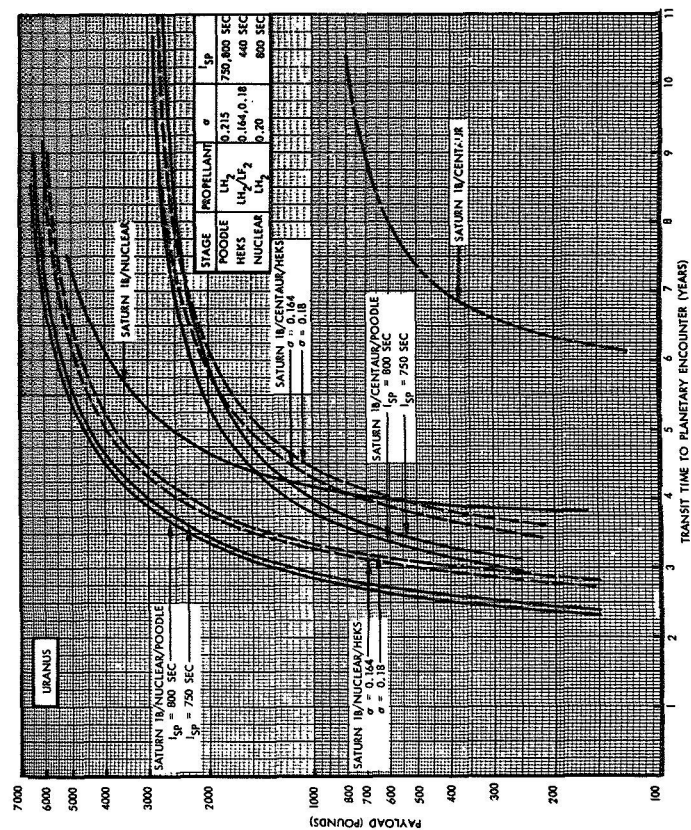


Figure 4-13. Variation of Payload with Transit Time to Encounter With the Planet Uranus (Direct Trajectory)

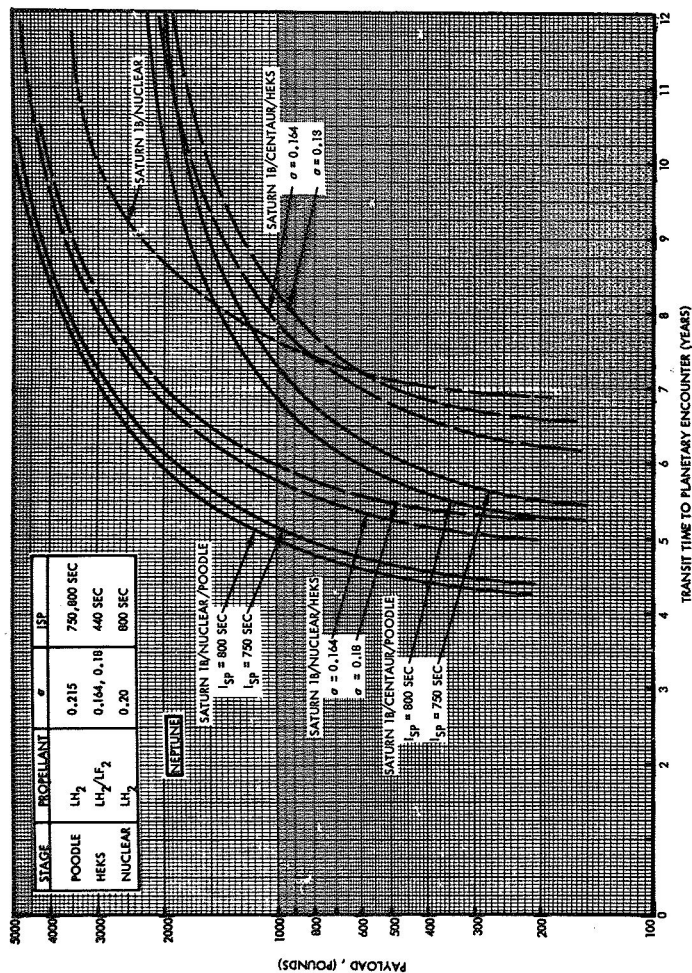


Figure 4-14. Variation of Payload with Transit Time to Encounter With the Planet Neptune (Direct Trajectory)

4.4.4 Orbital Transfers

Orbital transfers represent an important class of missions of definite NASA and USAF interest. These missions have been evaluated by TRW Systems and have been reported previously (Reference 4-4). The orbital transfer can be accomplished with POODLE by spiralling out from an initial parking orbit, as illustrated schematically in Figure 4-15. Because of the low thrust/weight ratio, POODLE must provide a greater ΔV to perform an orbital transfer than that which must be provided by a high-thrust system.* Orbital altitudes achieved as a function of velocity increment for high- and low-thrust propulsion systems are shown in Figure 4-16. Table 4-5 summarizes results obtained for orbital transfer missions.

A POODLE stage has a unique capability not applicable to chemical propulsion systems. When performing an orbit transfer, the POODLE stage will have a speed about equal to the circular orbital velocity. Any part of the payload jettisoned will go into a near circular orbit at the altitude it is released. Therefore, it is feasible to drop off satellites at various altitudes in order to provide continuous and simultaneous mapping of Earth's radiation fields.

4.5 CONCLUSIONS

The performance of a POODLE upper stage on Saturn-class launch vehicles has been evaluated for a variety of planetary and interplanetary missions of potential interest to NASA. The results obtained were then compared to the performance of the most likely competitor, the hydrogen-fluorine upper stage (HEKS). In all cases, it was shown that POODLE will outperform HEKS when the following principal propulsion tradeoffs are considered:

- Solar probes Payload versus perihelion distance
- Out-of-ecliptic probes Payload versus angle
- Outer-planet flybys Payload versus transit time
- Orbital transfers Payload versus altitude

* See Appendix A.

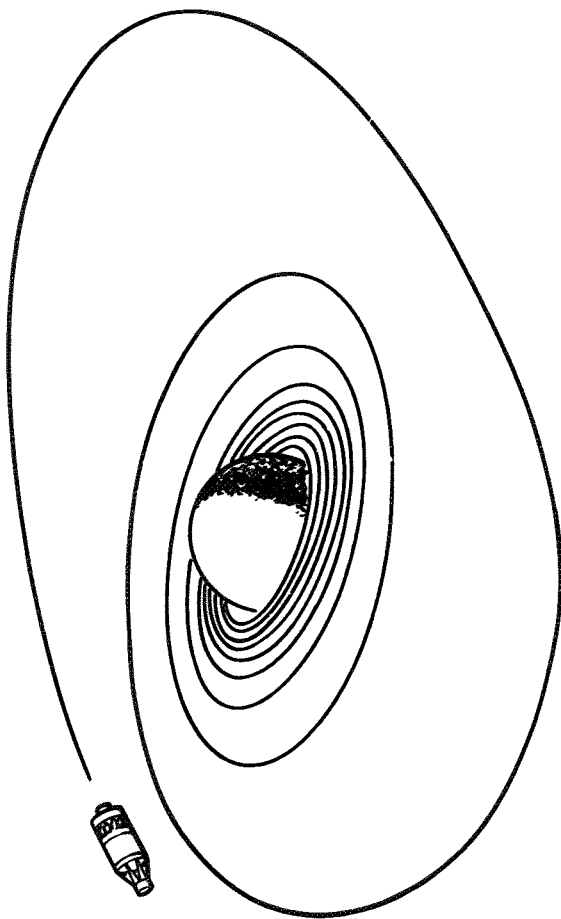


Figure 4-15. Low Thrust Orbit Transfer Trajectory

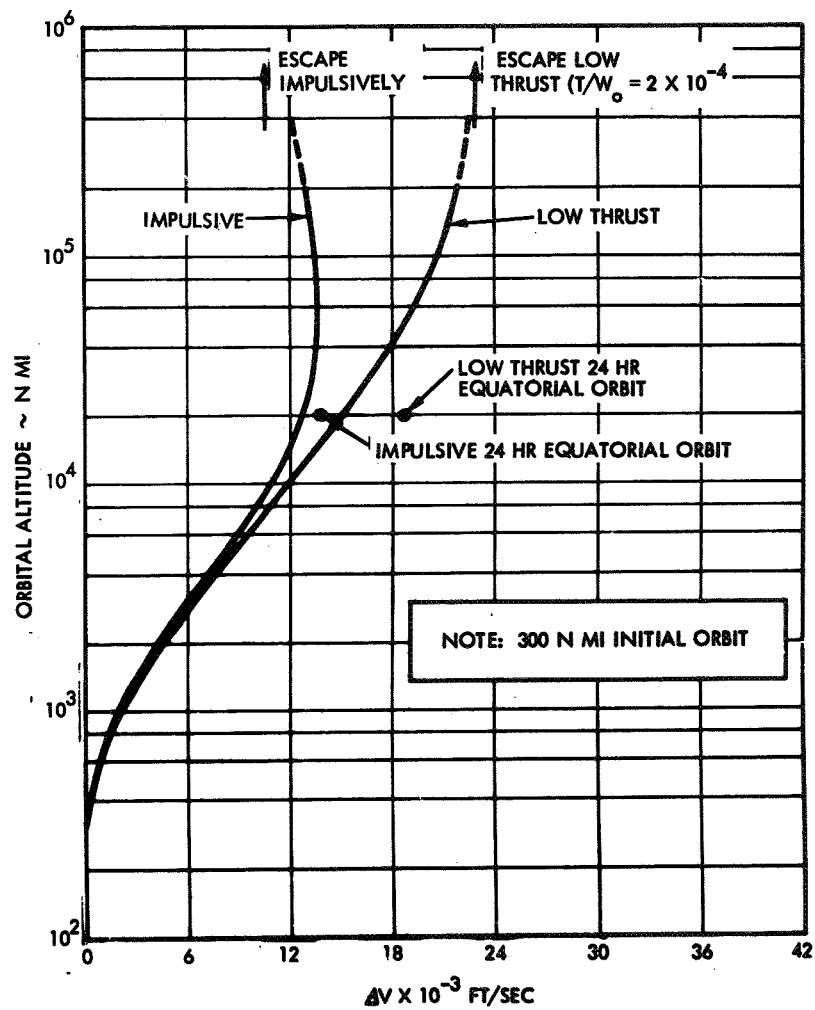


Figure 4-16. Orbital Transfer Velocity Requirements

Table 4-5. Comparative Orbital Payload Capabilities

<u>Vehicle Combination</u>	<u>12 Hr Orbit</u>	<u>Payload (lbs) 24 Hr Orbit</u>	<u>24 Hr Equatorial</u>
Atlas - Agena	575	280	100
Atlas - Centaur	1775	1200	735
Atlas - POODLE (2.5K)	1450	1280	930
Titan II - Agena	1125	650	325
Titan IIIA* - Centaur	2625	1900	1325
Titan II-H ₂ /F ₂ (7K)	2680	2200	1830
Titan II-POODLE (4.6K)	3275	2910	2260
Titan IIIA* - Centaur-H ₂ /F ₂ (7K)	3850	3300	2850
Titan IIIA* - Centaur-POODLE (7.2K)	5800	5200	4150
Titan IIIC* - Agena	5500	4300	3450
Titan IIIC* - Centaur	10,750	9100	7800
Titan IIIC-POODLE (14.5K)	11,900	10,800	8500
Saturn IB - Centaur	12,250	10,300	8900
Saturn IB-POODLE (20K)	16,250	14,600	11,600

*No Transtage

The payload capability for each launch vehicle combination is summarized in Table 4-6. POODLE will generally be most useful for the most difficult missions, i.e., those with highest characteristic velocities. A POODLE stage in the 5000-pound class provides significant capability for a variety of missions.

Future stages of intermediate size with which POODLE can be combined are indeed possible. Consideration has been given here to a nuclear reactor stage competitive with Centaur. With the nuclear reactor stage POODLE will perform a variety of missions previously considered extremely difficult. It is possible for a Saturn V/Nuclear/POODLE to inject a small payload (250 pounds) into the Sun without a planetary swingby maneuver. In addition, the same Nuclear/POODLE combination on the Saturn IB competes with the more expensive Saturn V/Centaur for a variety of missions.

Table 4-6. Mission Payloads (pounds) for Boost Vehicle Combinations

Vehicle Combination	Solar Probe			Out-of-Ecliptic Probe					Jupiter Flyby Mission		Saturn Flyby Mission		Uranus Flyby Mission			Neptune Flyby Mission				
	0.01 AU	0.05 AU	0.1 AU	0.2 AU	25°	30°	35°	40°	45°	360 days	400 days	500 days	1.5 yrs	2 yrs	3 yrs	4 yrs	5 yrs	6 yrs	8 yrs	
Saturn IB/Centaur	0	0	0	100	0	0	0	0	0	0	0	1200	0	0	640	0	0	0	0	
Saturn IB/Centaur/HEKS	0	0	150	2200	1800	550	0	0	0	1500	1100	1400	<100	1400	2600	0	700	1500	0	100
Saturn IB/Centaur/POODLE	0	0	600	2200	2000	1000	320	0	0	1800	2400	3000	400	1700	2700	300	1200	1850	0	500
Saturn IB/Nuclear	0	0	0	4000	3000	115	0	0	0	2400	4200	6200	0	2100	5000	0	700	2600	0	1350
Saturn IB/Nuclear/HEKS	0	200	1100	5500	4200	2000	650	0	0	3900	5100	7000	800	3700	5900	500	2500	4000	250	1200
Saturn IB/Nuclear/POODLE	0	800	2000	5500	4900	2900	1500	730	100	4500	5800	7500	1700	4300	6400	1250	3200	4600	1000	2050
Saturn V/Centaur	0	0	2500	>10,000	>10,000	6000	2000	0	0											
Saturn V/Nuclear	0	2000	8000	>10,000	>10,000	>10,000	6200	1800	0											
Saturn V/Nuclear/HEKS	400	3400	9000	>10,000	>10,000	>10,000	6400	3200	1200											
Saturn V/Nuclear/POODLE	1400	4800	10,000	>10,000	>10,000	>10,000	8200	4600	2500											

APPENDIX A

VELOCITY PENALTY ASSOCIATED WITH POODLE FOR ESCAPE MISSIONS

For Earth-escape missions, POODLE incurs a velocity penalty relative to a high thrust system because it cannot supply its velocity increment impulsively at the low Earth parking orbit. It is assumed here that a stage thrust of one pound is sufficient to preclude further penalty in the Sun's gravitational field. The high-thrust system provides its velocity increment in the parking orbit (impulsive approximation). The resultant hyperbolic excess velocity (relative to Earth) is related to the equivalent burnout velocity by:

$$V_{\infty} = \sqrt{V_{BO}^2 - 2V_{CIR}^2}$$

where

V_{BO} = high-thrust burnout velocity

V_{CIR} = circular velocity in parking orbit

V_{∞} = hyperbolic excess velocity

If V_{BO} is less than the required escape velocity, the POODLE stage and payload will go into an elliptical orbit. Escape from an elliptical orbit can be accomplished with POODLE. The low-thrust ΔV depends on the booster burnout velocity, V_{BO} , at injection.

For $V_{BO} > V_{escape}$

$$\Delta V_{LT} = V_{\infty 2} - V_{\infty 1} = V_{\infty 2} - \sqrt{V_{BO}^2 - 2V_{CIR}^2}$$

For $V_{BO} < V_{escape}$

$$\Delta V_{LT} = V_{\infty 2} + \sqrt{2V_{CIR}^2 - V_{BO}^2}$$

To evaluate the low-thrust ΔV penalty relative to a high-thrust system, it is necessary to determine the increment in the high-thrust ΔV necessary to achieve the final velocity. It must be recalled that all the high-thrust ΔV necessary to achieve $V_{\infty 2}$ can be provided from the 100 nautical mile parking orbit. In this case, the additional ΔV_{HT} required to achieve $V_{\infty 2}$ can be related to the burnout velocity in the low-thrust case by

$$\Delta V_{HT} = \sqrt{V_{\infty 2}^2 + 2V_{CIR}^2} - V_{BO}$$

The ΔV penalty, the ratio of $\Delta V_{LT}/\Delta V_{HT}$, is shown in Figures A-1 and A-2 for $V_{BO} < V_{escape}$ and $V_{BO} > V_{escape}$, respectively. If a low-thrust POODLE stage is to compete with a high-thrust system, the ΔV penalty must be less than the I_{sp} advantage. The I_{sp} advantage for POODLE, relative to chemical propulsion systems is approximately a factor of 2. Therefore, except for very large values of final hyperbolic excess velocities, the POODLE stage must have at least escape velocity before operating if it is to deliver a greater payload relative to a high-thrust upper stage.

A-2

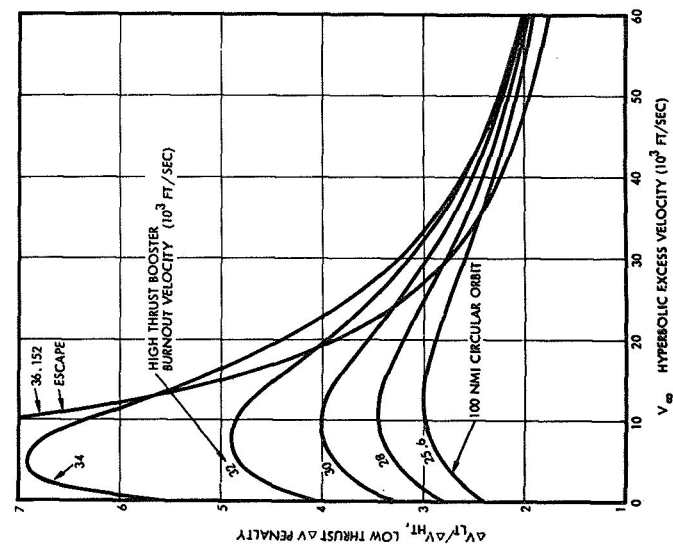


Figure A-1. Low-Thrust Penalty for Low-Thrust Escape from Elliptical Orbits

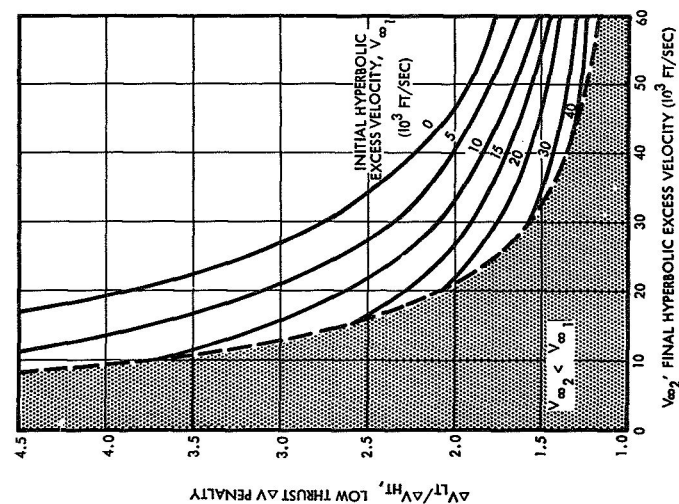


Figure A-2. Low-Thrust Penalty for High-Thrust Escape from Parking Orbit

A-3

REFERENCES

- 4-1 J. S. Martin z, "Isotope/Thermal Thrusters and Applications," presented to Second AGARD/NATO Lecture Series on Nuclear Propulsion, Brussels, 2 October 1964.
- 4-2 "Radioisotope Applications in Space - Final Report," STL-517-0016, Vol. V, February 1965.
- 4-3 W. C. Strack, "Solar-Electric Propulsion System Performance for the 0.1-AU Solar Probe Mission," AIAA Paper 66-496, June 1966.
- 4-4 "Radioisotope Applications in Space - Final Report," STL-517-0016, Vol. VI, February 1965.

R-1

END

DATE FILMED

11 / 9 / 67